Investigation of Ordered Pd based Intermetallic Nanoparticles as Efficient and Stable Catalysts in Fuel Cell Application

A Thesis

Submitted in partial fulfillment for the degree of

Master of Science

as a part of

Integrated PhD Programme (Chemical Science)

By

Mr. Rajkumar Jana

New Chemistry Unit

Jawaharlal Nehru Centre for Advanced Scientific Research

(A Deemed University)

Bangalore - 560064 (INDIA)

MARCH-2015

Dedicated to my Parents

Declaration

I hereby declare that the matter embodied in the thesis entitled "**Investigation of Ordered Pd based Intermetallic Nanoparticles as Efficient and Stable Catalysts in Fuel Cell Application**" is the result of investigations carried out by me at the New Chemistry Unit, Jawaharlal Nehru Centre for Advanced Scientific Research, Bangalore, India under the supervision of Dr. Sebastian C. Peter and that it has not been submitted elsewhere for the award of any degree or diploma.

In keeping with the general practice in reporting scientific observations, due acknowledgement has been made whenever the work described is based on the findings of other investigators. Any omission that might have occurred by oversight or error of judgment is regretted.

Date :

Bangalore, India Rajkumar Jana

Certificate

I hereby certify that the matter embodied in this thesis entitled "**Investigation of Ordered Pd based Intermetallic Nanoparticles as Efficient and Stable Catalysts in Fuel Cell Application**" has been carried out by Mr. Rajkumar Jana at the New Chemistry Unit, Jawaharlal Nehru Centre for Advanced Scientific Research, Bangalore, India under my supervision and that it has not been submitted elsewhere for the award of any degree or diploma.

Date : 31-03-2015

Bangalore, India

Dr. Sebastian C. Peter

New Chemistry Unit
JNCASR
(Research Supervisor)

Acknowledgements

First of all, I am highly grateful to my research supervisor Dr. Sebastian C. Peter for his constant support, inspiration and enthusiasm and the kind of freedom he has given me for my work. His suggestions pertaining to my work and his way of tackling problems has helped me immensely. It has been a great pleasure for me to work under his guidance. So, I take this opportunity to express my immense gratitude to him.

I have been extremely fortunate to have got encouragement from Prof. C. N. R. Rao, F.R.S. at the beginning of my research career. I owe a deep sense of gratitude to his great personality and immense contribution to science. He has been a great source of inspiration during my MS work.

I am also thankful to all the faculty members of New Chemistry Unit for selecting me as one of the candidates for Int. PhD Program 2012 and giving me the opportunity to carry out my research.

I convey my sincere thanks to NCU chairman Prof. C.N.R. Rao, F.R.S., conveners, Prof. T. Govindaraju and Dr. Ranjani Viswanatha.

I would like to thank my collaborators Prof. S. Sampath, Prof. Umesh V. Waghmare, Ms. Anju V.G. and Mr. Balamurugan Tappa.

I would like to thank Prof. H. Ila, Dr. Sridhar Rajaram, Dr. Jayanta Haldar, Dr. Subi J. George, Dr. M. Eswaramoorthy, Dr. T. Govindaraju, Dr. Ranjani Viswanatha, Dr. Sebastian C. Peter, Dr. Tapas K. Maji, Dr. Ujjal Gautam, Dr. Kanishka Biswas, Prof. A. Sundaresan, Prof. Umesh V. Waghmare, Prof. S. M. Shivaprasad and Prof. S. Sampath for the various courses which were extremely helpful to me.

I shall never forget the contributions of my lab-mates. I extend my deep sense of gratitude to Sumanta, Subba, Soumya, Aloke, Abhishek, Deepti, Pramod, Pradeep, Prakthi, Ramesh, Duddappa, Saurav, Sweta, Vijay for their help, encouragement and for maintain a

friendly environment in the lab. I would like to thank the visiting students Anupam, Paramita who have helped me in synthesis of the compounds during their summer fellowship.

I would also like to acknowledge my undergraduate and school teachers, who have taught me the basics of science and ensured that I have a strong pedestal for achieving my goals. I would like to thank Mrs. Uma, Mr. Satyakum, Mr. Tapanjyoti, Dr. Tapan, Mr. Kajal, Mr. Kishore, Dr. A.V.S, Dr. Pr.G, Dr. B.K.S and all the teachers of chemistry department of Narendrapur, Balighai F.D. high school, Egra J.L high school.

I would like to thank all my Integrated Ph.D. chemical science and material science batch mates Shantanu, Kushagra, Promit, Ananya Mishra, Ananya Banik, Sohini, Vikas and Shivkumar for being there when I needed most.

I also thank my friends, seniors and juniors, Satya, Rana, Arindom, Abhijit, Mohini, Somnath, Ritesh, Prolok, Debu, Suman, Arpan, Moumita, Sunita, Tarak, Rajib, Anirban, Avijit, Anindita, Sisir, Koushik, Chandan, Papri, Syamantak, Jiaul, Krishnendu, Debopreeti, Jiarul and all others whom I have missed to mention for helping me in various cases and making my stay in JNCASR pleasant and enjoyable.

I would like to express my sincere thanks to all the academic, administrative, security, library, complab and health center staff for making our campus life smooth and easy.

I would like to thank technical staff Mrs. Usha, Mrs. Bhavya, Mr. Anil, Mrs. Selvi, Mr. Basu for their helps in various measurements.

Above all, I would like to thank my parents, grandparents and my relatives for all the love, affection and support they gave. Especially, I have been fortunate enough to have such a parents who stood by me during my bad time and led me to find out the correct way.

Last but not the least; I thank Almighty God for providing me a wonderful life.

Preface

Energy crisis is one of the major challenges that the world is facing today. Under the circumstances research related to energy storage and conversion have become very much essential. "Fuel Cell" is one of the remedies against such looming crisis of energy. This M.S. thesis presents the results of investigations of the synthesis of Pd based intermetallic nanocrystals in various sizes and shapes and their applications in fuel cell both as cathode and anode catalyst materials. Due to low cost, less poisoning effect and remarkable activity and durability in comparison with state of art Pt electrode materials, Pd based electrocatalysts have gained a lot of attention from research community. The thesis consists of four chapters.

Chapter 1 gives a brief overview of fuel cells, urgency of fuel cell research and discusses about some fundamental aspects of electrocatalysis. It also describes the importance of noble metal based nanocrystals as cathode and anode materials.

Chapter 2 deals with the rational design, characterization and electrocatalytic properties of ordered Pd_3Pb intermetallic nanocrystals as an efficient and durable anode electrocatalysts in both acid and alkaline medium. The ordered Pd_3Pb compound has been synthesized in different size and morphology both hydrothermal and polyol method. The polyol method requires just 10 seconds for the ordered structure formation.

Chapter 3 describes synthesis, characterizations and electrocatalytic properties of novel Pd_2Ge intermetallic nanoparticle. The catalyst is highly efficient and stable for the electrochemical oxidation of ethanol in alkaline medium. The experimentally observed data have been with the DFT calculations in terms of combined effect of adsorption energies of CH_3CO and OH radicals, d- band center model and work function of the corresponding catalyst surfaces.

Chapter 4 articulates about the shape tailoring of ordered $PdCu_3$ nanocrystals simply by solvothermal method and the effect of crystal facets in Oxygen Reduction Reaction (ORR) in alkaline medium. This chapter shows how control in morphology enhances the kinetics of ORR.

Finally the results have been summarized with some future plans to improve the activity of the materials studied.

Table of Contents

Chapter 2. Facile and Ultrafast Synthesis of Pd_3Pb Nanocrystals towards Enhanced Activity and Durability in Direct Ethanol and Formic acid Fuel Cells

Chapter 3. Ordered Pd_2Ge Intermetallic Nanoparticles for Enhanced Activity and Stability towards Ethanol Oxidation

Chapter 1

Introduction

1.1. Background

Search of sustainable solutions to the looming energy crisis has become one of the major challenges on the way to get rid of our dependence on fossil fuels.[1,2] Over the last few years several technologies have been implemented to provide electrical energy from different renewable sources such as solar energy, wind power generators.[3] But the mismatch between supply and demand leads researchers to find out integrated solutions with advanced energy conversion and storage.[1,2,4-6] In recent years noble metal nanocrystals have been considered as the benchmark materials due to their superior catalytic performances in the field of "electrochemical energy conversion and storage.[7] Noble metal based materials have been widely used in various electrochemical reactions like hydrogen or small molecule oxidation, oxygen reduction in fuel cells.[8,9] The catalytic performance mainly depends on activity, selectivity and stability. The catalytic performances of noble metal based materials are influenced mainly by three factors; (1) ensemble effect, (2) electronic effect, (3) geometric effect.[10] Ensemble effect comes into play when a catalyst consisting of multiple metals provides different reaction sites.[11,12] For electronic effect, the electronic structure of the noble metal surface modifies from the electronic charge transfer between different components leading to the improvement of the catalytic activity.[13,14] In case of geometric effect, the strain induced in different structures (different exposed facets) enhances the catalytic activity indirectly by changing electronic structure and atomic arrangements of the surface of the catalyst.[15-18] Thus control synthesis of noble metal nanostructures with different morphology has a profound effect in designing efficient and stable catalysts.

Among the various methods towards nanocrystal synthesis, the colloidal method is still considered as one of the facile, cost-effective method.[19,20] Through this method one can get both kinetic and thermodynamic controlled structures.[18] However shape selective

synthesis of noble metal alloys are more complicated because of the various reduction potential and different nucleation or growth habits of the different metals present in the same structure.[18]

1.2. Fuel Cells

1.2.1. What is fuel cell?

A fuel cell is a device that converts chemical energy stored in a fuel into electrical energy through a chemical reaction with oxygen or other oxidizing agents (**Figure 1**).

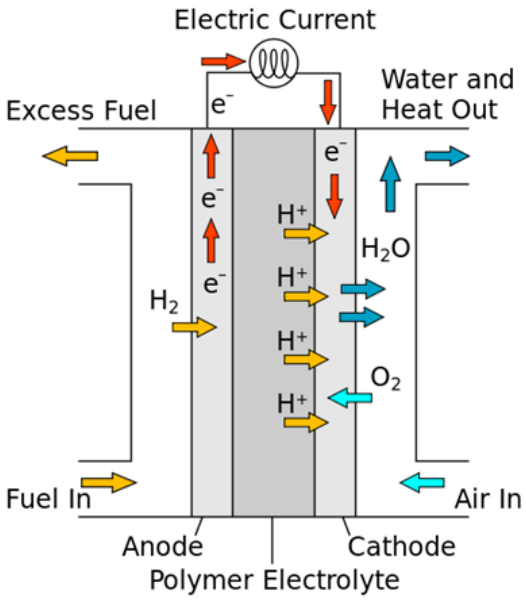

Figure 1. Fuel cell diagram (Figure generated from http://en.wikipedia.org/wiki/File: Solid_oxide_fuel_cell.svg)

The fuel gas (mainly hydrogen rich) is passed towards the anode where the following oxidation occurs.

$$H_2\ (gas) \longrightarrow 2H^+ + 2e^-$$

The liberated electrons pass through external circuit and go to cathode and positive hydrogen ion (H^+) migrates through electrolyte towards cathode. At the cathode H+ ions react with oxygen (from air) to form water and heat and electricity generated.

$$H_2 + ½\ O_2 \longrightarrow H_2O + \text{electricity} + \text{heat}$$

In the area of energy storage and conversion devices, electrochemical systems play an important role. The electrochemical energy conversion means the conversion of chemical energy to electrical energy of vice versa. Electrochemical energy systems possess several advantages, (1) chemical energy is directly converted to electrical energy without Carnot limitation and hence they are very efficient; (2) low emission of pollutants and (3) they are easily transportable.[21-23] Among the three types of electrochemical energy systems namely, fuel cells, batteries and capacitors, fuel cell occupies a special position owing to its high specific energy associated with the device (**Table 1**).[23] Evidently, specific energy of a fuel cell is far superior to a battery and a capacitor. This is further supported from the plot of specific power (the rate at which energy can be released) vs. specific energy which is known as Ragone plot (**Figure 2**). However, fuel cells do not possess high power density. Hence, fuel cell should be coupled with a capacitor when both energy density and power density requirements are high.

Table 1. Comparison of energy densities among various electrochemical energy systems.

Electrochemical systems	Specific energy (Wh/Kg)
Lead acid battery	35-40
Li-ion battery	150-200
H_2-O_2 fuel cell	33500
CH_3OH-O_2 fuel cell	6100

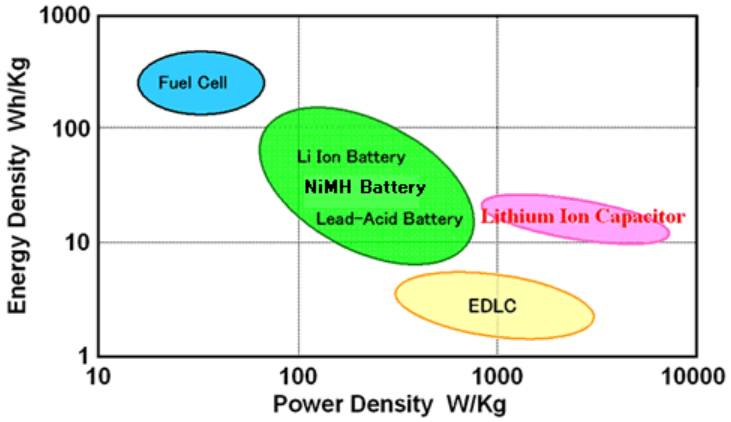

Figure 2. Ragone plot for electrochemical energy systems (Figure generated from http://commons.wikimedia.org/wiki/File:Lithium_Ion_Capacitor_Chart.png).

1.2.2. History

Electrocatalysis and search for promising electrocatalysts effectively initiated after two distinct developments in science in the 19th century when i) Sir William Robert Grove reported the reverse of water electrolysis (in 1839) and his discovery of energy device named as '*gas voltaic battery'* and theoretical definition of (H_2/O_2) fuel cells and their fundamental structure in 1842 and (ii) introduction of Tafel polarization studies. In 1894, Ostwald discussed the advantages of electrochemical energy conversion methods over the thermal counterparts.[21] Horiuti and Polanyi in 1935 first reported the experimental treatment on electrocatalysis, but the most intensive growth in the field of electrocatalysis started in the early 1960s and continuous to develop when Francis Thomas Bacon initiated work on fuel cells developed by Mond and Langer.[24] He constructed a cell with less expensive electrode material (nickel gauze) and less corrosive electrolyte (alkali) that operated under pressure as high as 3000 psi.[25] Subsequently, Pratt & Whitney Company developed Bacon's work for 'Apollo' spacecraft fuel cells. General Motors (GM) and Union Carbide (UC) in 1966 initiated work on fuel cells for general applications and introduced the first earthbound fuel cell vehicle called the 'Electrovan'.[26]

1.2.3. Types of Fuel Cell

According to electrolyte and operation temperature fuel cells are classified in various types such that polymer electrolyte membrane fuel cell (PEMFC), phosphoric acid fuel cell (PAFC), direct alcohol fuel cell (DAFC), direct formic acid fuel cell (DFAFC), alkaline fuel cell (AFC), molten carbonate fuel cell (MCFC), and solid oxide fuel cell (SOFC). The characteristics and efficiency of different fuel cells are summarized in **Table 2**. Half-cell reactions of various fuel cells are shown in **Table 3**.[27] PEMFCs and DAFCs have drawn more attention for transportation and consumer electronics due to its low operating temperature, rapid start up, light weight and simplicity.

Table 2. Efficiency and working temperature of different types of fuel cells.

Types of fuel cell	Working temperature (°C)	Efficiency (%)
PEM	80	40-60
AFC	90-100	60-70
DAFC	50-120	< 40
PAFC	100-250	< 40
MCFC	600-700	50-60
SOFC	700-1000	50-60

Table 3. Electrochemical characteristics of different fuel cells.

Fuel cell	Anode reaction	Cathode reaction	Mobile ion
PEMFC	$H_2 \rightarrow 2H^+ + e^-$	$½\ O_2 + 2H^+ + 2e^- \rightarrow H_2O$	H^+
DMFC	$CH_3OH + H_2 \longrightarrow CO_2 + 6H^+ + 6e^-$	$½\ O_2 + 2H^+ + 2e^- \rightarrow H_2O$	H^+
AFC	$H_2 + 2OH^- \rightarrow 2H_2O + 2e^-$	$½\ O_2 + 2H_2O + 2e^- \rightarrow 2OH^-$	OH^-
PAFC	$H_2 \rightarrow 2H^+ + e^-$	$½\ O_2 + 2H^+ + 2e^- \rightarrow H_2O$	H^+
MCFC	$H_2 + CO_3^{2-} \rightarrow H_2O + CO_2 + 2e^-$	$½\ O_2 + CO_2 + 2e^- \rightarrow CO_3^{2-}$	CO_3^{2-}
SOFC	$H_2 + O^{2-} \rightarrow H_2O + 2e^-$	$½\ O2 + 2e- \rightarrow O^{2-}$	O^{2-}

1.2.3.1. Proton exchange membrane fuel cells

Proton exchange membrane fuel cells (PEMFC) also known as polymer electrolyte membrane fuel cells, consist of a proton conducting polymer electrolyte. The generally used electrolyte is a perfluorosulfonic acid membrane (Nafion, DuPont, USA) consisting of hydrophilic and hydrophobic part.[28] The CF_2 groups in the polymer (**Figure 3**) are equivalent to Teflon giving high stability in oxidizing and reducing environments.[27,29-32] A very thin membrane (50-100 µm) is used to achieve high efficiency as it reduces ohmic resistance loss considerably. Corrosion related issues are minimal in case of PEMFCs as it uses solid electrolyte and the reaction product is only water. PEMFCs can produce high power densities and offer advantages of low weight and small volume.

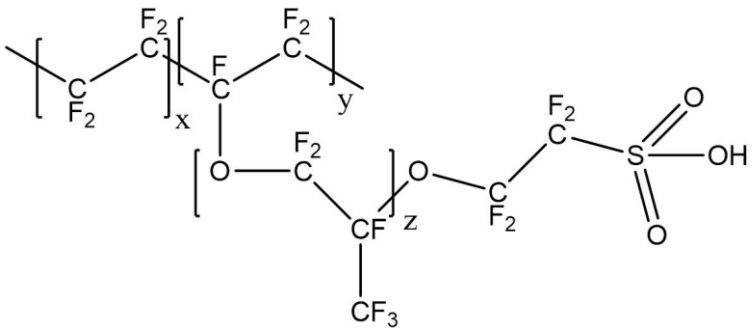

Figure 3. Structure of Nafion.

1.2.3.2. Direct alcohol fuel cell

The problems associated with H_2 - O_2 fuel cells have led to a class of liquid feed fuel cells i.e. direct fuel cells where liquid fuel solutions are fed to the anode compartment.[33-35] Some of the fed fuels include methanol, ethanol, hydrazine, glycerol and ascorbic acid.[33,36-38] In direct alcohol fuel cells, alcoholic solutions are used along with either gaseous oxygen or liquid hydrogen peroxide as fuel and oxidant respectively. The most used alcohols in direct alcohol fuel cells (DAFC) are methanol and ethanol, which can be produced from natural gas or renewable biomass resources.[33,36,39-42] Since the fuels are fed as liquids, storage and transport problems associated with H_2 - O_2 fuel cells are minimized.[33,36,38] The DAFCs are generally projected for low power applications such as consumer electronics.

1.2.3.3. Alkaline fuel cells

Ever since National Aeronautics and Space Administration (NASA, USA) used alkaline fuel cells (AFC) in their manned space mission, AFCs have drawn enormous attention from scientific community across the globe. The advantages of AFCs are improved reaction kinetics of fuel oxidation combined with reduced poisoning of the electrocatalysts[43-45] and use of inexpensive catalyst in alkaline media.[33,36,38] The fuels used under alkaline conditions are H_2, methanol, ethanol, ethylene glycol, borohydride and hydrazine.[33,36,38] Across the membrane, the ion transport is by OH^- ions and proceeds from cathode to anode. Due to the reversal of electro-osmotic drag methanol permeation rate is reduced resulting in reduced cross-over.[46] However, some of the issues related to AFCs are the unavailability of stable OH^- conducting membrane, thermal instability and low OH^- conductivity.[46-49]

1.2.3.4. Phosphoric acid fuel cell

The phosphoric acid fuel cell (PAFC) is the one of the few fuel cell types that has reached commercialization stage in the twentieth century.[27] Phosphoric acid (H_3PO_4), excellent electrolyte for fuel cells, use hydrogen produced by steam-reforming/shift conversion of organic hydrocarbons (e.g. natural gas) and alcohols (methanol or ethanol). Unlike other acid electrolyte systems, water is not involved in the transport mechanism; the protons are conducted directly by the acid, which also serves as the solvent. The phosphonium ion, similar to the hydronium ion is formed, and proton hopping occurs via phosphoric acid molecules. The advantages of PAFC are that (*a*) the electrolyte is inert and stable in an oxidizing or reducing environment; (*b*) it is capable of operation up to 200°C; and (*c*) the CO tolerance at the anode is 1%–2%. Added advantages are that (*a*) the product, water, is removed from the cell as vapour and (*b*) waste heat rejection is efficient because of high temperature, compared with AFCs and PEMFCs, which operate at <100 °C.[22,27]

1.2.3.5. Molten carbonate fuel cells

The molten carbonate fuel cell (MCFC) is promising in terms of high electricity-generating efficiencies and the ability to consume coal-based fuels. In MCFCs, oxygen and carbon dioxide is consumed in cathodic reaction to produce carbonate ions.[27,50]

1.2.3.6. Solid oxide fuel cells

The solid oxide fuel cell (SOFC) operates at high temperatures, of the order of 1000°C. One of the major advantages of the SOFC is that it uses a solid electrolyte,[51] unlike other types of fuel cells. Since it is a two-phase system (solid/gas), the problems connected with mass transport of reactants and products in liquid phase within the electrode are eliminated.

1.2.4. Fundamental aspects of fuel cell

The goal of research on electrocatalysis is to obtain maximum efficiency of conversion with minimum overpotential. Fuel cells should be able to provide substantial electrical energy when reasonably large currents are drawn. However, when there is a current load, the cell voltage (V) decreases due to various irreversible processes, called 'polarization losses'. Three different polarization limitations are identified (i) ohmic polarization (η_{ohm}), (ii) concentration polarization (η_{conc}) and (iii) activation polarization (η_{act}).

Ohmic polarization is due to the movement of ions within electrolyte and resistance to electron flow. η_{ohm} can be expressed by

$$\eta_{ohm} = I.\ R$$

where I is the cell current and R is the overall cell resistance including electronic, ionic and contact resistances.[52,53]

Concentration polarization arises at high reaction rates, where a high concentration gradient develops between concentration of reactant at the electrode surface (C_s) and bulk (C_{bulk}) of the solution. Fuel cell polarization losses are mainly influenced by η_{conc}, especially at high current densities due to diffusion limited mass transport. The mass transport can be described by applying Fick's law of diffusion.[54]

$$i = [nFD\ (C_{bulk}-C_s)]/\delta$$

where D is diffusion co-efficient, F is Faraday constant and δ is thickness of diffusion layer. At the limiting current condition when $C_s=0$,

$$i_L = (nFDC_{bulk})/\delta$$

η_{conc} can be defined as the difference between the equilibrium potential for which $C_s=C_{bulk}$ (E_{Cb}) and the equilibrium potential in case of $C_s<C_{bulk}$ (E_{Cs}). The following

expression can be obtained, when Nernst equation is combined with Fick's law of diffusion.

$$\eta_{conc} = (RT/nF) \ln(C_s/C_{bulk}) = (RT/nF) \ln (1-i/i_L)$$

Activation polarization, η_{act} comes into play in case of sluggish reaction kinetics. It is greatly influenced by adsorption/desorption of reactant and/or product species. Also, the transfer of electrons across double layer and nature of electrode surface (smooth or rough) dictates activation polarization. η_{act} is generally described by Tafel equation,

$$\eta_{act} = (RT/\alpha nF) \ln (i/i_o)$$

where α is transfer coefficient and i_o is exchange current density.

The Butler−Volmer equation generally governs the kinetics and thermodynamics of electrochemical reactions. The Tafel analysis is used in extreme cases when the reaction is taken away from equilibrium, where either the anodic or the cathodic current is dominating the total current measured. The logarithm of the current density log |i| (i = current density) is then plotted as a function of over potential η (= E(i)-E°) and the plot is used to calculate the kinetics of the reaction.

1.3. The Need for Fuel cell

Energy is one of the basic and most required resources in everyday life. Over several decades, fossil fuels could feed to our needs. It has been estimated that by around 2100 all the fossil fuel will be depleted. The depletion of fossil fuel coupled with increased global demand has led to search for alternate sources of energy. This pursuit has been further motivated by serious environmental concerns such as global warming and the effect of increase in carbon emissions on the environment. As of 2013, the level

of CO_2 is 398.5 ppm and about to reach 400 ppm.[55] In this aspect, we need to provide green alternative source of energy for future generation. Several alternative forms of energy emit less greenhouse gas including more efficient include photovoltaic solar cells, geothermal energy etc. However, among all of this form of alternative energy technologies fuel cell provide one of the best alternatives by virtue of their high efficiency and minimal greenhouse gas emission and long term deployment.[56] Therefore focus of research has been emphasized on electrochemical energy devices where chemical energy is directly converted into electrical energy. The process known as electrocatalysis is defined as the catalytic influence of electrode material on different electrode reactions.[21]

1.4. Electrocatalysis and metal nanoparticles

1.4.1. Catalytic aspects

1.4.1.1. Small molecule oxidation (SOMs)

It is evident from general discussion that a fuel cell consists of three important architectural components namely, (1) fuel, the energy source, (2) membrane, which allows internal communication between anode and cathode and (3) electrocatalysts over which the fuel undergoes oxidation or reduction reactions. Several small organic molecules (SOMs) like methanol, ethanol, formic acid etc in liquid state have been projected as alternate fuels to hydrogen in order to overcome the issues related to safety and storage.[33,35] These molecules have drawn the attention of fuel cell community because of the low temperature application due to their appreciable energy density and attractive theoretical voltage.[57,58] It is possible to achieve complete oxidation of methanol and formic acid into CO_2 as compared to ethanol which requires breakage of C-C bond. Among methanol, ethanol and formic acid, ethanol is less toxic than others. Among various liquid fuels, formic acid has been proposed as a promising fuel due to

good oxidation kinetics, less fuel cross-over problem.[57,59] One of the common features among these three fuels is the involvement of several reaction pathways during electrochemical oxidation. The conversion of fuel to CO_2 involves several sequential steps resulting in the generation of various intermediates, carbon monoxide (CO) being common in several reactions. Pt is known to be the best catalyst for alcohols and formic acid oxidation.

Methanol electrooxidation on Pt follows parallel reaction pathways as shown in **Figure 5**.[60,61] Methanol gets oxidized to CO_2 through two pathways simultaneously[60,61] and the domination of one pathway over the other one depends on the potential. In one pathway, methanol first dehydrogenates to CO at low overpotentials and CO gets adsorbed on to Pt. The adsorbed CO is further oxidized to CO_2 at high anodic potentials. In other pathway, direct oxidation of methanol to CO_2 occurs without the intermediate step of CO. A good electrocatalyst should favour the direct pathway as the poisoning effect of CO on Pt surface is well known. It has been reported that Pt alloys like PtRu, PtNi, PtIr, $PtRuO_2$ and PtRuIr possess superior CO tolerance properties compared to pure Pt.[62-69] Slow oxidation kinetics of methanol[70,71] and its cross-over through the polymer electrolyte membrane to cathode compartment.[72-75]

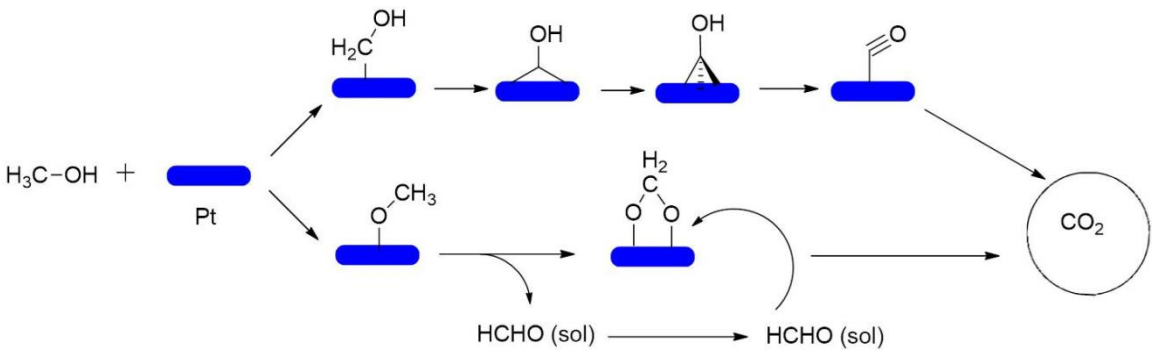

Figure 5. Methanol oxidation pathways on Pt.

Ethanol is a potential renewable fuel[76,77] having theoretical energy density (8 KWh Kg^{-1} as against 6.1 KWh Kg^{-1} for methanol).[78,79] However, complete oxidation of

ethanol to CO_2 demands high activation energies to overcome as it involves 12 electrons and also the breaking of C-C bond.[78,80-83] Many of the intermediates (mainly CO and –CHO) produced during the oxidation reaction poison the anode electrocatalyst and reduce the catalytic efficiency.[80] Ethanol oxidation has been reported to be very facile on Pt and its alloys such as PtSn, PtRu, PtNi and PtIr. Ethanol oxidation on Pt also follows a parallel pathway mechanism as in the case of methanol (**Figure 6**).[84-87] In the first pathway, ethanol oxidizes to acetaldehyde and acetic acid via four electron transfer without breaking C-C bond. The other pathway involves the cleavage of C-C bond, which results in the accumulation of CO on Pt sites. An efficient electrocatalyst should favour the second pathway of cleavage of C-C bond, which corresponds to a 12 electron transfer. Kowal et al have reported a ternary catalyst comprising Pt, Rh and SnO_2 for the complete oxidation of ethanol to CO_2.[85]

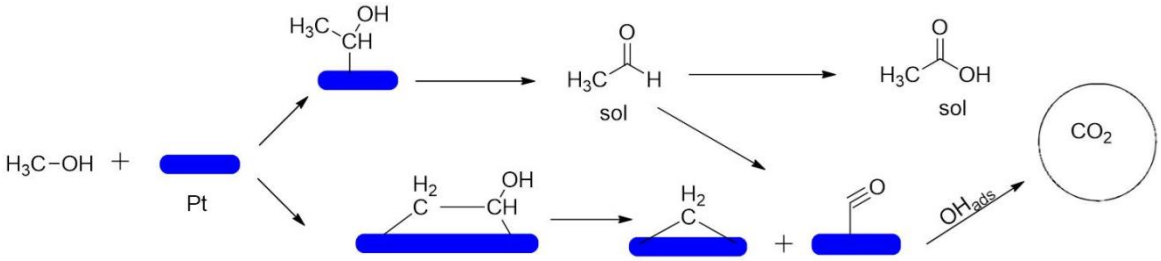

Figure 6. Schematic illustration of the oxidation of ethanol on Pt surface oxidation via different pathways.

Due to less fuel crossover problem and good oxidation kinetics at anode formic acid has been considered as a promising fuel. On platinum, formic acid oxidation mainly occurs mainly either direct pathway or indirect pathway (**Figure 7**).[88] In direct pathway formic acid oxidizes to CO_2 directly without the adsorbed CO intermediate step, thereby enhancing the overall turnover number. The indirect pathway involves dehydration of formic acid to form adsorbed CO on Pt surface. Then adsorbed –OH group on Pt surface oxidizes CO intermediate to gaseous CO_2. Another possibility is the formate pathway

has been proposed where CO_2 formation occurs via adsorbed formate intermediate (**Figure 7**).[89]

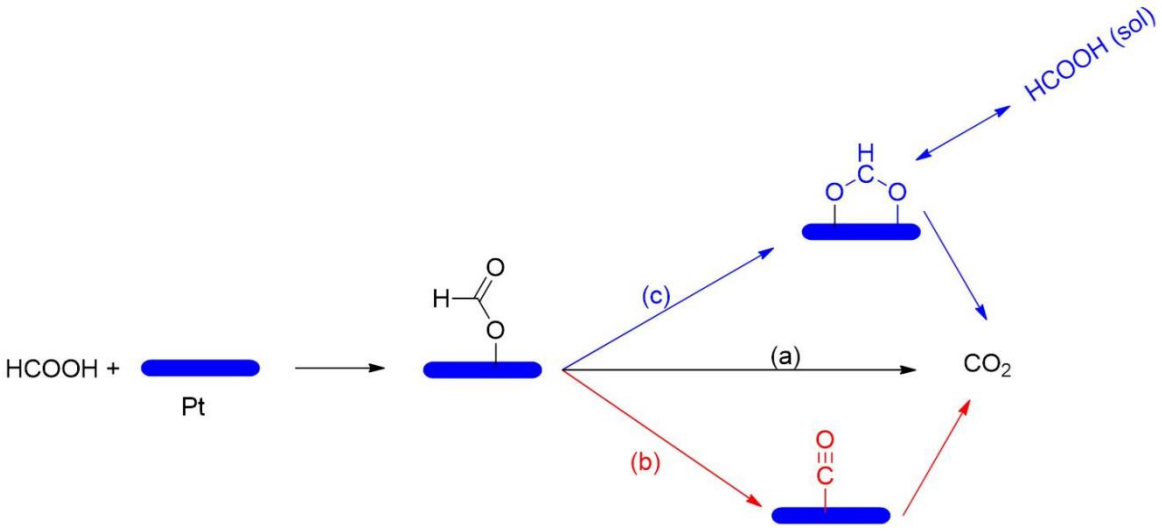

Figure 7. Schematic illustration of formic acid oxidation pathways on Pt (a) direct, (b) indirect and (c) formate ion pathways.

From the above mechanistic details of SOMs oxidation, it is evident that CO is one of the most common intermediates in all types of fuel. CO is known to be surface poison that drastically reduces the performance of the electrocatalysts. Alleviation of CO poisoning is necessary to improve the performance. Several ways have been proposed to mitigate poisoning of CO. One of the main issues related to the use of the best known Pt catalyst for SOMs oxidation is CO poisoning. Even in H_2-O_2 fuel cells, CO poisoning is of serious concern because CO is produced as a by-product of hydrocarbon reforming to hydrogen.[27] About 10-50 ppm concentration of CO is sufficient to poison the catalyst which causes severe degradation of performance over time.[22,27,32,90-92] After dehydrogenative adsorption and reorientation of methanol, the formed CO gets adsorbed on Pt. There is synergetic interaction between CO and Pt. According to molecular orbital diagram of metal-CO (M-CO) bonding, there is electron donation from the highest occupied molecular orbital (HOMO) of the CO molecule (sp-hybrid orbital based on carbon) to the metal. Then back donation of electron from to metal to lowest unoccupied

molecular orbital (LUMO) occurs. The LUMO is the empty antibonding π* orbital. Thus CO bond weakens due to the population of electron in the antibonding π* with the increase in back donation, the bond order (bond strength) of M-C bond increases whereas bond order of C-O bond decreases. High activation energies are to be overcome to free the Pt surface from CO, which in turn reduces the efficiency of the fuel cell dramatically. Hence, a good promoter in the catalyst should reduce the extent of back donation from Pt to adsorbed CO thereby weakening the Pt-C bonding strength. This will free the Pt sites for further reaction.

In order to remove CO from the Pt surface, adsorption of hydroxyl species on its surface should happen[58,93-98] and then CO will be removed as shown below.

$$Pt\text{-}CO_{ads} + Pt\text{-}OH_{ads} \longrightarrow 2Pt + CO_2 + H^+ + e^-$$

$$Pt + H_2O \longrightarrow Pt\text{-}OH_{ads} + H^+ + e^-$$

The formation of –OH groups on Pt surface happens only at very high anodic potentials (> 0.6 V vs. SHE), while accumulation of CO occurs at low over potentials.[58,93-97] But under normal fuel cell condition Pt-OH formation by decomposing water and subsequent removal of CO is not possible as fuel cell equilibrium working potential is not very high. The well-established strategy is to have a second metal like Ru, Ni, Ir, Rh, Fe, Pb and Bi along with Pt.[98-106] Among all these, Ru has drawn enormous attention because of its ability to decompose water at remarkably low overpotentials of 0.25 V vs. SHE .[100,102,103] In PtRu system, Pt dehydrogenates methanol to form Pt-CO and Ru decomposes water to form Ru-OH as shown in **Figure 8**. Both the reactions happen at low over potentials and hence adsorbed CO on Pt can be removed by the mechanism called ‘bifunctional mechanism’ as shown below.

$$CH_3OH + Pt \longrightarrow Pt\text{-}CO_{ads} + H^+ + e^-$$

$$Ru + H_2O \longrightarrow Ru\text{-}OH_{ads} + H^+ + e^-$$

$$Pt\text{-}CO_{ads} + Ru\text{-}OH_{ads} \longrightarrow Pt + Ru + CO_2 + H^+ + e^-$$

The proximity of Pt and Ru are very important in achieving CO removal by this mechanism. Alloying of Pt with Ru, Fe, Ni, Co have also been reported to modify the electronic structure of Pt, which is known as 'ligand effect'.[107,108]

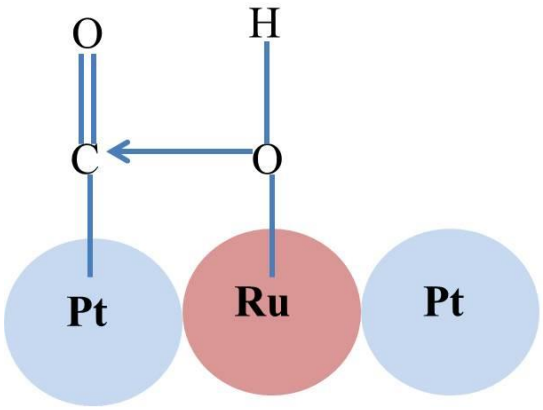

Figure 8. Schematic presentation of bi-functional mechanism in PtRu catalyst.

In order to develop cost effective fuel cell catalysts, non-platinum based materials like Pd, Au, Ag, Ni based electrocatalysts have been reported.[33,109,110] Use of Pd is justified by the fact that Pd is 50 times more abundant than Pt and their activities are comparable.[33] However, the electrocatalytic activity of Pd is limited to alkaline media because of the scarcity of adsorbed hydroxyl groups on Pd surface in acidic media.[38] Other non-platinum based electrocatalysts such as NiCu[111] alloy reported for alcohol oxidation and tungsten monocarbide (WC)[112] for methanol oxidation but electrochemical stability of the later at high anodic polarization is found to be poor.

1.4.1.2. Oxygen Reduction Reaction (ORR)

Crucial to the performance of Polymer Electrolyte Membrane Fuel Cells (PEMFC) is the efficiency of the reaction in which protons (passed through the

electrolyte) from the anode reduce O_2 at the cathode to form H_2O, the oxygen reduction reaction (ORR). Oxygen reduction reaction (ORR) has been of particular interest over past few decades due to its significance in fuel cells and metal-air batteries.[113,114] It is known that ORR kinetics is six fold slower than the kinetics of fuel (methanol, for example) oxidation reaction.[115] ORR in aqueous solutions depends on the nature of catalyst and pH and can proceed in two ways (i) an efficient direct, 4-electron conversion into water or (ii) formation of H_2O_2 as an intermediate via 2-electron process. In non-aqueous aprotic solvents and/or in alkaline solutions, the 1-electron reduction pathway, the intermediate step, is the formation of superoxide (O^{2-}) from O_2. **Table 4** describes different types of reactions involved in ORR depending on pH of the aqueous solution.[116]

Table 4. Thermodynamic potentials of electrochemical O_2 reduction reactions.

Electrolyte	ORR reaction mechanisms	Pathways	Thermodynamic potential (V vs RHE)
Acidic	$O_2 + 4H^+ 4e^- \rightarrow H_2O$	Direct	1.229
	$O_2 + 2H^+ + 2e^- \rightarrow H_2O_2$	Indirect	0.70
	$H_2O_2 + 2H^+ + 2e^- \rightarrow 2H_2O$		1.76
Alkaline	$O_2 + H_2O + 4e^- \rightarrow 4OH^-$	Direct	0.401
	$O_2 + H_2O + 2e^- \rightarrow HO_2^- + OH^-$	Indirect	–0.065
	$HO_2^- + H_2O + 2e^- \rightarrow 3OH^-$		0.867

Norskov et al following Sabatier's analysis plotted the activities of various metal catalysts as a function of oxygen adsorption energy and constructed "volcano curve".[117] The" volcano plot" indicates that Pt, among the metals, has been an efficient catalyst with high activity for ORR and the reduction of oxygen proceeds via four electron pathway (**Figure 9**). Pt thus is considered as the 'state-of-the-art' electrocatalyst for electrochemical reduction of oxygen as well as also the only catalyst shown in long

term operations in acidic and corrosive medium present in proton exchange membrane fuel cells (PEMFC).

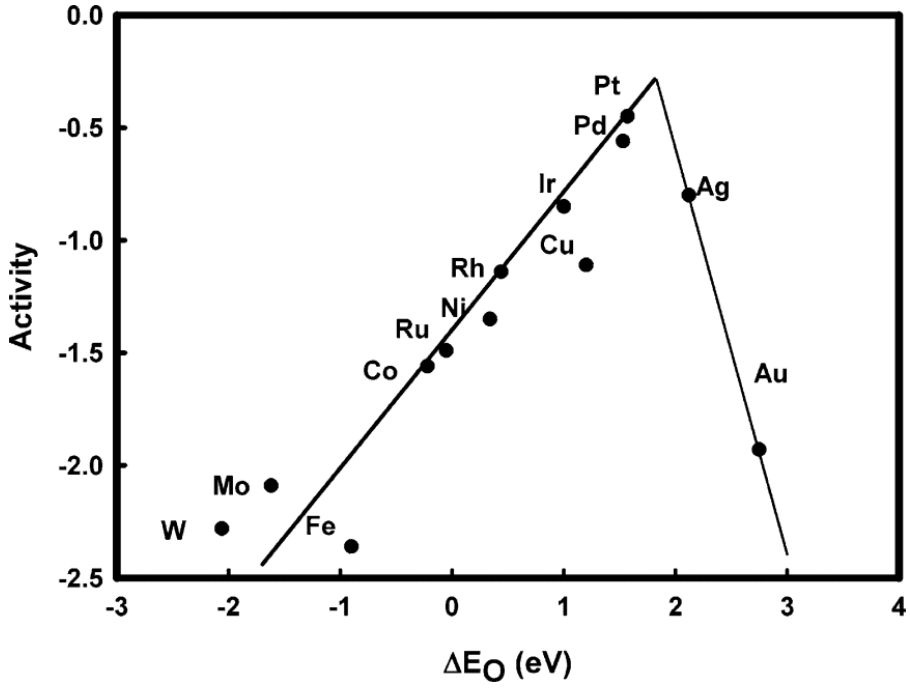

Figure 9. Trends in ORR activity as a function of oxygen binding energy (adapted with permission from ref. 117. © 2004 American Chemical Society).

The involvement of different pathways is a consequence of different adsorption states and catalytic nature of the electrodes.[54] The possibility of different adsorption configurations are schematically presented in **Figure 10**.[116,118]

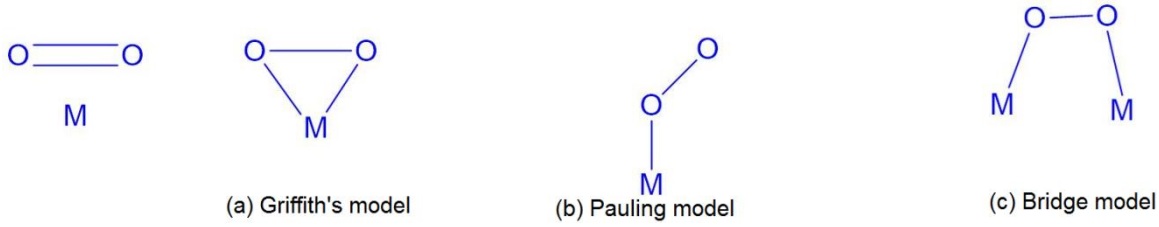

Figure 10. Possible adsorption modes for ORR on catalyst surface.

If oxygen adsorbs on a catalytic site according to Pauling's model (**Figure 11b**), the O-O bond distance remains almost unaltered. Therefore pathway II is favoured with the formation of H_2O_2. If adsorption of oxygen occurs on both sides as shown in **Figures 11a and 11c**, the O-O bond distance is stretched and in turn facilitates rupture of O-O bond. Accordingly, four electron reductions to water are preferred. (Pathway I

or III as given in **Figure 11**).[118,119] Two adjacent adsorption sites are required for molecular oxygen to give water as product with four electron transfer. Apart from this pre-condition, type of catalyst, presence or absence of adsorbing anions and pH of the electrolyte strongly determine the chosen reaction pathway.

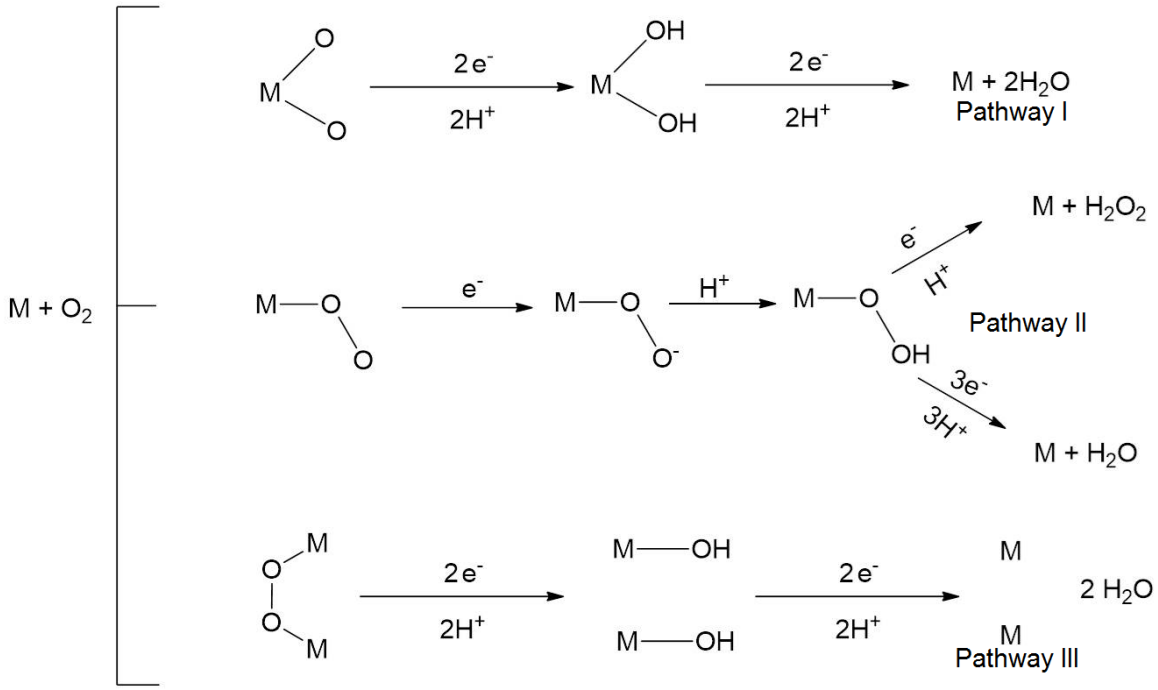

Figure 11. Different reaction pathways for ORR in acidic medium on Pt catalyst.

The sluggish kinetics of ORR can be attributed to the difficulty in the cleavage of O-O bond of oxygen whose bond dissociation energy is 498 kJ $mol^{-1.}$ Platinum, among the pure noble metals, has been identified as an efficient catalyst with low overpotential for ORR and the reaction proceeds via four electron pathway thus serving as 'state-of–the-art' catalyst as mentioned earlier for oxygen/air electrode in PEMFC.[120] It is noteworthy that lattice contraction of Pt achieved by alloying, results in favourable Pt-Pt spacing leading to dissociative adsorption of O_2. Various forms of Pt and Pt alloys have been extensively used in ORR.[121-124] Several Pt-free materials have been investigated to overcome the problem associated with fuel crossover observed in direct alcohol fuel cell.[125-128] These non-Pt based compounds are showing activity comparable to Pt

catalyst. Carbon-based materials have also been the subject of focus for ORR. Among them carbon nanotubes (CNTs), non-metal (N, B, P) doped CNTs, graphene, non-metal (N, B, S, P) doped graphene have been reported as efficient catalysts for ORR.[129-133] Other non-Pt based catalysts include transition metal nitrides such as TiN, Cu_3N and MoN, transition metal carbides like W_2C, TiC, transition metal oxides such as MnO_2, Co_3O_4, Cu_2O and transition metal chalcogenides like Rh_xS_y, Ru_xS_y, Rh_xSe_y, Ru_xSe_y, Co_xS_y (124-129).[134-139]

1.4.2. Synthesis of metal nanoparticles

In recent years, nanoparticles have attracted tremendous research interests because of their application in various fields like magnetism, optics, biology and catalysis.[140-146] FePt, PtCo, PtSn, PtNi, rare earth alloys fall into this category.

1.4.2.1. General approach to the synthesis of nanoparticles

Metal nanoparticles (monometallic, alloy, bimetallic, intermetallic) can be synthesized through either "bottom-up" (from molecular to nanoscale) or "top-down" (from large to small dimension) approaches. Top-down approach involves breaking of bulk materials to nano-sized particles. These processes are associated with mechanical milling or grinding.

A large variety of nanoparticles are synthesized through "bottom-up" approach which is based on chemical methods which involves pyrolysis, solvothermal, sol-gel methods etc. For metal and metal alloys the precursor salts are typically dissolved in either aqueous or organic solvent. Formation of nanoparticles is triggered by the reduction of salts using reducing agent or through the controlled decomposition of organometallic compounds. Reaction time, temperature, concentration of reagents, concentration of stabilizer/surfactants plays a crucial role in controlling the size and shape of the nanoparticles. Stabilizers are generally used to control the growth and aggregation

of the nanoparticles. Most of the growth mechanism has been attributed to the "Oswald ripening" process where large particle continues to increase in size with time.

1.4.2.2. Synthesis of Metal nanoparticles

Various synthetic strategies have been adopted to synthesize metal nanoparticles. Ahmadi and co-workers have reported synthesis of Pt nanoparticles with different morphologies like cubes, tetrahedron by changing the molar ratio of capping agent (sodium polyacrylate) and hexachloroplatinate salt.[147] Herricks *et al* reported synthesis of shape variant Pt nanoparticles by ethylene glycol reduction at 160 °C. By changing the molar ratio of $NaNO_3$ and H_2PtCl_6 they are able to control the shapes from irregular to tetrahedron and octahedron.[148] Xiong et al. have showed shape controlled synthesis of Pd nanoparticle.[149] Yang et al reported solvothermal synthesis approach towards multiple shapes of silver nanoparticle.[150]

1.4.2.3. Synthesis of metal alloys/bimetallic/intermetallic nanoparticles

Recently more attention has been paid to the synthesis of bimetallic or alloy structures because of their potential application in catalysis. But synthesis of alloys, bimetallic and intermetallic is more difficult compared to the pure metal because of the difficulty associated with the atomic diffusion (**Figure 12**).[151-153] Wang et al reported the

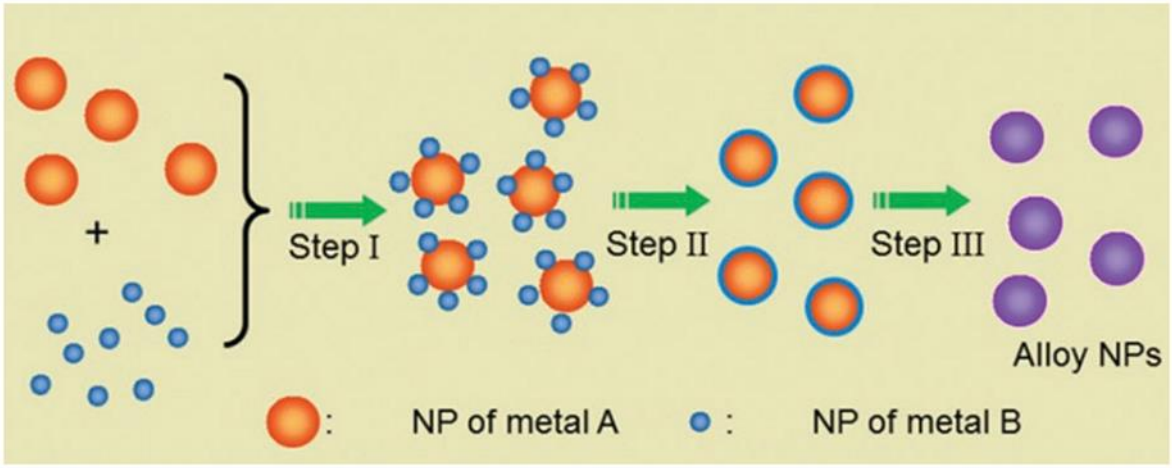

Figure 12. Formation of intermetallic nanoparticle through diffusion (adapted with permission from ref. 153. ©2013 Royal Society of Chemistry).

solvothermal synthesis of AgAu alloy through interfacial diffusion of core-shell structures. Another way to the formation of alloys/intermetallics is the co-reduction of metal precursor salts.[74,154] Schaak group developed low temperature solution based synthetic approaches to the synthesis of alloy and intermetallic nanoparticles.[155] They have reported M-Zn (M=Au, Cu, Pd),[156,157] M-Pt (M=Sn, Pb, Sb, Cu),[158] M-Sn (M=Co, Ni, Cu, Ag, Au, Pt, Ru)[159] and M-Au (M= Fe, Co, Ni)[160] alloy and intermetallic nanoparticles with various morphology from pre synthesized nanoparticles with a second metal precursor in hot organic solvent under reducing condition.

1.5. References

(1) *The future of energy supply: challenges and opportunities*; Armaroli, N.; Balzani, V., **2007**; Vol. 46, pp 52-66.

(2) Lewis, N. S.; Nocera, D. G. *PNAS* **2006**, *103*, 15729-15735.

(3) Jacobson, M. Z. *Energ. Environ. Sci.* **2009**, *2*, 148-173.

(4) Gust, D.; Moore, T. A.; Moore, A. L. *Acc. Chem. Res.* **2009**, *42*, 1890-1898.

(5) Yang, Z.; Zhang, J.; Kintner-Meyer, M. C.; Lu, X.; Choi, D.; Lemmon, J. P.; Liu, J. *Chem. Rev.* **2011**, *111*, 3577-3613.

(6) Katsounaros, I.; Cherevko, S.; Zeradjanin, A. R.; Mayrhofer, K. J.: Oxygen electrochemistry as a cornerstone for sustainable energy conversion. *Angew. Chem. Int. Ed.* **2014**, *53*, 102-121.

(7) Yu, W.; Porosoff, M. D.; Chen, J. G. *Chem. Rev.* **2012**, *112*, 5780-5817.

(8) Debe, M. K. *Nature* **2012**, *486*, 43-51.

(9) Jung, N.; Chung, D. Y.; Ryu, J.; Yoo, S. J.; Sung, Y.E. *Nano Today* **2014**, *9*, 433-456.

(10) Strasser, P.; Koh, S.; Anniyev, T.; Greeley, J.; More, K.; Yu, C. F.; Liu, Z. C.; Kaya, S.; Nordlund, D.; Ogasawara, H.; Toney, M. F.; Nilsson, A. *Nat. Chem.* **2010**, *2*, 454-460.

(11) Chen, M.; Kumar, D.; Yi, C.W.; Goodman, D. W. *Science* **2005**, *310*, 291-293.

(12) Maroun, F.; Ozanam, F.; Magnussen, O.; Behm, R. *Science* **2001**, *293*, 1811-1814.

(13) Ruban, A.; Hammer, B.; Stoltze, P.; Skriver, H. L.; Nørskov, J. K. *J. Mol. Catal. A: Chem.* **1997**, *115*, 421-429.

(14) Stamenkovic, V. R.; Mun, B. S.; Arenz, M.; Mayrhofer, K. J.; Lucas, C. A.; Wang, G.; Ross, P. N.; Markovic, N. M. *Nat. Mater.* **2007**, *6*, 241-247.

(15) Stamenkovic, V. R.; Fowler, B.; Mun, B. S.; Wang, G.; Ross, P. N.; Lucas, C. A.; Marković, N. M. *Science* **2007**, *315*, 493-497.

(16) Zhang, J.; Yang, H.; Fang, J.; Zou, S. *Nano Lett.* **2010**, *10*, 638-644.

(17) Yin, A.-X.; Min, X.Q.; Zhang, Y.W.; Yan, C.H. *J. Am. Chem. Soc.* **2011**, *133*, 3816-3819.

(18) Liu, H.l.; Nosheen, F.; Wang, X. *Chem. Soc. Rev.* **2015**.

(19) Yin, Y.; Alivisatos, A. P. *Nature* **2005**, *437*, 664-670.

(20) Xia, Y.; Xiong, Y.; Lim, B.; Skrabalak, S. E. *Angew. Chem. Int. Ed.* **2009**, *48*, 60-103.

(21) Ostwald, F. W.: *J. Electrochem.* **1894**, *1*, 122.

(22) Kordesch, K. V.; Simader, G. R. *Chem. Rev.* **1995**, *95*, 191-207.

(23) Winter, M.; Brodd, R. J. *Chem. Rev.* **2004**, *104*, 4245-4270.

(24) Jaksic, M. M.; Schmickleer, W.; Botton, G. *Adv. Phys. Chem.* **2012**, *2012*.

(25) Bacon, F. *Electrochim. Acta* **1969**, *14*, 569-585.

(26) Wand, G.: FuelCellToday, fuel cell history, Part 2, **2007**.

(27) Srinivasan, S.; Mosdale, R.; Stevens, P.; Yang, C.: Fuel cells: Reaching the era of clean and efficient power generation in the twenty-first century. *Annu. Rev. Energy Env.***1999**, *24*, 281-328.

(28) Sheng, W.: Electrocatalytic Activities of Supported Pt Nanoparticles for Low-Temperature Fuel Cell Applications. *Dissertation* **2010**.

(29) James, P. J. M., T. J.; Newton, J. M.; Miles, N.J. : *Polymer* **2000**, *41*, 4223.

(30) Wakizoe, M.; Velev, O. A.; Srinivasan, S. *Electrochim. Acta* **1995**, *40*, 335-344.

(31) Kim Y. S.; Wang, F. H. M. M. S. H., Y. T.; Harrison, W.; Zawodzinski, T. A. M., J. E. *J. Poly. Sci. Part B: Poly. Phys.* **2003**, *41*, 2816.

(32) Devanathan, R. *Energ. Environ. Sci.* **2008**, *1*, 101-119.

(33) Bianchini, C.; Shen, P. K. *Chem. Rev.* **2009**, *109*, 4183-4206.

(34) Qi, Z. G.; Kaufman, A. *J. Power Sources* **2002**, *110*, 177-185.

(35) Santasalo, A.; Kallio, T.; Kontturi, K. *Platin. Met. Rev.* **2009**, *53*, 58-66.

(36) Lee, C.-G.; Umeda, M.; Uchida, I. *J. Power Sources* **2006**, *160*, 78-89.

(37) Zeng, Y. Z.; Fujiwara, N.; Yamazaki, S.; Tanimoto, K.; Wu, P. *J. Power Sources* **2008**, *185*, 95-103.

(38) Asazawa, K. Y., K.; Tanaka, H.; Oka, A.; Taniguchi, M., Kobayashi, T: *Angew. Chem. Int. Ed.* **2007**, *46*, 8024.

(39) Lamy, C.; Lima, A.; LeRhun, V.; Delime, F.; Coutanceau, C.; Leger, J. M. *J. Power Sources* **2002**, *105*, 283-296.

(40) Richter, B. S., L. D. *Science* **2004**, *305*, 340.

(41) Uda, T. B., D. A.; Chisholm, C. R. I.; Haile, S. M. , *J. Electrochem. Soc.* **2006**, *9*, A261.

(42) Kumar, J. A. K., P.; Saravanan, R.: *Int. J. Electrochem. Sci.* **2008**, *3*, 961.

(43) Markovic, N. M.; Schmidt, T. J.; Grgur, B. N.; Gasteiger, H. A.; Behm, R. J.; Ross, P. N. *J. Phys. Chem. B* **1999**, *103*, 8568-8577.

(44) Yang, L. X.; Yang, W. Y.; Cai, Q. Y. *J. Phys. Chem. C* **2007**, *111*, 16613-16617.

(45) Tripkovic, A. V.; Popovic, K. D.; Momcilovic, J. D.; Drazic, D. M. *J. Electroanal. Chem.* **1996**, *418*, 9-20.

(46) Yu, E. H.; Scott, K. *J. Power Sources* **2004**, *137*, 248-256.

(47) Hou, H.; Sun, G.; He, R.; Sun, B.; Jin, W.; Liu, H.; Xin, Q. *Int. J. Hydrogen Energy* **2008**, *33*, 7172-7176.

(48) Hou, H.; Sun, G.; He, R.; Wu, Z.; Sun, B. *J. Power Sources* **2008**, *182*, 95-99.

(49) Yu, E. H. S., K.; Reeve, R. W. *J. Appl. Electrochem.* **2006** , *36*, 25.

(50) Lunghi, P. B., R.; Desideri, U.: *J. Power Sources* **2004**, *137*, 239.

(51) Modius, H. H.: *J. Solid-State Electrochem.* **1997**, *1*, 2.

(52) Bockris, J. O. M. R., A. K. N. : 'Modern electrochemistry-Electrodics in Chemistry, Engineering, Biology and environmental science. **2000**.

(53) Kinoshita, K.; McLarnon, F.; Cairns, E. "Fuel cell handbook," Lawrence Berkeley Lab., CA (USA), **1988**.

(54) Hamann, C. H.; Hamnett, A.; Vielstich, W.: Electrochemistry.Wiley-VCH, **1998**.

(55) Ewald, J.: Carbon Dioxide at NOAA's Mauna Loa Observatory reaches new milestone: Tops 400 ppm'. *NOAA Research, 10 May,* **2013**.

(56) O'Hayre, R., Cha, S.W.,Colella,W.,Prinz, F.B. : Fuel Cell Fundamenals. **2006**.

(57) Uhm, S.; Lee, H. J.; Lee, J. *Phys. Chem. Chem. Phys.* **2009**, *11*, 9326-9336.

(58) Wasmus, S.; Küver, A. *J. Electroanal. Chem.* **1999**, *461*, 14-31.

(59) Wang, C.Y. *Chem. Rev.* **2004**, *104*, 4727-4766.

(60) Herrero, E.; Chrzanowski, W.; Wieckowski, A. *J. Phys. Chem.* **1995**, *99*, 10423-10424.

(61) Jarvi, T. D.; Sriramulu, S.; Stuve, E. M. *J. Phys. Chem. B* **1997**, *101*, 3649-3652.

(62) Deivaraj, T. C.; Chen, W. X.; Lee, J. Y. *J. Mater. Chem.* **2003**, *13*, 2555-2560.

(63) Moore, J. T.; Chu, D.; Jiang, R.; Deluga, G. A.; Lukehart, C. *Chem. Mater.* **2003**, *15*, 1119-1124.

(64) Park, K. W.; Choi, J. H.; Kwon, B. K.; Lee, S. A.; Sung, Y. E.; Ha, H. Y.; Hong, S. A.; Kim, H.; Wieckowski, A. *J. Phys. Chem. B* **2002**, *106*, 1869-1877.

(65) Liu, Z. L.; Lee, J. Y.; Han, M.; Chen, W. X.; Gan, L. M. *J. Mater. Chem.* **2002**, *12*, 2453-2458.

(66) Boxall, D. L.; Kenik, E. A.; Lukehart, C. *Chem. Mater.* **2002**, *14*, 1715-1720.

(67) Steigerwalt, E. S.; Deluga, G. A.; Lukehart, C. M. *J. Phys. Chem. B* **2002**, *106*, 760-766.

(68) Lee, S. A.; Park, K. W.; Choi, J. H.; Kwon, B. K.; Sung, Y. E. *J. Electrochem. Soc.* **2002**, *149*, A1299-A1304.

(69) Liao, S.; Holmes, K.A.; Tsaprailis, H.; Birss, V. I. *J. Am. Chem. Soc.* **2006**, *128*, 3504-3505.

(70) Bagotzsky, V. S. V., Y. B.; Khazova. O. A.: *J. Electroanal. Chem.* **1977**, *81*, 229.

(71) Ganesan, R. L. J. S.: *J. Power Sources* **2006**, *157*, 217.

(72) Küver, A.; Potje-Kamloth, K. *Electrochim. Acta* **1998**, *43*, 2527-2535.

(73) Kim, Y. J.; Bae, B.; Scibioh, M. A.; Cho, E.; Ha, H. Y. *J. Power Sources* **2006**, *157*, 253-259.

(74) Antolini, E.; Salgado, J.; Dos Santos, A.; Gonzalez, E. *Electrochem. and Solid-State Lett.* **2005**, *8*, A226-A230.

(75) Service, R. F. *Science* **2002**, *296*, 1222-1224.

(76) Cosmi, C.; Macchiato, M.; Mangiamele, L.; Marmo, G.; Pietrapertosa, F.; Salvia, M.: Environmental and economic effects of renewable energy sources use on a local case study. *Energy Policy* **2003**, *31*, 443-457.

(77) Wachsmann, U.; Tolmasquim, M. T.: Wind power in Brazil—transition using German experience. *Renewable Energy* **2003**, *28*, 1029-1038.

(78) Vigier, F.; Coutanceau, C.; Hahn, F.; Belgsir, E. M.; Lamy, C. *J. Electroanal. Chem.* **2004**, *563*, 81-89.

(79) Caillard, A.; Coutanceau, C.; Brault, P.; Mathias, J.; Léger, J.M. *J. Power Sources* **2006**, *162*, 66-73.

(80) Song, S. Q. Z., W. J.; Liang, Z. X.; Cai, R.; Sun, G. Q.; Xin, Q.; Stergiopoulos, V.; Tsiakaras, P. *Appl. Catal., B* **2005**, *55*, 65.

(81) Cao, L. S., G. Q.; Li, H. Q.; Xin, Q.: *Electrochem. Commun.* **2007**, *9*, 2541.

(82) Park, K.W.; Choi, J.H.; Kwon, B.K.; Lee, S.A.; Sung, Y.E.; Ha, H.Y.; Hong, S.A.; Kim, H.; Wieckowski, A. *J. Phys. Chem. B* **2002**, *106*, 1869-1877.

(83) Russell, A. E.; Rose, A. *Chem. Rev.* **2004**, *104*, 4613-4636.

(84) dos Anjos, D. M.; Hahn, F.; Leger, J. M.; Kokoh, K. B.; Tremiliosi, G. *J. Brazilian Chem. Soc.* **2008**, *19*, 795-802.

(85) Kowal, A.; Li, M.; Shao, M.; Sasaki, K.; Vukmirovic, M.; Zhang, J.; Marinkovic, N.; Liu, P.; Frenkel, A.; Adzic, R. *Nat. Mater.* **2009**, *8*, 325-330.

(86) Neto, A. O.; Linardi, M.; dos Anjos, D. M.; Tremiliosi, G.; Spinace, E. V. *J. Appl. Electrochem.* **2009**, *39*, 1153-1156.

(87) Shin, J.; Tornquist, W. J.; Korzeniewski, C.; Hoaglund, C. S. *Surf. Sci.* **1996**, *364*, 122-130.

(88) Rice, C.; Ha, S.; Masel, R.; Waszczuk, P.; Wieckowski, A.; Barnard, T. *J. Power Sources* **2002**, *111*, 83-89.

(89) Chen, Y. X. H., M.; Jusys, Z.; Behm, R. J: *Angew. Chem. Int. Ed.* **2006**, *45*, 981.

(90) Divisek, J.; Oetjen, H.-F.; Peinecke, V.; Schmidt, V.; Stimming, U. *Electrochim. Acta* **1998**, *43*, 3811-3815.

(91) Bellows, R. J.; Marucchi-Soos, E. P.; Buckley, D. T. *Ind. Eng. Chem. Res.* **1996**, *35*, 1235-1242.

(92) Watkins, D. S.: Research, development and demonstration of solid polymer fuel cell systems. In Fuel Cell Systems, Blomen L, Mugerwa M (ed.), **1993**.

(93) Schultz, T.; Zhou, S.; Sundmacher, K.: Current status of and recent developments in the direct methanol fuel cell. *Chem. Eng. Tech.* **2001**, *24*, 1223-1233.

(94) Gasteiger, H. A.; Markovic, N.; Ross Jr, P. N.; Cairns, E. J. *J. Phys. Chem.* **1993**, *97*, 12020-12029.

(95) Kauranen, P.; Skou, E.; Munk, J. *J. Electroanal. Chem.* **1996**, *404*, 1-13.

(96) Krewer, U.; Christov, M.; Vidakovic, T.; Sundmacher, K. *J. Electroanal. Chem.* **2006**, *589*, 148-159.

(97) Shivhare, M.; Jackson, C.; Scott, K.; Martin, E. *J. Power Sources* **2007**, *173*, 240-248.

(98) Luo, J.; Njoki, P. N.; Lin, Y.; Mott, D.; Wang, L.; Zhong, C.J. *Langmuir* **2006**, *22*, 2892-2898.

(99) Holstein, W. L.; Rosenfeld, H. D. *J. Phys. Chem. B* **2005**, *109*, 2176-2186.

(100) Lin, Y. H.; Cui, X. L.; Yen, C. H.; Wai, C. M. *Langmuir* **2005**, *21*, 11474-11479.

(101) Casado-Rivera, E.; Volpe, D. J.; Alden, L.; Lind, C.; Downie, C.; Vazquez-Alvarez, T.; Angelo, A. C. D.; DiSalvo, F. J.; Abruna, H. D. *J. Am. Chem. Soc.* **2004**, *126*, 4043-4049.

(102) Park, K.-W.; Choi, J.-H.; Sung, Y.E. *J. Phys. Chem. B* **2003**, *107*, 5851-5856.

(103) Wang, H.; Alden, L. R.; DiSalvo, F.; Abruna, H. D. *Langmuir* **2009**, *25*, 7725-7735.

(104) Huang, J. J.; Yang, H.; Huang, Q. H.; Tang, Y. W.; Lu, T. H.; Akins, D. L. *J. Electrochem. Soc.* **2004**, *151*, A1810-A1815.

(105) Umeda, M.; Ojima, H.; Mohamedi, M.; Uchida, I. *J. Power Sources* **2004**, *136*, 10-15.

(106) Liu, H. C.; Gaigneaux, E. M.; Imoto, H.; Shido, T.; Iwasawa, Y. *J. Phys. Chem. B* **2000**, *104*, 2033-2043.

(107) Giorgi, L. P., A.; Bracchini, C.; Giorgi, R.; Turtuá, S. : *J. Appl. Electrochem.* **2001**, *31*, 325.

(108) Toda, T.; Igarashi, H.; Uchida, H.; Watanabe, M. *J. Electrochem. Soc.* **1999**, *146*, 3750-3756.

(109) Xu, C.; Cheng, L.; Shen, P.; Liu, Y. *Electrochem. Commun.* **2007**, *9*, 997-1001.

(110) Zhang, K. F. G., D. J.; Liu, X.; Li, J.; Li, H. L.; Su, Z. X. : *J. Power Sources* **2006**, *162*, 1077.

(111) Tian, X. K.; Zhao, X. Y.; Zhang, L. D.; Yang, C.; Pi, Z. B.; Zhang, S. X. *Nanotechnology* **2008**, *19*.

(112) Weigert, E. C.; Stottlemyer, A. L.; Zellner, M. B.; Chen, J. G. G. *J. Phys. Chem. C* **2007**, *111*, 14617-14620.

(113) Wang, S. Y.; Jiang, S. P.; White, T. J.; Guo, J.; Wang, X. *J. Phys. Chem. C* **2009**, *113*, 18935-18945.

(114) Lee, J. S.; Kim, S. T.; Cao, R.; Choi, N. S.; Liu, M.; Lee, K. T.; Cho, J. *Adv. Energy Mater.* **2011**, *1*, 34-50.

(115) Ma, G. X.; Jia, R. R.; Zhao, J. H.; Wang, Z. J.; Song, C.; Jia, S. P.; Zhu, Z. P. *J. Phys. Chem. C* **2011**, *115*, 25148-25154.

(116) Kleiner, K. *Nature* **2006**, *441*, 1046.

(117) Norskov, J. K.; Rossmeisl, J.; Logadottir, A.; Lindqvist, L.; Kitchin, J. R.; Bligaard, T.; Jonsson, H. *J. Phys. Chem. B* **2004**, *108*, 17886-17892.

(118) Tarasevich, M. R. S., A.; Yeager, E.; Bockris, J. O.; Conway, E. E.; Yeager, E.; Khan, S. U. M.; White, R. E.: Oxygen Electrochemistry', in'Comprehensive Treatise of Electrochemistry. **1983**.

(119) Yeager, E.: *J. Mol. Catal.* **1986**, *38*, 5-25.

(120) Gottesfeld, S.; Zawodzinski, T. A.: Polymer electrolyte fuel cells. *Adv. Electrochem. Sci. Eng.* **1997**, *5*, 195-302.

(121) Wang, C.; Chi, M.; Li, D.; van der Vliet, D.; Wang, G.; Lin, Q.; F. Mitchell, J.; More, K. L.; Markovic, N. M.; Stamenkovic, V. R. *ACS Catal.* **2011**, *1*, 1355-1359.

(122) Chen, C.; Kang, Y.; Huo, Z.; Zhu, Z.; Huang, W.; Xin, H. L.; Snyder, J. D.; Li, D.; Herron, J. A.; Mavrikakis, M. *Science* **2014**, *343*, 1339-1343.

(123) Xia, D.; Chen, G.; Wang, Z.; Zhang, J.; Hui, S.; Ghosh, D.; Wang, H. *Chem. Mater.* **2006**, *18*, 5746-5749.

(124) Liang, Y.; Li, Y.; Wang, H.; Zhou, J.; Wang, J.; Regier, T.; Dai, H. *Nat. Mater.* **2011**, *10*, 780-786.

(125) Zhang, L.; Hou, F.; Tan, Y. *Chem. Comunm.* **2012**, *48*, 7152-7154.

(126) Yang, R. Z.; Bian, W. Y.; Strasser, P.; Toney, M. F. *J. Power Sources* **2013**, *222*, 169-176.

(127) Holewinski, A.; Idrobo, J.-C.; Linic, S. *Nat. Chem.* **2014**, *6*, 828-834.

(128) Zhang, N.; Chen, X.; Lu, Y.; An, L.; Li, X.; Xia, D.; Zhang, Z.; Li, J. *Small* **2014**, *10*, 2662-2669.

(129) Yang, L. J., S.; Zhao, Y.; Zhu, L.; Chen, S.; Wang, X.; Wu, Q.; Ma, J.; Ma, Y.; Hu, Z.: *Angew. Chem. Int. Ed.* **2011**, *50*, 7132.

(130) Wang, S.; Yu, D.; Dai, L.; Chang, D. W.; Baek, J.B. *ACS Nano* **2011**, *5*, 6202-6209.

(131) Yang, Z.; Yao, Z.; Li, G.; Fang, G.; Nie, H.; Liu, Z.; Zhou, X.; Chen, X. a.; Huang, S. *ACS Nano* **2011**, *6*, 205-211.

(132) Wang, S. I., E.; Roy, A.; Xue, Y.; Yu, D.; Dai, L.: *Angew. Chem. Int.Ed.* **2011**, *123*, 11960.

(133) Wang, S. Y.; Yu, D. S.; Dai, L. M. *J. Am. Chem. Soc.* **2011**, *133*, 5182-5185.

(134) Chen, J.; Takanabe, K.; Ohnishi, R.; Lu, D.; Okada, S.; Hatasawa, H.; Morioka, H.; Antonietti, M.; Kubota, J.; Domen, K. *Chem. Commun.* **2010**, *46*, 7492-7494.

(135) Ziegelbauer, J. M.; Gatewood, D.; Gulla, A. F.; Guinel, M. J. F.; Ernst, F.; Ramaker, D. E.; Mukerjee, S. *J. Phys. Chem. C* **2009**, *113*, 6955-6968.

(136) Xu, J.; Gao, P.; Zhao, T. *Energ. Environ. Sci.* **2012**, *5*, 5333-5339.

(137) Cheng, F.; Shen, J.; Peng, B.; Pan, Y.; Tao, Z.; Chen, J. *Nat. Chem.* **2011**, *3*, 79-84.

(138) Feng, Y.; He, T.; Alonso-Vante, N. *Fuel Cells* **2010**, *10*, 77-83.

(139) Cao, D. X.; Wieckowski, A.; Inukai, J.; Alonso-Vante, N. *J. Electrochem. Soc.* **2006**, *153*, A869-A874.

(140) Caruso, F.: Nanoengineering of particle surfaces. *Adv. Mater.* **2001**, *13*, 11.

(141) Hyeon, T.: Chemical synthesis of magnetic nanoparticles. *Chem. Commun.* **2003**, 927-934.

(142) Ross, C.: Annu. Rev. Mater. Res. **2001**, *31*, 203-235.

(143) Sellimyer, D.; Luo, C.; Yan, M.; Liu, Y.: High-anisotropy nanocomposite films for magnetic recording. *Magnetics, IEEE Transactions on* **2001**, *37*, 1286-1291.

(144) Sun, S. H.; Murray, C. B.; Weller, D.; Folks, L.; Moser, A. *Science* **2000**, *287*, 1989-1992.

(145) Weller, D.; Moser, A.; Folks, L.; Best, M. E.; Lee, W.; Toney, M. F.; Schwickert, M.; Thiele, J.U.; Doerner, M. F.: High K u materials approach to 100 Gbits/in 2. *Magnetics, IEEE Transactions on* **2000**, *36*, 10-15.

(146) Laurent, S.; Forge, D.; Port, M.; Roch, A.; Robic, C.; Elst, L. V.; Muller, R. N.: Magnetic iron oxide nanoparticles *Chem. Rev.* **2008**, *108*, 2064-2110.

(147) Ahmadi, T. S.; Wang, Z. L.; Green, T. C.; Henglein, A.; ElSayed, M. A. *Science* **1996**, *272*, 1924-1926.

(148) Herricks, T.; Chen, J. Y.; Xia, Y. N. *Nano Lett.* **2004**, *4*, 2367-2371.

(149) Xiong, Y.; Xia, Y. *Adv. Mater.* **2007**, *19*, 3385-3391.

(150) Yang, Y.; Matsubara, S.; Xiong, L.; Hayakawa, T.; Nogami, M. *J. Phys. Chem. C* **2007**, *111*, 9095-9104.

(151) Radziuk, D. V.; Zhang, W.; Shchukin, D.; Möhwald, H. *Small* **2010**, *6*, 545-553.

(152) Lee, D. K.; Hwang, N. M. *Scr. Mater.* **2009**, *61*, 304-307.

(153) You, H.; Yang, S.; Ding, B.; Yang, H. *Chem. Soc. Rev.* **2013**, *42*, 2880-2904.

(154) Alden, L. R.; Roychowdhury, C.; Matsumoto, F.; Han, D. K.; Zeldovich, V. B.; Abruña, H. D.; DiSalvo, F. J. *Langmuir* **2006**, *22*, 10465-10471.

(155) Leonard, B. M.; Anderson, M. E.; Oyler, K. D.; Phan, T. H.; Schaak, R. E. *ACS Nano* **2009**, *3*, 940-948.

(156) Cable, R. E.; Schaak, R. E. *Chem. Mater.* **2007**, *19*, 4098-4104.

(157) Schaefer, Z. L.; Vaughn, D. D.; Schaak, R. E. *J. Alloys Compd.* **2010**, *490*, 98-102.

(158) Bauer, J. C.; Chen, X.; Liu, Q.; Phan, T.-H.; Schaak, R. E. *J. Mater. Chem.* **2008**, *18*, 275-282.

(159) Chou, N. H.; Schaak, R. E. *Chem. Mater.* **2008**, *20*, 2081-2085.

(160) Vasquez, Y.; Luo, Z.; Schaak, R. E. *J. Am. Chem. Soc.* **2008**, *130*, 11866-11867.

Chapter 2

Facile and Ultrafast Synthesis of Pd_3Pb Nanocrystals towards Enhanced Activity and Durability in Direct Ethanol and Formic acid Fuel Cells

Abstract

This work discusses about the controlled synthesis of the compound Pd_3Pb as nanocrystals in different morphologies having superior electrocatalytic activity. Two synthetic strategies, polyol and hydrothermal, were employed along with tuning other reaction conditions to produce the nanocrystals from the metal precursors. Powder X-ray diffraction and transmission electron microscopy data suggest that the compound was formed in the ordered Cu_3Au cubic structure type with Pd and Pb atoms occupying different crystallographic positions. The catalytic activity and durability of the materials were tested for the electro oxidation of formic acid and ethanol, which is found to be far superior than the commercial Pd on carbon (Pd/C). The morphological variation of nanocrystals has shown a profound electrocatalytic effect on the oxidation of formic acid and ethanol. Among all the catalysts, the flower-like Pd_3Pb catalyst that formed within 10 seconds by polyol method, had enhanced specific and mass activity and superior stability in cyclic voltammetric (CV) and chronoamperometric (CA) measurements. The current density and mass activity of our catalyst are 2.5 times and 2.4 times higher than that of commercial Pd/C for the formic acid oxidation and 1.5 times each higher for ethanol oxidation. Commercial Pd/C catalyst is found to be less stable compared to all the Pd_3Pb catalysts as observed in CA study.

2.1. Introduction

Due to the dominance of the indirect reaction pathway and strong poisoning effect, the studies on the formic acid (HCOOH) based fuel cell are very much limited.[1,2] In general, Pt metal [3] and Pt based alloys and intermetallics (PtPb,[4] Pt_3Pb,[5] PtSn,[6] PtBi,[7] PtCo,[8] PtZn,[9] AuPt,[10] PtM [M = Ni, Cu, Mn, Cr, V, Co],[11-13] PtRuFe[14] and FePtAu[15]) are mostly considered as efficient anode materials in the fuel cell. Recently, Pd nanoparticles (NPs) were found to be more active than the commonly used Pt catalysts in catalyzing formic acid oxidation (FAO) in polymer electrolyte membrane fuel cell.[16,17] Alloys,[18,19] bimetallics[20] and intermetallics[21] based on Pd and monometal[22] have drawn more attention for formic acid oxidation compared to Pt due to their ability to oxidize HCOOH to carbon dioxide (CO_2) in direct pathway. This in fact, automatically reduces the poisoning effect by avoiding the formation of carbon monoxide (CO), which is one of the common problems for Pt-based catalysts.[18] The limiting step for activity enhancement of FAO is believed to be the enhancement in the adsorption/dissociation of HCOOH on Pd surface.[23] The desired enhancement of adsorption/dissociation properties can be achieved through alloying Pd with oxophilic metals (M) like Co and Cu through so called ligand effect, which basically needs manipulating Pd-M bonding.[18]

Alloyed and oxide supported Pd-M (M = Ru, Au, Ni, Ag, Sn, Ir and Ti) binary electrocatalysts have been extensively reported in the literature.[24-30] The catalytic activities of the NPs are found to be highly dependent on its sizes and shapes.[31-33] By varying the morphology, the catalytic activity of these materials can be tuned.[34-36] On the other hand, many studies have revealed that Pb has promoting effect on the electrode oxidation of SOMs.[37-39] For example, Li et al found that after the addition of Pb, the catalytic activity of carbon supported Pt and Pt/Ru catalysts towards ethanol oxidation has increased remarkably.[37] Liu et al reported PtPb/C with enhanced electrocatalytic activity

towards both formic acid and methanol compared to the commercially available Pt/C and PtRu/C catalysts.[39] In other report, Wang et al found that PdPb/C bimetallic catalyst is more active than Pd/C for the electrooxidation of ethanol in alkaline medium.[40]

Inspired by the good catalytic activity of Pd and promoting effect of Pb on the electrooxidation of alcohols and other organic fuels, we have synthesized ordered intermetallic Pd_3Pb nanomaterial using different methods (solvothermal and polyol). The compound Pd_3Pb crystallizes in the Cu_3Au type crystal structure with two independent crystallographic positions of Pd and Pb.[41] Instead of disordered alloys and bimetallics (such as Pt-Ru, Pt-Pb), the use of intermetallic nanoparticles (such as PtPb and PtBi) is advantageous due to their excellent electrocatalytic properties in terms of current density, CO tolerance and sulfur impurities.[42,43] The advantage of ordered structure comes from its uniform surroundings of active sites. The number and distance between active sites play an important role in the catalytic activity. Interestingly, Pd_3Pb has formed within 10 seconds by polyol method, which is assumed to be an ultrafast diffusion of constituent elements leading to the formation of an ordered intermetallic compound. We have studied the electrochemical oxidation of HCOOH in acidic medium and EOR in alkaline medium using the Pd_3Pb catalysts synthesized at different conditions. The increase in catalytic activity for the compound formed by polyol method in ultrafast condition clearly indicates that the morphology of the nanoparticles plays crucial role in the electrocatalysis. The catalytic activity of all the samples reported here is far superior to the commercial Pd on carbon (Pd/C).

2.2. Experimental Section

2.2.1. Chemicals

Potassium tetrachloropalladate (K_2PdCl_4), palladium acetylacetonate ($Pd(acac)_2$), sodium borohydride ($NaBH_4$) and nafion binder (5 wt%) were purchased from Sigma-Aldrich, lead acetate trihydrate ($Pb(OAc)_2.3H_2O$) and polyvinyl pyrrollidone (PVP) were purchased from SDFCL and tetra ethylene glycol (TEG) was purchased from Alfa Aesar. All the chemicals (more than 99% purity) were used as purchased without further purification. Millipore water of conductivity 18.2 MΩcm was used for the synthesis and all other studies.

2.2.2. Synthesis

2.2.2.1. Polyol Method

The compound Pd_3Pb was obtained in different morphologies by polyol method without using any surfactant. In a typical synthesis procedure, 0.3 mmol (91.4 mg) of $Pd(acac)_2$ and 0.1 mmol (0.0379 g) $Pb(OAc)_2.3H_2O$ with 18 ml TEG were taken in a two neck round bottom (RB) flask. The solution mixture was made homogeneous using magnetic stirrer under Ar atmosphere at 60 °C for 10 minutes. Then the temperature was raised to 180 °C followed by quick injection of $NaBH_4$ solution (0.045 g in 2 ml TEG) through rubber septa and quenching the reaction in ice bath after stirring for different reaction time. Pure phases of Pd_3Pb intermetallic nanocompounds was obtained for different reaction times 10 sec (Pd_3Pb_P10s), 1 min (Pd_3Pb_P1m), 2 min (Pd_3Pb_P2m), 5min (Pd_3Pb_P5m) and 15 min (Pd_3Pb_P15m).

2.2.2.2. Hydrothermal Method

In a typical hydrothermal method, 0.3 mmol (0.0978 g) K_2PdCl_4 and 0.1 mmol (0.0379 g) $Pb(OAc)_2.3H_2O$ were mixed in 18 ml water and taken in a 23 ml teflon lined

autoclave. The autoclave was shaken in an orbital shaker for 30 minutes to obtain a homogenous solution. More than one equivalent of $NaBH_4$ (0.045 g) was added to the solution and the autoclave was kept at 240 °C with different reactions times 24, 48 and 72 hrs. The syntheses were performed both in absence and presence of the surfactant. After the reaction, the autoclave was cooled down to room temperature naturally. The precipitate obtained was washed six times with ethanol and three times with water. The obtained product was dried in vacuum oven for 12 hrs at 60 °C. All the characterisations were carried out on dried powder sample. Pure phase of Pd_3Pb intermetallic nanoparticle was obtained for different reactions times: 24 hrs (Pd_3Pb_HP24), 48 hrs (Pd_3Pb_HP48) and 72 hrs (Pd_3Pb_HP72) in the presence of PVP and 72 hrs (Pd_3Pb_HN72) in the absence of surfactant.

2.2.3. Powder X-ray Diffraction (PXRD)

PXRD measurements were done at room temperature on a Rigaku Miniflex X-ray diffractometer with Cu-K_α X-ray source (λ = 1.5406 Å), equipped with a position sensitive detector in the angular range $20^o \leq 2\theta \leq 80^o$ with the step size 0.02^o and scan rate of 0.5 s/step calibrated against corundum standards. The experimental patterns were compared to the pattern simulated from the data reported in the literature.[41]

2.2.4. Elemental Analysis

Quantitative microanalysis on all the samples were performed with a FEI NOVA NANOSEM 600 instrument equipped with an EDAX® instrument. Data were acquired with an accelerating voltage of 20 kV and a 100 s accumulation time. The EDAX analysis was performed using P/B-ZAF standardless method (where, Z = atomic no. correction factor, A = absorption correction factor, F = fluorescence factor, P/B = peak to background model) on selected spots and points.

2.2.5. Transmission electron microscopy (TEM)

TEM and high resolution TEM (HRTEM) images, selected area electron diffraction (SAED) patterns were collected using a JEOL 200 TEM instrument. Samples for these measurements were prepared by dropping a small volume of sonicated nanocrystalline powders in ethanol onto a carbon-coated copper grid.

2.2.6. Electrochemical Studies

All the electrochemical measurements were performed on a CHI 608E electrochemical workstation with three electrode channels at room temperature. Three electrode set-up consists of a glassy carbon (GC) (having diameter 3 mm) as working electrode, platinum wire as counter electrode and Hg/HgO (MMO) (alkaline medium) and Ag/AgCl (acidic medium) as reference electrodes. All the solutions were purged with nitrogen gas for 25 minutes prior to the measurement. The catalyst ink was prepared by dispersing 2 mg of catalyst in 1 mL of mixed solvent solution (IPA: H_2O=1:1 v/v) and 10 μL of 1 wt% nafion binder. The nafion binder (5 wt%) was diluted to 1 wt% with isopropyl alcohol (IPA). From the prepared catalyst ink 10 μL was dropcasted on GC electrode and dried overnight in air. Before depositing the catalyst, the GC electrode was polished with 0.05 μm alumina slurry, washed several times with distilled water. Commercial Pd/C (10 wt%, Sigma Aldrich) was used for comparison of activity with the Pd_3Pb catalysts. Cyclic voltammetry (CV) measurement was carried out with 0.5M $HClO_4$, 0.5M KOH aqueous solution as well as 0.5M $HClO_4$/1M HCOOH, 0.5M KOH/1M EtOH electrolyte solution at a scan rate 50 mV/sec. Chronoamperometry (CA) was performed in 0.5M $HClO_4$/1M HCOOH, 0.5M KOH/1M EtOH electrolyte solution.

2.3. Results and Discussions

2.3.1. Structure, Synthesis, Shape and Morphology

Palladium is considered as the more promising catalyst for the oxidation of ethanol and formic acid due to its abundance, decent catalytic activity and low cost compared to Pt. The other way of reducing the cost and increase the catalytic activity is alloying Pd with low cost metals. The compound Pd_3Pb is such an example, which has a primitive cubic crystal structure crystallizing in the Cu_3Au structure type with $Pm\bar{3}m$ space group. A typical representation of unit cell of the Pd_3Pb crystal structure in comparison with Pd structure is shown in **Figure 1**. Pure palladium metal has a face centered cubic crystal structure ($Fm\bar{3}m$) where all the corners and faces are occupied by the Pd atoms (Wyckoff no. 4*a*). While, in Pd_3Pb the Pb atoms occupy the corner positions (Wyckoff no. 1*a*) and the Pd atoms occupy half of the octahedral holes (Wyckoff no. 3*c*). Such an ordered arrangement of Pd atoms within the lattice of Pb is expected to increase the catalytic activity.

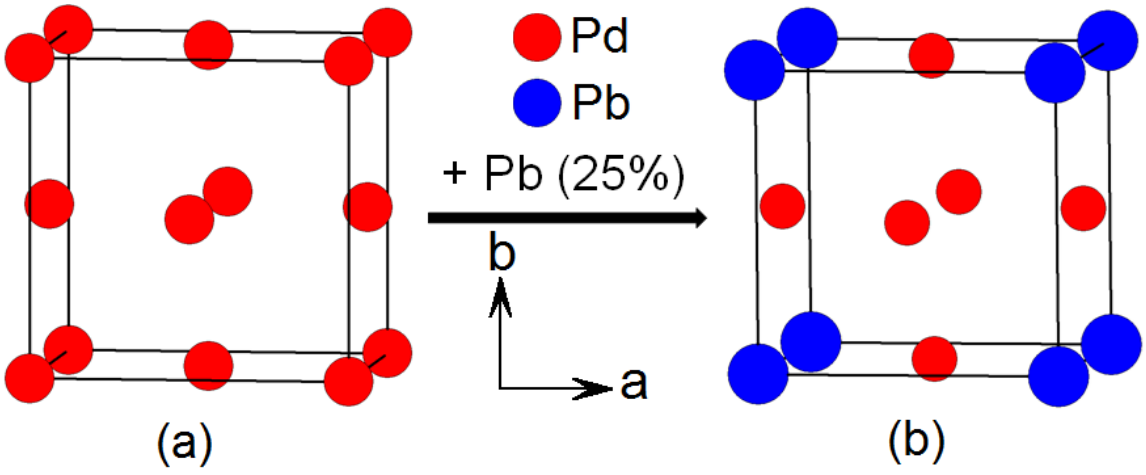

Figure 1. The crystal structure comparison of Pd (a) and Pd_3Pb (b) along the *c*-direction.

We were successful in synthesizing pure phase of intermetallic Pd_3Pb nanocrystals by different methods (hydrothermal, polyol) in different morphologies. The details of the various synthesis parameters are listed in **Table 1**. The crystallite sizes of all the hydrothermally synthesized nanoparticles calculated from the Scherer formula are also listed in **Table 1**. As the particles are of interconnected network type, there is slight deviation of the crystallite size calculated from the Scherer formula in comparison with the TEM measurements. Comparison of PXRD for the samples Pd_3Pb_P10s, Pd_3Pb_P1m, Pd_3Pb_P2m, Pd_3Pb_P5m, Pd_3Pb_P15m, Pd_3Pb_HP24, Pd_3Pb_HP48, Pd_3Pb_HP72 and Pd_3Pb_HN72 with simulated pattern of the reported data[41] clearly indicates that compound has been formed in pure ordered intermetallic phases without any impurity (**Figures 2 and 3**). The PXRD pattern of the selected catalysts (Pd_3Pb_P10s, Pd_3Pb_HP24 and Pd_3Pb_HN72) is compared with the simulated pattern (**Figure 2**).

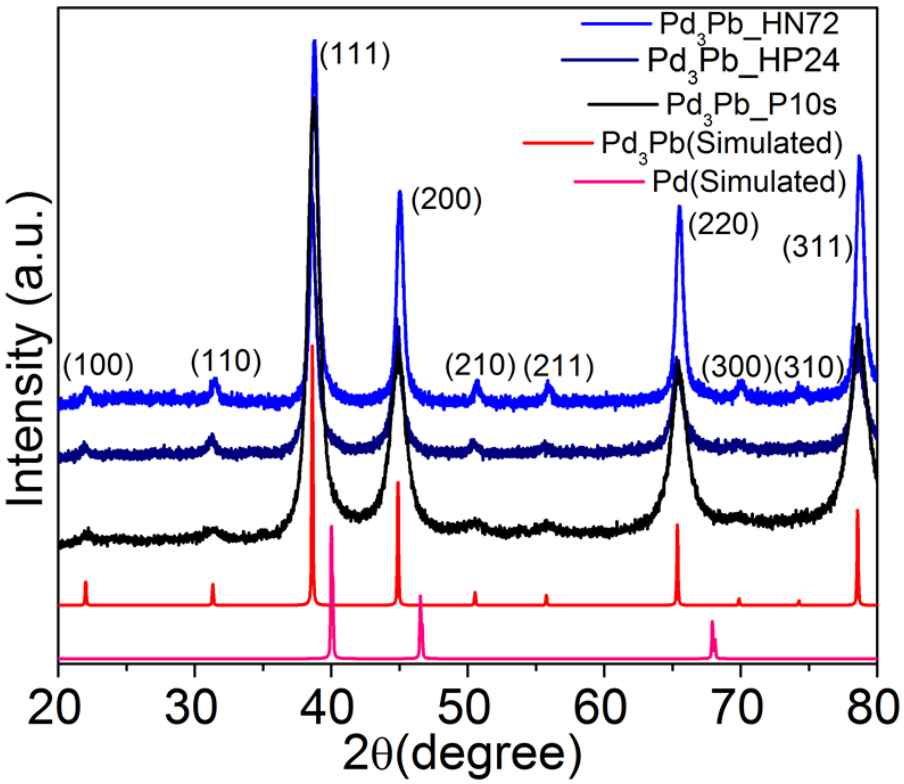

Figure 2. Comparison of PXRD patterns of the selected Pd_3Pb intermetallic nanoparticle synthesized by polyol and solvothermal methods with the simulated powder patterns of Pd_3Pb.

Table 1. Summary of the synthesis protocols on the formation of pure phase Pd_3Pb intermetallic nanocrystals.

Compounds	Methods	Conditions				Crystallite size from Scherer formula (nm)
		Precursors	Solvent	Surfactant	Time	
Pd_3Pb_P10s	Polyol	$Pd(acac)_2$ and $Pb(OAc)_2.3H_2O$	TEG	None	10 sec	9
Pd_3Pb_P1m					1 min	12.8
Pd_3Pb_P2m					2 min	15.4
Pd_3Pb_P5m					5 min	16.3
Pd_3Pb_P15m					15min	15.6
Pd_3Pb_HP24	Hydro-thermal	K_2PdCl_4 and $Pb(OAc)_2.3H_2O$	Water	PVP	24 hr	13
Pd_3Pb_HP48					48 hr	13.6
Pd_3Pb_HP72					72 hr	19.2
Pd_3Pb_HN72				None	72 hr	15

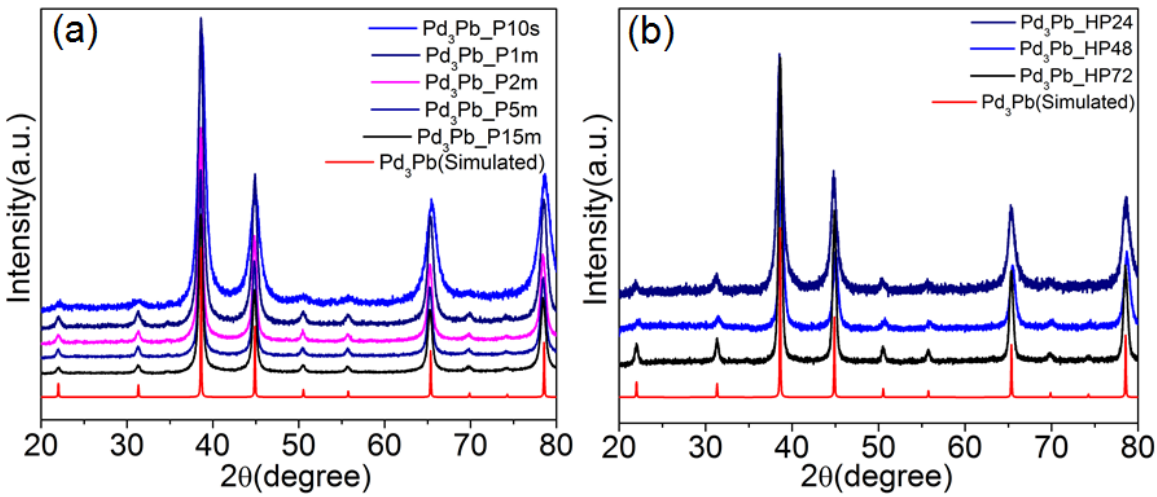

Figure 3. PXRD pattern of Pd_3Pb nanoparticle (a) synthesized at 180 °C by polyol method in different time interval (10 seconds – 15 minutes), (b) 240 °C by hydrothermal method in different time interval (24, 48, 72 hrs) using PVP as surfactant. The patterns are compared with the simulated pattern of Pd_3Pb reported in the literature.

In general, intermetallic compounds are synthesized at high temperature by ceramic, arc melting and high frequency induction heating methods. The high temperature syntheses are required in the formation of the ordered compounds, as it demands high kinetic energy for the better diffusion of the reactants. With an increase in reaction temperature, the thermal vibration of the atoms increases, as a result, the diffusion of the metals will enhance and tend to be occupied in the ordered positions. On

the other hand, in solution methods, it is well known fact that the formation of alloy or intermetallic nanoparticles requires co-reduction of metal salts.[44,45] Though there is large difference in redox potentials for $Pd^{2+/}Pd$ (0.83 V vs NHE) and $Pb^{2+/}Pb$ (-0.13V vs NHE), use of strong reducing agent like $NaBH_4$ favours the co-reduction, which is the key step in the formation of ordered intermetallic compound. However, interestingly, polyol method adopted in this work leads to the formation of the ordered compound within just 10 seconds. To the best of our knowledge, the synthesis of ordered intermetallic nanomaterial within such short period is not reported so far. Although the exact reason for this extremely fast phase formation is not known, fast kinetics of the insertion of Pb atoms into Pd lattice may be the probable reason for this ultrafast diffusion and alloying.

Our attempts to synthesize Pd_3Pb nanoparticles by solvothermal method adopting the conditions from the polyol method were not successful probably because of inhomogeneity of the precursor salt solution before the addition of $NaBH_4$. This was due to the poor solubility of the precursor salts at room temperature. However, using water soluble salts, we were able to synthesize the pure phase (hydrothermally) indicating the requirement of homogeneous solution for the co-reduction and the formation of the ordered intermetallic phase. In hydrothermal method, in the absence of surfactant even after 48 hrs we did not get pure phase .The formation of the pure phase required 72 hrs of reaction time. In the presence of surfactant (PVP), pure phase was formed within 24 hrs of reaction, which could be due to the mild reducing ability of PVP.[46] However, we were unsuccessful in synthesizing the pure intermetallic phase within shorter period (12 hrs) even in the presence of PVP. Our attempts to synthesize the ordered intermetallic phase below 240 °C in the presence of PVP were also not successful. All these controlled experimental conditions suggest that the optimum conditions required for the formation

of pure phase by hydrothermal method are the presence of PVP, temperature as high as 240 °C and 24 hrs of reaction time.

In contrast and as mentioned before, the pure ordered compound was formed within 10 seconds after the addition of $NaBH_4$ in polyol method. TEM image of the sample obtained by ultra-fast synthesis (Pd_3Pb-P10s) in **Figure 4a** shows flower-like morphology. A close look at the magnified TEM image (**Figure 4b**) reveals that the flower-like nanocrystals are constructed by many of the elongated irregular shaped primary nanoparticles. **Figure 4c** represents the SAED pattern containing (111), (200), (300) and (222) crystallographic planes, which further confirms the formation of ordered intermetallic Pd_3Pb nanoparticle. The d-spacing (inter-planar spacing of the lattice fringes),calculated from HRTEM images of the sample Pd_3Pb_P10s (**Figure 4d**) is 0.232 nm corresponding to the (111) plane of Pd_3Pb, which is another proof of ordering of the atomic positions.

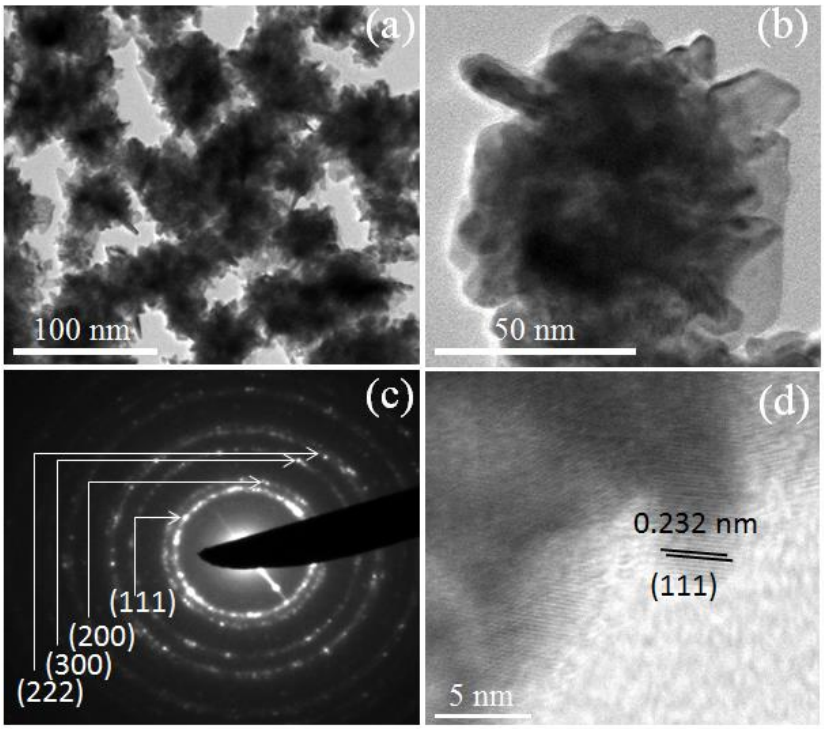

Figure 4. TEM image (a), magnified TEM image (b), SAED pattern (c) and HRTEM image (d) of Pd_3Pb flower-like nanocrystals.

As the reaction time was increased (1-15 minutes), the particles were agglomerated slowly (**Figure 5**), which made it difficult to propose the actual morphology of the particles. Among all the nanocrystals synthesized by the polyol method or hydrothermal method, the flower-like shaped morphology has more exposed surface area and was expected to show better catalytic activity, which is indeed observed in our catalysis experiments.

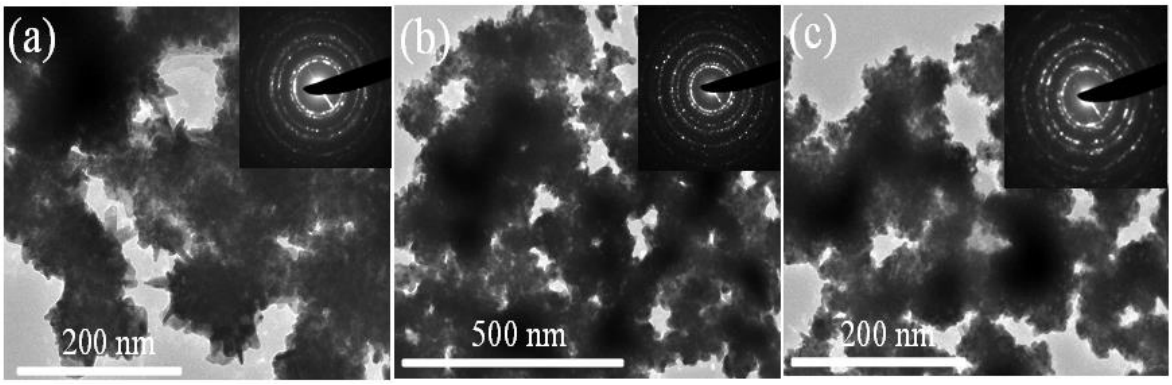

Figure 5. TEM images of Pd_3Pb_P1m (a), Pd_3Pb_P2m (b), Pd_3Pb_P15m (c). The inset in each figure represents the SAED patterns of the corresponding sample.

Although the mechanism of formation of the flower-like Pd_3Pb intermetallic nanocrystal is not clear, it is highly probable that unstable small nuclei of metal atoms aggregate into three dimensional flower-shaped NPs. "Seeded growth" and "self-organization" mechanisms are well established for the formation of branched/multipodal structures.[34,47,48] By incorporating these concepts, a probable mechanism can be speculated for the formation of Pd_3Pb-P10s in three steps- i) co-reduction of metal salts and nucleation, ii) random growth of spherical nanoparticles to form irregular shaped (plate-like and rod-like) nanoparticles, iii) and finally three dimensional assembly of those irregular shaped particles to the flower-like morphology (**Figure 6a**). Le et al. proposed a similar mechanism for flower-shaped Au-Pd alloy nanoparticles.[49] It is also known that $NaBH_4$ might promote the formation of flower-shaped Pd alloy.[50] In the case of hydrothermal synthesis, interconnected network type morphology can be explained

through the oriented attachment mechanism.[51] After the co-reduction of bigger spherical nanoparticles join to smaller ones, which leads to the formation of interconnected network (**Figures 6b, 7**).

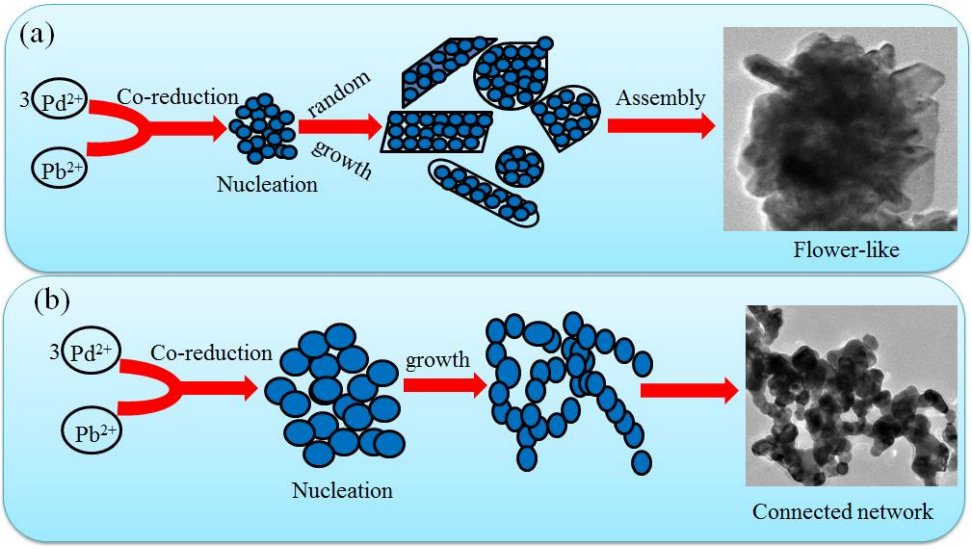

Figure 6. The mechanism on the formation of (a) flower-like nanocrystal and (b) interconnected network type structure.

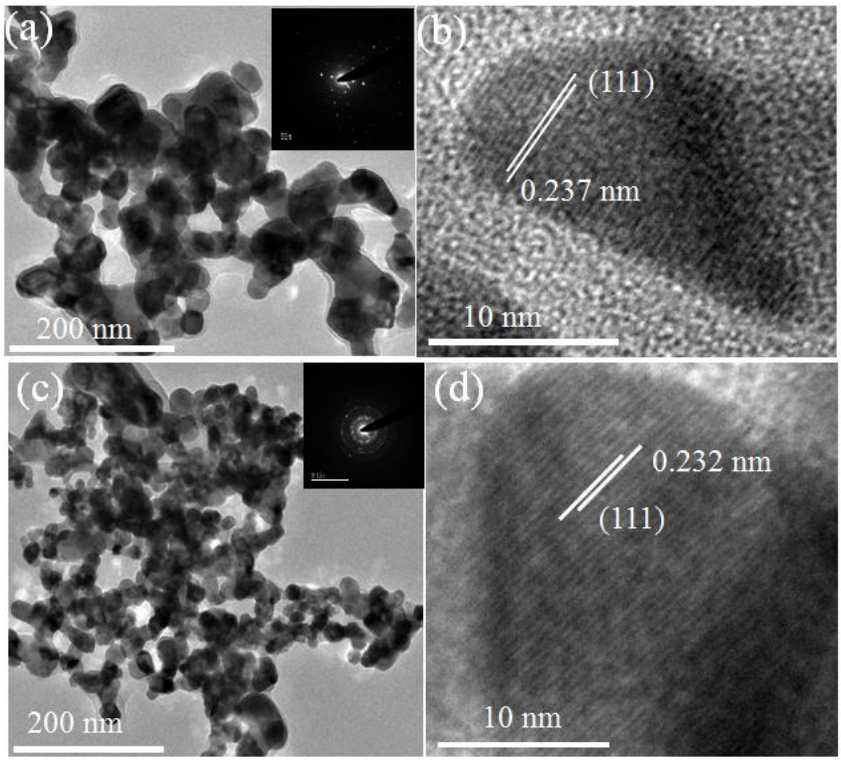

Figure 7. TEM (a) and HRTEM (b) images of Pd_3Pb_HP24 and TEM (c) and HRTEM (d) images of Pd_3Pb_HN72. The inset in figures (a) and (c) represent the corresponding SAED patterns.

The d-spacing calculated from HRTEM images are 0.237 nm and 0.232 nm for Pd_3Pb_HP24 (**Figures 7b**) and Pd_3Pb_HN72 (**Figures 7d**), respectively, which are the characteristics of (111) plane of Pd_3Pb. Pd_3Pb_HP48 and Pd_3Pb_HP72 samples show more agglomeration in the connected type structure. EDAX elemental analysis provide the atomic percentage of the elements 75.07±1.9%, 72±1.9%, 74.72±2.2% and 24.93±2.7%, 28±2.8%, 25.28±3.7% for Pd and Pb, respectively, which is in good agreement with the expected stoichiometric ratio of 3:1 for the compounds Pd_3Pb_P10s, Pd_3Pb_HN72 and Pd_3Pb_HP24 (**Figure 8**).

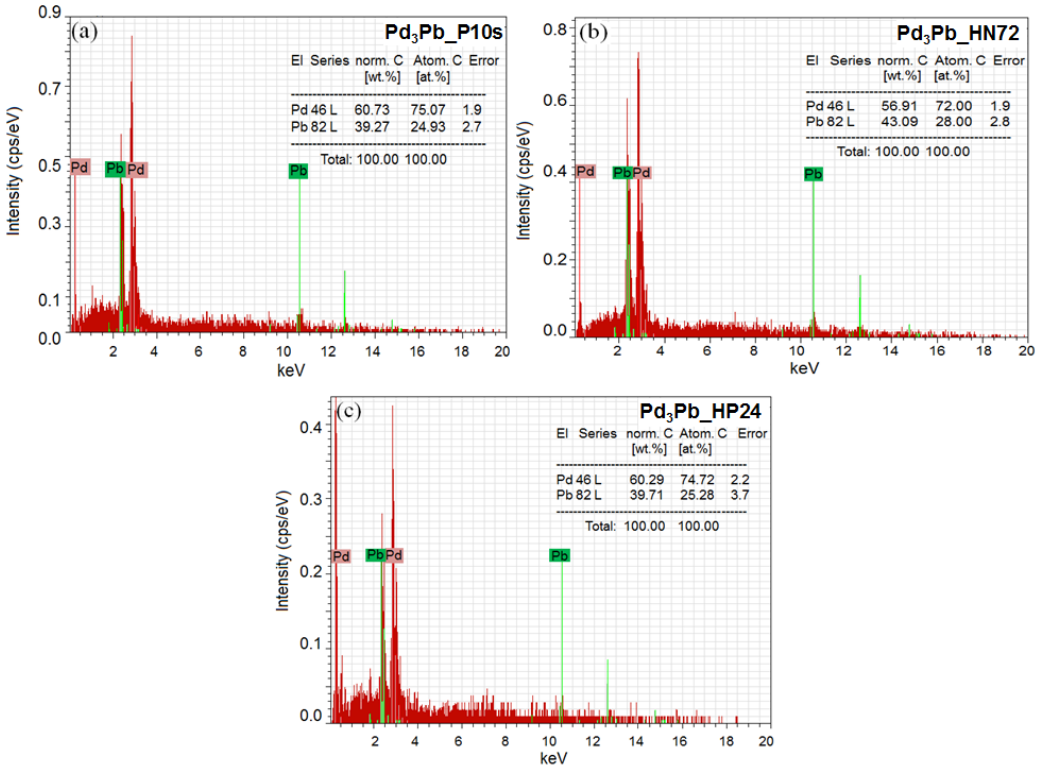

Figure 8. EDAX spectrum of (a) Pd_3Pb_P10s, (b) Pd_3Pb_HN72 and (c) Pd_3Pb_HP24.

2.3.2. Electrochemical Catalytic Activity

The FAO studies using pure Pd_3Pb samples and commercial Pd/C were performed in acidic medium (0.5 M $HClO_4$) by running CV in the potential ranges (-0.2-1.0V) (shown in **Figure 9**). The CV curves show potential regions in the ranges -0.2-

0.15V, 0.15-0.4 V and 0.4-1.0 V are characteristics of hydrogen adsorption-desorption, double layer charge and the formation and reduction of PdO, respectively.

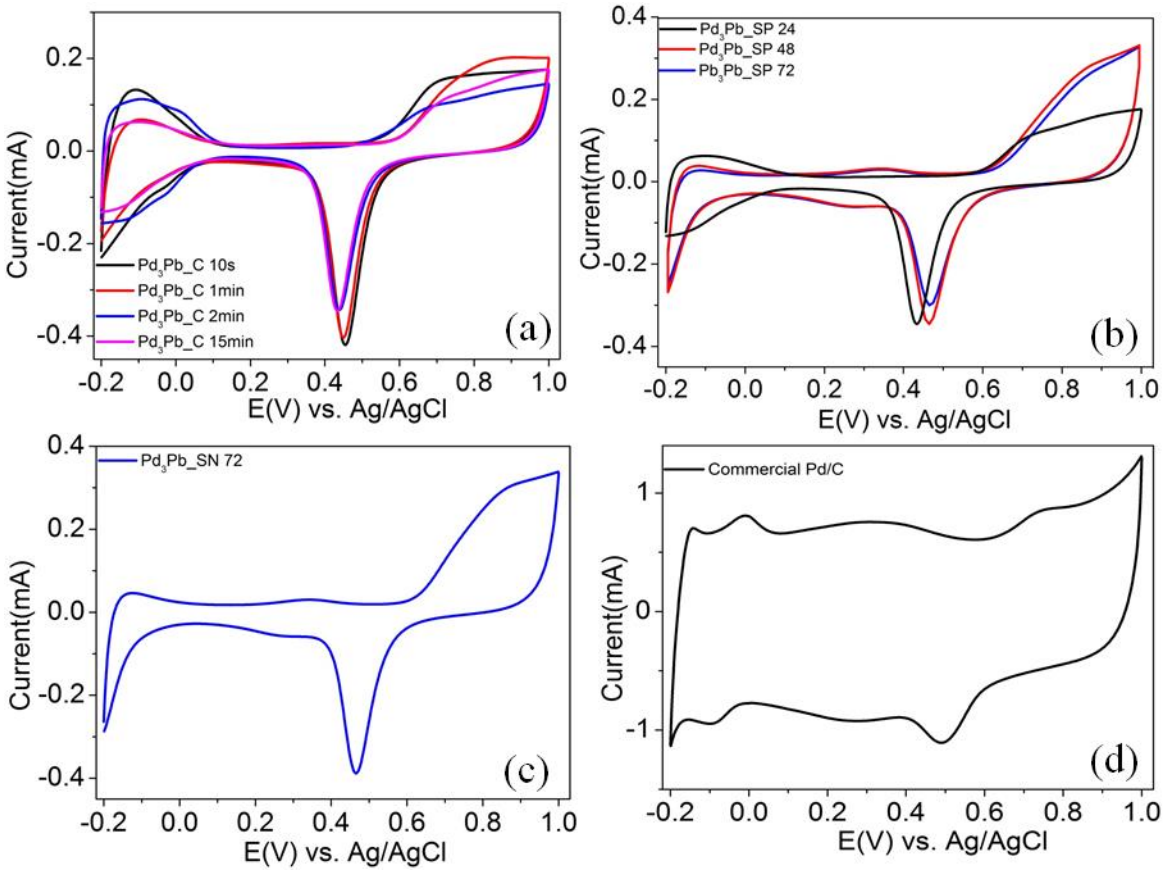

Figure 9. CV curves of Pd_3Pb modified GC electrodes and commercial Pd/C in 0.5M $HClO_4$ solution (a) synthesized by polyol method (b) hydrothermal method in presence of PVP, (c) hydrothermal method in absence of PVP, (d) commercial Pd/C at a scan rate of 50mV/s.

The electrochemical active surface area (ECSA) was estimated from the value of 430 µC/cm^2 for PdO monolayer reduction in acidic[52] medium (**Table 2**). The CV measurement proves that Pd_3Pb modified electrodes are electrochemically accessible, which is important for the electrocatalytic reaction.[19] **Table 2** shows that the ECSA for Pd_3Pb_P10s is higher than other samples synthesized by polyol method with longer reaction time (1-15 minutes), which is quite obvious because of agglomeration in the latter samples due to longer reaction time. ECSA value for Pd_3Pb_P10s also indicates that more active surface area is available in case of the material with flowerlike morphology.

Similarly, due to the same agglomeration effect, PVP assisted hydrothermally synthesized samples with longer reaction time show decrease in ECSA value (**Table 2**).

Table 2. ECSA values obtained for all the catalysts in 0.5M $HClO_4$

Compounds	ECSA (cm^2) (0.5M $HClO_4$)
Pd_3Pb_P10s	1.70
Pd_3Pb_P1m	1.55
Pd_3Pb_P2m	1.40
Pd_3Pb_P15m	1.34
Pd_3Pb_HN72	1.42
Pd_3Pb_HP24	1.35
Pd_3Pb_HP48	1.29
Pd_3Pb_HP72	1.14
Commercial Pd/C	1.77

The agglomeration effect is further confirmed by mass activity and specific activity measurements of all the samples for FAO (**Figure 10**). A peak current near 0.4 V corresponds to the FAO via direct pathway.[18,19] From **Figures 10-11**, it was observed that both mass and specific activities of the less agglomerated samples (Pd_3Pb_P10s, Pd_3Pb_HP24) are enhanced compared to the agglomerated materials. Pd_3Pb_P10s and Pd_3Pb_HN72, Pd_3Pb_HP24 are found to be the more active catalysts, respectively for the samples synthesized from polyol and hydrothermal methods (without surfactant, PVP assisted). Though in case of PVP assisted samples with increasing reaction time, there is negative shift of peak potential which can be attributed to the increase in alloying effect with increasing reaction time.[53] The activities of the better catalysts synthesized by different methods are compared in **Figure 12**. The specific current density value of the catalysts for FAO in the anodic scan at peak potential is in the order of Pd_3Pb_HP24 (5.68 $mAcm^{-2}$) < Pd_3Pb_HN72 (5.81 $mAcm^{-2}$) < Pd_3Pb_P10s (6.83 $mAcm^{-2}$). The peak current density value for Pd_3Pb_P10s catalyst is 1.20 and 1.17 times than that for Pd_3Pb_HP24 and Pd_3Pb_HN72, respectively (**Figure 12a, Table 3**). It was observed that mass activity of the catalysts also follows the same trend as Pd_3Pb_HP24 < Pd_3Pb_HN72 <

Pd_3Pb_P10s. The mass activity of the most active catalyst, Pd_3Pb_P10s, is 1.05A/mg_{Pd} (**Figure 12b and Table 3**).

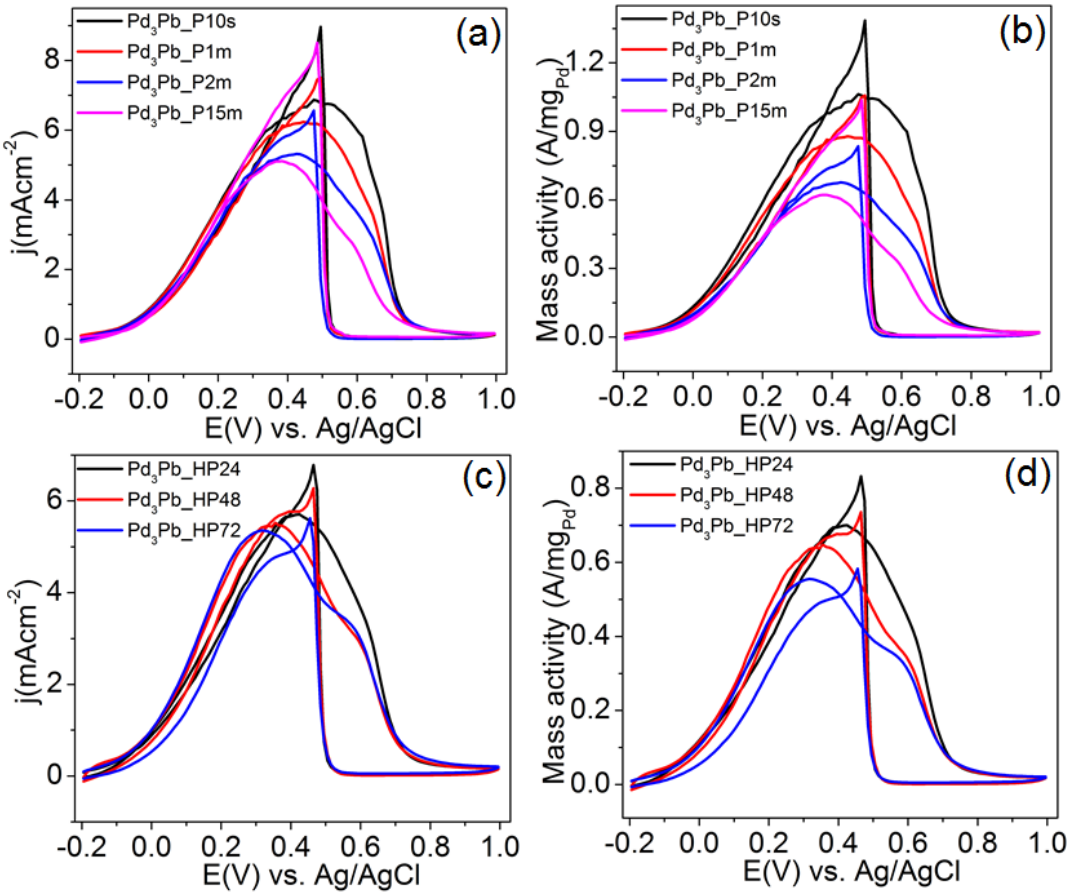

Figure 10. CV measurements of all Pd_3Pb catalysts in 0.5 M HClO4 + 1 M HCOOH solution at a scan rate of 50mV/s. (a) specific activity, (b) mass activity of the catalysts synthesized by polyol method, (c) specific activity and (d) mass activity of the catalysts synthesized by PVP assisted hydrothermal method.

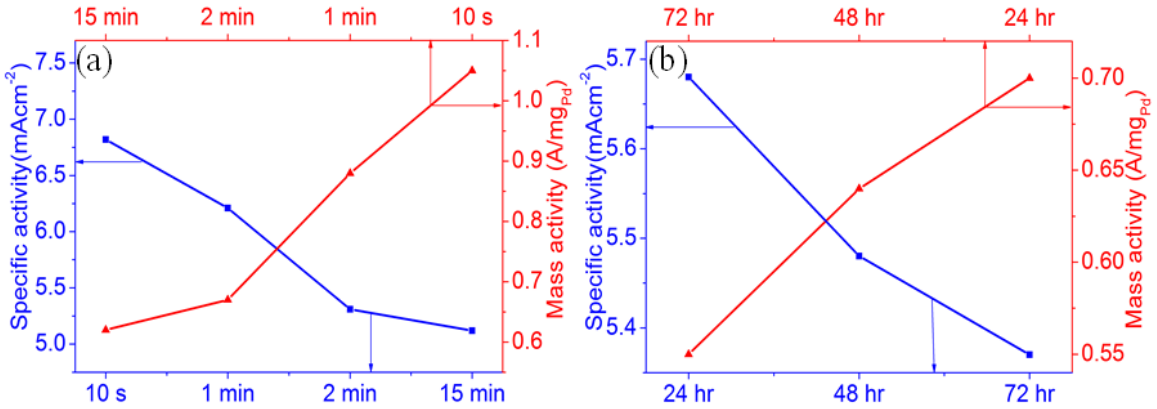

Figure 11. The trend of mass and specific activities data of all Pd_3Pb nanocatalysts synthesized by polyol method (a) and PVP assisted hydrothermal method (b).

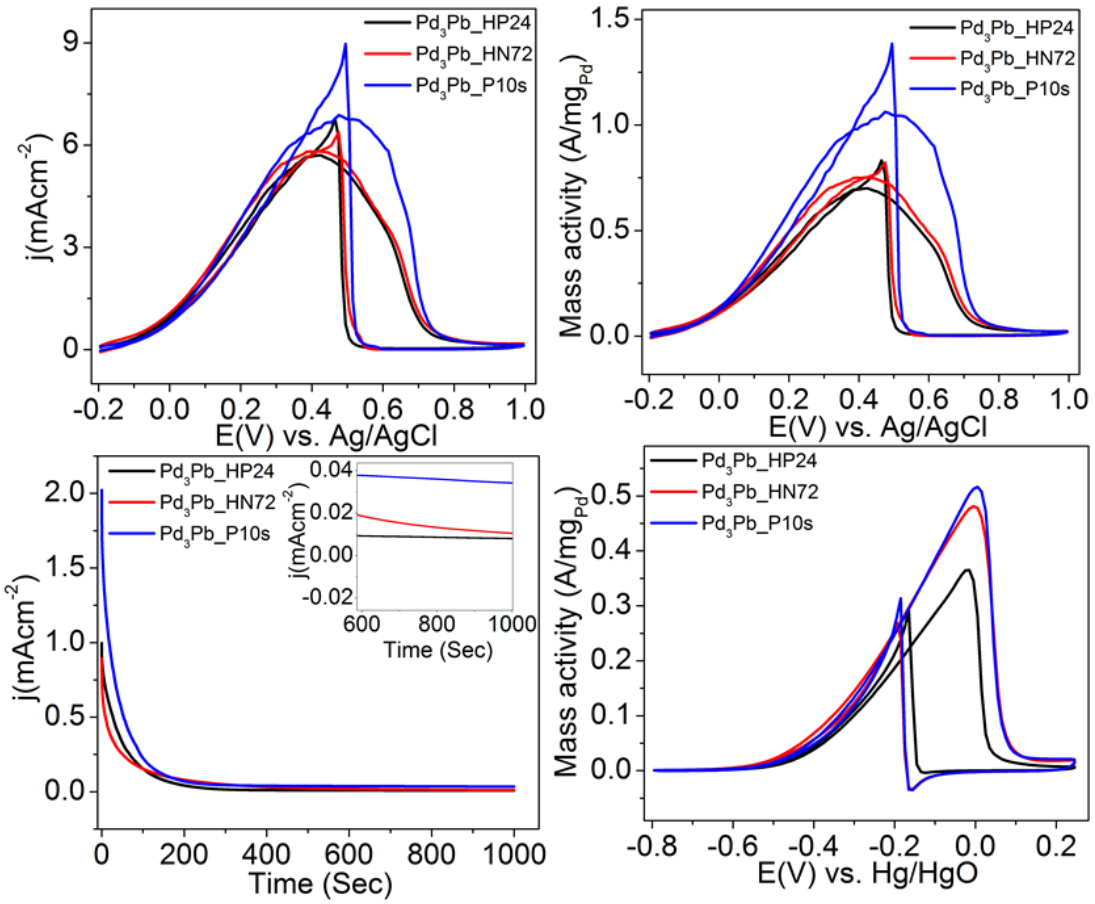

Figure 12. (a) CV measurements obtained for the Pd_3Pb catalysts in 0.5 M HClO4 + 1 M HCOOH solution at a scan rate of 50mV/s, (b) comparison of mass activities of all Pd_3Pb catalysts in 0.5 M HClO4 + 1 M HCOOH solution at a scan rate of 50mV/s, (c) CA measurement obtained for all Pd_3Pb catalysts in 0.5 M $HClO_4$ + 1 M HCOOH solution at 0.4V and (d) comparison of the mass activities of all Pd_3Pb catalysts in 0.5 M KOH + 1 M ethanol solution at a scan rate of 50mV/s.

Table 3. Electro-catalytic activity results for the oxidation of formic acid and ethanol on different Pd_3Pb nanocatalysts.

Catalysts	ECSA(cm^2)		Activity(at peak potential)			
			FAO		EOR	
	0.5M $HClO_4$	0.5M KOH	Mass activity (A/mg_{Pd})	Specific activity ($mAcm^{-2}$)	Mass activity (A/mg_{Pd})	Specific activity ($mAcm^{-2}$)
Pd_3Pb_P10s	1.70	2.82	1.05	6.83	0.51	2.02
Pd_3Pb_HN72	1.42	2.80	0.75	5.81	0.48	1.88
Pd_3Pb_HP24	1.35	2.42	0.70	5.68	0.36	1.66
Commercial Pd/C	1.77	2.85	0.14	0.60	0.36	1.42

The stability of the Pd_3Pb NPs for FAO was investigated by CA technique at 0.4V (**Figure 12c**). It can be clearly observed that current decay is slower for

Pd_3Pb_P10s, which indicates superior electrochemical stability during 1000s test. The CA curve shows that Pd_3Pb_P10s has good tolerance towards formic acid electro-oxidation. The better activity of Pd_3Pb_HN72 catalyst over Pd_3Pb_HP24 may be due to surface coverage of the latter with PVP, which decreases the available surface area for electrocatalysis. Among the three chosen catalysts (Pd_3Pb_HP24, Pd_3Pb_HN72, Pd_3Pb_P10s) Pd_3Pb_HP24 is found to be the least active in terms of peak current density, mass activity and stability.

The catalysts showing best activities towards FAO were subjected for electrooxidation towards ethanol in alkaline medium. The ECSA of the catalysts in 0.5M KOH were calculated from the value of 405 $\mu C/cm^2$ for PdO monolayer reduction[54] (**Table 3**). Similarly electrocatalytic activity towards ethanol was carried out by CV technique in the mixture of 0.5M KOH/1M ethanol aqueous solution. From **Figure 12d**, we can conclude the order of mass activity for ethanol oxidation reaction (EOR) to be Pd_3Pb_HP24 < Pd_3Pb_HN72 < Pd_3Pb_P10s. The mass activity of superior catalyst (Pd_3Pb_P10s) was calculated to be 0.52 A/mg_{Pd}, which is 1.40 times higher than Pd_3Pb_HP24 catalyst. The peak current density of the catalysts also follows the same order as Pd_3Pb_HP24 < Pd_3Pb_HN72 < Pd_3Pb_P10s (**Figure 13a**). To evaluate stability of the catalysts CA was employed in a mixture of 0.5M KOH and 1M ethanol solution at a constant applied potential of -0.1V. As shown in **Figure 13b**, after initial rapid decrease in current density due to accumulation of strongly adsorbed reaction intermediates on active surface, a pseudosteady state was reached. The activity order for EOR in terms of current density is Pd_3Pb_HP24 < Pd_3Pb_HN72 < Pd_3Pb_P10s. After 1000s reaction Pd_3Pb_P10s catalyst shows 1.56 and 1.24 times higher current density than Pd_3Pb_HP24 and Pd_3Pb_HN72, respectively.

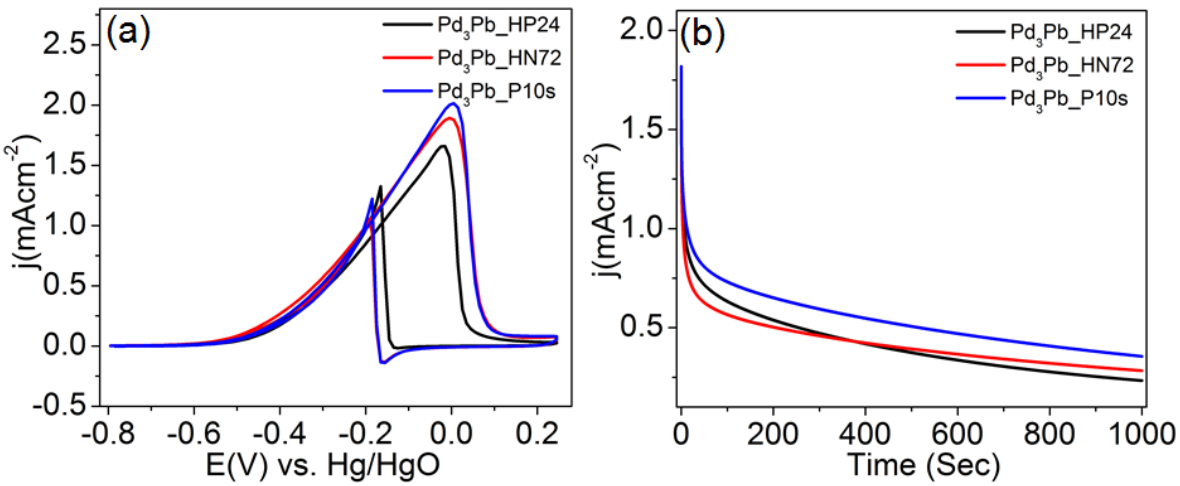

Figure 13. a) current density comparison of Pd3Pb catalysts in 0.5 M KOH + 1 M ethanol solution at a scan rate of 50mV/s, b) CA measurement at -0.1V in 0.5 M KOH + 1 M ethanol solution.

A comparison study of commercial Pd/C with the three most active catalysts has been carried out in both acidic and alkaline medium (**Figure 14, 15**). The current density and mass activity of Pd_3Pb_P10s catalyst observed for FAO is respectively 2.5 times and 2.4 times higher than the commercial Pd/C (**Figure 14a-b, 15a**) in 0.5M $HClO_4$ medium. The current density and mass activity of Pd_3Pb catalysts are also higher than commercial Pd/C in 0.5M KOH medium (**Figure 14c-d, 15c**). Commercial Pd/C catalyst is found to be less stable compared to all Pd_3Pb catalysts in CA study (**Figure 15b and d**). These results clearly show the better activity and stability of the Pd_3Pb catalysts over the Pd/C.

Both CV and CA measurements for FAO and EOR suggest that Pd_3Pb_P10s is the superior catalyst among all the Pd_3Pb catalyst synthesized by different methods (**Figure 14, 15**). Although Pb does not have any catalytic activity, promotional effect of Pb to enhance electrocatalytic oxidation activity as well as CO-poisoning tolerance is well known in literature[39,55,56] due to bi-functional mechanism and electronic effects (d-band theory).[57-59] Wang and co-workers[40] have already shown enhancement in the EOR activity in alkaline medium by alloying Pb with Pd compared to monometal Pd. It has been reported that flower-like nanostructures of Au,[60] Pt,[61] Pd,[34] Pd alloy[50] and Pt alloy[62]

have shown enhancement in the electrocatalytic oxidation properties. Here, flowerlike nanostructure of Pd_3Pb could greatly increase the surface area, which may be the reason for the enhancement of the electrocatalytic activity.

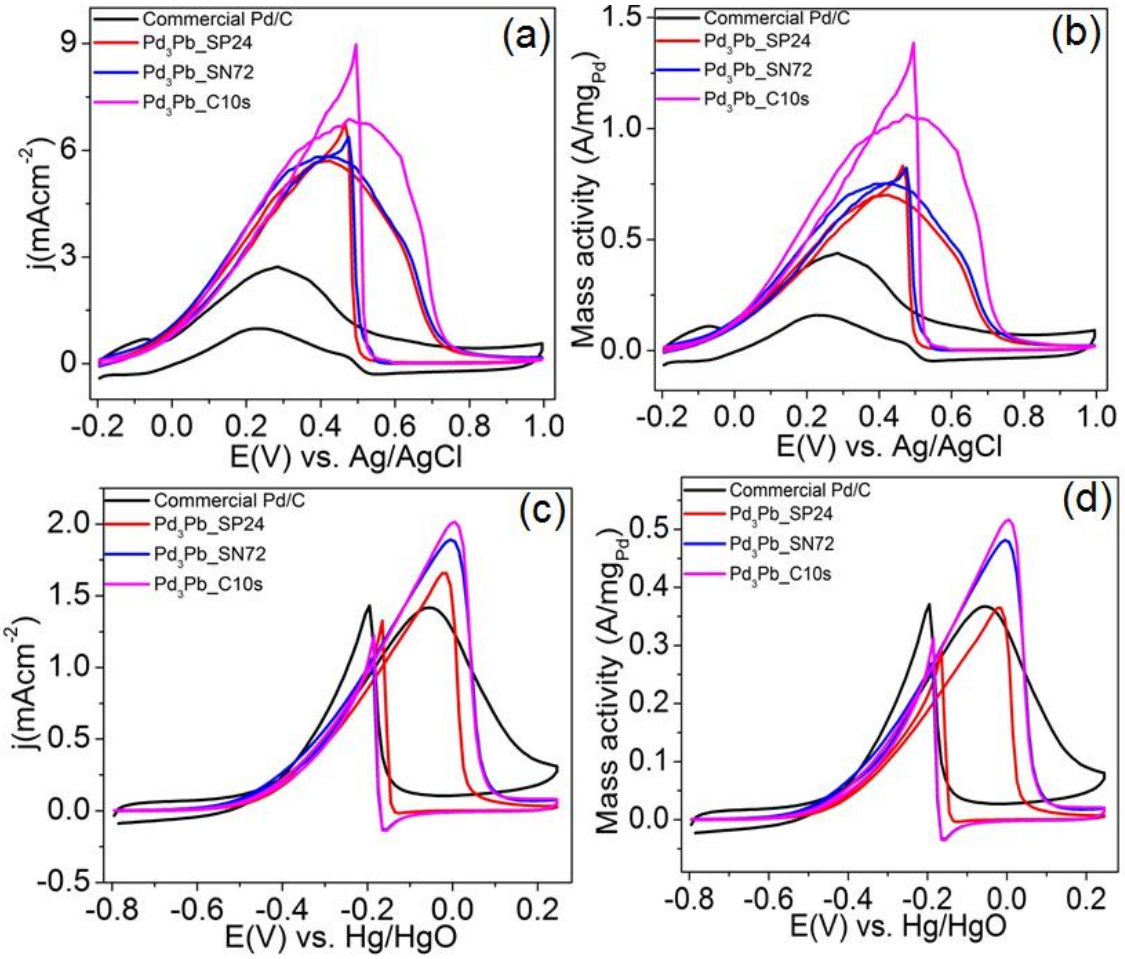

Figure 14. CV curves obtained for different Pd_3Pb catalysts and commercial Pd/C at a scan rate of 50mV/s (a) specific activity, (b) mass activity in 0.5M HClO4 solution containing 1M HCOOH, (c) specific activity and (d) mass activity in 0.5 KOH solution containing 1M ethanol.

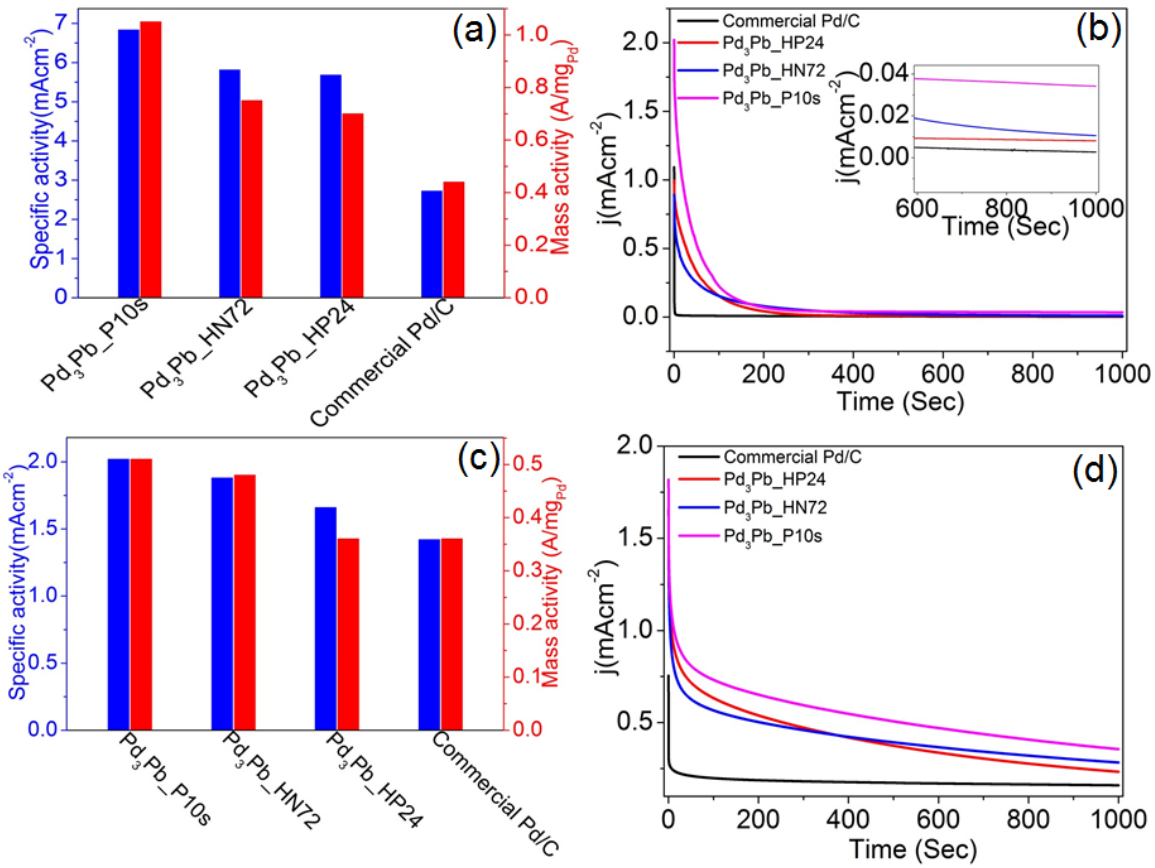

Figure 15. The comparison for the elcterochemical activity for FAO and EOR of the catalyst Pd_3Pb and commercial Pd/C. (a) comparison of specific and mass activity for FAO (0.5 M HClO4 + 1 M HCOOH, scan rate of 50mV/s), (b) CA at 0.4V for 1000s in 0.5 M HClO4 + 1 M HCOOH solution (the inset shows stability curve in the range 600-1000s), (c) comparison of specific and mass activity for EOR (in 0.5 M KOH + 1 M ethanol solution, scan rate of 50mV/s) and (d) CA at -0.1V for 1000s in 0.5 M KOH solution containing 1M ethanol.

2.4. Conclusion

Facile and ultrafast synthetic methods (polyol, hydrothermal) for the preparation of Pd_3Pb intermetallic nanoparticles has been developed through solution based chemistry for the first time. The ordered nature of the compounds has been confirmed through the PXRD and TEM techniques. Polyol method assisted in the formation of Pd_3Pb within short period of 10 seconds, which is found to be the ultrafast synthesis of ordered intermetallic compounds by the solution methods. The electrochemical oxidation of formic acid and ethanol was studied on differently shaped/morphed Pd_3Pb nanoparticles in different supporting electrolytes (KOH, $HClO_4$). Among all the catalysts flowerlike Pd_3Pb catalyst has shown superior performance in terms of both catalytic activity and

stability. The synthesis methods can be extended for the formation of other Pd and group IV metal based intermetallics by choosing appropriate precursor salts. Therefore, the present work suggests that Pb can be a potential constituent with noble metals in form of alloy, bimetallic or intermetallic for electrochemical oxidation reaction in direct fuel cell. The size, morphology, ordering and alloying plays crucial roles in improving the catalytic activity towards selected electrochemical reactions.

2.5. References

(1) Rice, C.; Ha, S.; Masel, R. I.; Wieckowski, A. *J. Power Sources* **2003**, *115*, 229-235.

(2) Capon, A. P., R. : *J. Electroanal. Chem.* **1973**, *45*, 205 –231.

(3) Wang, L.; Yamauchi, Y. *Chem. Mater.* **2009**, *21*, 3562-3569.

(4) Roychowdhury, C.; Matsumoto, F.; Zeldovich, V. B.; Warren, S. C.; Mutolo, P. F.; Ballesteros, M.; Wiesner, U.; Abruna, H. D.; DiSalvo, F. J. *Chem. Mater.* **2006**, *18*, 3365-3372.

(5) Kang, Y. J.; Qi, L.; Li, M.; Diaz, R. E.; Su, D.; Adzic, R. R.; Stach, E.; Li, J.; Murray, C. B. *ACS Nano* **2012**, *6*, 2818-2825.

(6) Hayden, B. E.; Rendall, M. E.; South, O. *J. Am. Chem. Soc.* **2003**, *125*, 7738-7742.

(7) Roychowdhury, C.; Matsumoto, F.; Mutolo, P. F.; Abruna, H. D.; DiSalvo, F. J. *Chem. Mater.* **2005**, *17*, 5871-5876.

(8) Koenigsmann, C.; Wong, S. S. *Energ. Environ. Sci.* **2011**, *4*, 1161-1176.

(9) Miura, A.; Wang, H. S.; Leonard, B. M.; Abruna, H. D.; DiSalvo, F. J. *Chem. Mater.* **2009**, *21*, 2661-2667.

(10) Iyyamperumal, R.; Zhang, L.; Henkelman, G.; Crooks, R. M. *J. Am. Chem. Soc.* **2013**, *135*, 5521-5524.

(11) Chen, G.; Xia, D. G.; Nie, Z. R.; Wang, Z. Y.; Wang, L.; Zhang, L.; Zhang, J. J. *Chem. Mater.* **2007**, *19*, 1840-1844.

(12) Ghosh, T.; Leonard, B. M.; Zhou, Q.; DiSalvo, F. J. *Chem. Mater.* **2010**, *22*, 2190-2202.

(13) Leonard, B. M.; Zhou, Q.; Wu, D. M.; DiSalvo, F. J. *Chem. Mater.* **2011**, *23*, 2499-2499.

(14) Scofield, M. E.; Koenigsmann, C.; Wang, L.; Liu, H.; Wong, S. S. *Energ. Environ. Sci.* **2015**, *2*, 915-931.

(15) Zhang, S.; Guo, S. J.; Zhu, H. Y.; Su, D.; Sun, S. H. *J. Am. Chem. Soc.* **2012**, *134*, 5060-5063.

(16) Wang, J. J.; Yin, G. P.; Chen, Y. G.; Li, R. Y.; Sun, X. L. *Int. J. Hydrogen Energy* **2009**, *34*, 8270-8275.

(17) Morales-Acosta, D.; Ledesma-Garcia, J.; Godinez, L. A.; Rodriguez, H. G.; Alvarez-Contreras, L.; Arriaga, L. G. *J. Power Sources* **2010**, *195*, 461-465.

(18) Mazumder, V.; Chi, M. F.; Mankin, M. N.; Liu, Y.; Metin, O.; Sun, D. H.; More, K. L.; Sun, S. H. *Nano Lett.* **2012**, *12*, 1102-1106.

(19) Liu, D.; Guo, Q. H.; Hou, H. Q.; Niwa, O.; You, T. Y. *ACS Catal.* **2014**, *4*, 1825-1829.

(20) Zhang, L.; Zhang, J. W.; Kuang, Q.; Xie, S. F.; Jiang, Z. Y.; Xie, Z. X.; Zheng, L. S. *J. Am. Chem. Soc.* **2011**, *133*, 17114-17117.

(21) Ji, X. L.; Lee, K. T.; Holden, R.; Zhang, L.; Zhang, J. J.; Botton, G. A.; Couillard, M.; Nazar, L. F. *Nat. Chem.* **2010**, *2*, 286-293.

(22) Wang, J. Y.; Zhang, H. X.; Jiang, K.; Cai, W. B. *J. Am. Chem. Soc.* **2011**, *133*, 14876-14879.

(23) Larsen, R.; Zakzeski, J.; Masel, R. I. *Electrochem. Solid State Commun.***2005**, *8*, A291-A293.

(24) Ha, S.; Larsen, R.; Masel, R. I. *J. Power Sources* **2005**, *144*, 28-34.

(25) Xu, C. W.; Wang, H.; Shen, P. K.; Jiang, S. P. *Adv. Mater.* **2007**, *19*, 4256.

(26) He, Q. G.; Chen, W.; Mukerjee, S.; Chen, S. W.; Laufek, F. *J. Power Sources* **2009**, *187*, 298-304.

(27) Antolini, E.; Zignani, S. C.; Santos, S. F.; Gonzalez, E. R. *Electrochim. Acta* **2011**, *56*, 2299-2305.

(28) Lu, C. L.; Prasad, K. S.; Wu, H. L.; Ho, J. A. A.; Huang, M. H. *J. Am. Chem. Soc.* **2010**, *132*, 14546-14553.

(29) Antolini, E.; Gonzalez, E. R. *Catal. Today* **2011**, *160*, 28-38.

(30) Ksar, F.; Ramos, L.; Keita, B.; Nadjo, L.; Beaunier, P.; Remita, H. *Chem. Mater.* **2009**, *21*, 3677-3683.

(31) Ksar, F.; Surendran, G.; Ramos, L.; Keita, B.; Nadjo, L.; Prouzet, E.; Beaunier, P.; Hagege, A.; Audonnet, F.; Remita, H. *Chem. Mater.* **2009**, *21*, 1612-1617.

(32) Zhang, J. F.; Feng, C.; Deng, Y. D.; Liu, L.; Wu, Y. T.; Shen, B.; Zhong, C.; Hu, W. B. *Chem. Mater.* **2014**, *26*, 1213-1218.

(33) Meng, H.; Sun, S.; Masse, J. P.; Dodelet, J. P. *Chem. Mater.* **2008**, *20*, 6998-7002.

(34) Yin, Z.; Zheng, H. J.; Ma, D.; Bao, X. H. *J. Phys. Chem. C* **2009**, *113*, 1001-1005.

(35) Yin, A. X.; Min, X. Q.; Zhang, Y. W.; Yan, C. H. *J. Am. Chem. Soc.* **2011**, *133*, 3816-3819.

(36) Wang, J. P.; Asmussen, R. M.; Adams, B.; Thomas, D. F.; Chen, A. C. *Chem. Mater.* **2009**, *21*, 1716-1724.

(37) Li, G. C.; Pickup, P. G. *Electrochim. Acta* **2006**, *52*, 1033-1037.

(38) Kelaidopoulou, A.; Abelidou, E.; Kokkinidis, G. *J. Appl. Electrochem.* **1999**, *29*, 1255-1261.

(39) Liu, Z. L.; Guo, B.; Tay, S. W.; Hong, L.; Zhang, X. H. *J. Power Sources* **2008**, *184*, 16-22.

(40) Wang, Y.; Nguyen, T. S.; Liu, X. W.; Wang, X. *J. Power Sources* **2010**, *195*, 2619-2622.

(41) Durussel, P.; Feschotte, P. *J. Alloys Compd.* **1996**, *236*, 195-202.

(42) Volpe, D.; Casado-Rivera, E.; Alden, L.; Lind, C.; Hagerdon, K.; Downie, C.; Korzeniewski, C.; DiSalvo, F. J.; Abruna, H. D. *J. Electrochem. Soc.* **2004**, *151*, A971-A977.

(43) Casado-Rivera, E.; Volpe, D. J.; Alden, L.; Lind, C.; Downie, C.; Vazquez-Alvarez, T.; Angelo, A. C. D.; DiSalvo, F. J.; Abruna, H. D. *J. Am. Chem. Soc.* **2004**, *126*, 4043-4049.

(44) Alden, L. R.; Roychowdhury, C.; Matsumoto, F.; Han, D. K.; Zeldovich, V. B.; Abruna, H. D.; DiSalvo, F. J. *Langmuir* **2006**, *22*, 10465-10471.

(45) Chai, G. S.; Yoon, S. B.; Yu, J. S.; Choi, J. H.; Sung, Y. E. *J. Phys. Chem. B* **2004**, *108*, 7074-7079.

(46) Xiong, Y. J.; Washio, I.; Chen, J. Y.; Cai, H. G.; Li, Z. Y.; Xia, Y. N. *Langmuir* **2006**, *22*, 8563-8570.

(47) Teng, X. W.; Liang, X. Y.; Maksimuk, S.; Yang, H. *Small* **2006**, *2*, 249-253.

(48) Hoefelmeyer, J. D.; Niesz, K.; Somorjai, G. A.; Tilley, T. D. *Nano Lett.* **2005**, *5*, 435-438.

(49) Lee, Y. W.; Kim, N. H.; Lee, K. Y.; Kwon, K.; Kim, M.; Han, S. W. *J. Phys. Chem. C* **2008**, *112*, 6717-6722.

(50) Chai, J.; Li, F. H.; Hu, Y. W.; Zhang, Q. X.; Han, D. X.; Niu, L. *J. Mater. Chem.* **2011**, *21*, 17922-17929.

(51) Shi, L. H.; Wang, A. Q.; Huang, Y. Q.; Chen, X. W.; Delgado, J. J.; Zhang, T. *Eur. J. Inorg. Chem.* **2012**, 2700-2706.

(52) Xiao, L.; Zhuang, L.; Liu, Y.; Lu, J. T.; Abruna, H. D. *J. Am. Chem. Soc.* **2009**, *131*, 602-608.

(53) Du, W. X.; Mackenzie, K. E.; Milano, D. F.; Deskins, N. A.; Su, D.; Teng, X. W. *ACS Catal.* **2012**, *2*, 287-297.

(54) Liang, Z. X.; Zhao, T. S.; Xu, J. B.; Zhu, L. D. *Electrochim. Acta* **2009**, *54*, 2203-2208.

(55) Alden, L. R.; Han, D. K.; Matsumoto, F.; Abruna, H. D.; DiSalvo, F. J. *Chem. Mater.* **2006**, *18*, 5591-5596.

(56) Wang, L. L.; Johnson, D. D. *J. Phys. Chem. C* **2008**, *112*, 8266-8275.

(57) Vigier, F.; Coutanceau, C.; Hahn, F.; Belgsir, E. M.; Lamy, C. *J. Electroanal. Chem.* **2004**, *563*, 81-89.

(58) Demirci, U. B. *J. Power Sources* **2007**, *173*, 11-18.

(59) Greeley, J.; Norskov, J. K. *Surf Sci* **2005**, *592*, 104-111.

(60) Jena, B. K.; Raj, C. R. *Langmuir* **2007**, *23*, 4064-4070.

(61) Ghosh, S.; Raj, C. R. *J. Phys. Chem. C* **2010**, *114*, 10843-10849.

(62) Habibi, B.; Delnavaz, N. *Int. J. Hydrogen Energ* **2011**, *36*, 9581-9590.

Chapter 3

Ordered Pd_2Ge Intermetallic Nanoparticles for Enhanced Activity and Stability towards Ethanol Oxidation

Abstract

In this work, Pd_2Ge nanoparticles were synthesized for the first time by superhydride reduction of K_2PdCl_4 and $GeCl_4$. The syntheses were performed using solvothermal method in the absence of surfactants and the size of the nanoparticles controlled by varying the reaction time. The powder X-ray diffraction (PXRD) and transmission electron microscopy (TEM) data suggest that Pd_2Ge nanoparticles were formed as ordered intermetallic phase. The catalyst is highly efficient for the electrochemical oxidation of ethanol (EOR) and is stable upto 250^{th} cycle in alkaline medium. In the crystal structure, Pd and Ge atoms occupy two crystallographically different positions with a vacancy in one of the Ge sites, which was proved by PXRD and energy-dispersive X-ray analysis, has crucial role in the catalytic activity towards the EOR. The specific activity of Pd_2Ge in the oxidation of ethanol is found to be 6.4 times better than the commercial Pd on carbon. The experimentally observed data were interpreted in terms of combined effect of adsorption energies of CH_3CO and OH radicals, d- band center model and work function of the corresponding catalyst surfaces.

3.1. Introduction

Although Pd proved to be a suitable electrocatalyst for ethanol oxidation reaction (EOR) in alkaline media, more effort is needed to further improve the electrocatalytic performance of Pd-based catalysts. Ethanol is relatively less studied than methanol, the reason could be because the C-C bond cleavage in ethanol requires very high dissociating energy (~350 KJ/mol).[18] However, the use of ethanol is advantageous over methanol because it is less toxic, highly abundant, low cost and results in 12 electrons per molecules when it is completely oxidized to CO_2 and H_2O. Some of the catalysts which have been used for electrochemical oxidation of ethanol are SnO_2 /Pt-Sn alloys,[19] Ni supported/Pt-Ru alloys[20] and Pt/C on other oxides like CeO_2 and NiO.[17] In alkaline medium, it has been shown that the reaction catalyzed by Pt is sluggish as compared to Pd. Hence, Pd on various support materials along with its alloys have been highly studied during last two decades. A few examples of this class are Pd on TiO_2/C,[21] Al_2O_3/C, VOx/C,[22] CeO_2/C,[23] Co_3O_4/C,[24] MnO_2/C,[25] NiO/C, In_2O_3/C,[26] CNts (both SWCNT and MWCNT),[24,27] and the alloys PdNi,[28] PdPt,[29] PdAu,[30] and PdRu.[31]

Apart from the above mentioned systems, several catalysts have been reported in the recent past for the electrooxidation of ethanol applying different strategies to improve both the activity and the durability of the catalyst. The examples are Pt-Sn[32] and Pd-Sn[33] based alloy nanoparticles are considered as superior catalyst in ethanol electrooxidation because of their high activity and durability in acidic and alkaline medium, respectively. However, these compounds do not form ordered intermetallic phases under normal reaction conditions. In the same manner $TaPt_3$ ordered intermetallic nanoparticles[34] were reported to show far better activity than Pt_3Sn nanoparticles. However, the ordered phase of $TaPt_3$ was obtained only after the post synthetic heating at a very high temperature (1000 ^oC). PtRh alloy nanocubes supported on graphene[35] were shown to have high

activity towards ethanol electrooxidation, however, both the constituents are costly. PdAu nanowires[36] were synthesized in presence of Br- and PVP as shape directing and stabilizing agent. Presence of an additive on the catalyst surface is detrimental to its catalytic activity as these polymer molecules significantly reduce the effective coverage of ethanol molecules.

Motivated by the incredible catalytic activity of Pd-Sn based alloy nanoparticles, we have synthesized the ordered intermetallic compound Pd_2Ge in nano dimension by modified polyol method at 220 ^oC without using any sort of additives or post synthetic heating. The compound Pd_2Ge crystallizes in the Fe_2P type crystal structure with two each independent crystallographic positions for Pd and Ge atoms.[37] We studied electrochemical oxidation of ethanol in alkaline medium using Pd_2Ge as a catalyst synthesized over a reaction time 24 hrs (Pd_2Ge_24) and 36 hrs (Pd_2Ge_36) of synthesis. Our compounds showed superior activity compared to the commercially available Pd/C, which is in the order of activity towards electrochemical oxidation of ethanol is: Pd_2Ge_36> Pd_2Ge_24> Pd/C. The presence of Ge deficiency in the Pd_2Ge_24 sample showed immense effect on the catalytic activity of the compound owing to the localized defects developed as deficiency. Interestingly, the increase in the catalytic activity for the Pd_2Ge_36 sample was due to the dealloying effect with the evolution of small amount of Pd, which outweighed the presence of localized defects in the Pd_2Ge_24 sample.

3.2. Experimental Section

3.2.1. Chemicals

Potassium tetrachloropalladate (K_2PdCl_4), tetraethylene glycol (TEG), and super-hydride ($Li(Et_3BH)$) were purchased from Sigma-Aldrich. Germanium (IV) chloride ($GeCl_4$) and ethylene glycol were purchased from Alfa Aesar. All materials were used as

purchased and all air-sensitive samples were handled inside an Ar filled glove box (H_2O, O_2 <0.1 ppm).

3.2.2. Synthesis

Pd_2Ge nanoparticles were synthesized by solvothermal method. In a typical solvothermal reaction, 0.2 mmol K_2PdCl_4 and 0.1 mmol $GeCl_4$ were mixed in 18 ml TEG with vigorous stirring and loaded in a 23 ml teflon lined autoclave. The autoclave was kept at 220 ^oC for 24 and 36 hrs. The product was repeatedly washed several times with ethanol.

3.2.3. Powder X-ray Diffraction (PXRD)

PXRD measurements were done at room temperature on a Rigaku Miniflex X-ray diffractometer with Cu-K_α X-ray source (λ = 1.5406 Å), equipped with a position sensitive detector in the angular range $30^o \leq 2\theta \leq 80^o$ with the step size 0.02^o and scan rate of 0.5 s/step calibrated against corundum standards. The experimental patterns were compared to the pattern calculated from the single crystal structure refinement.

3.2.4. Elemental Analysis

Quantitative microanalysis on all the samples were performed with a FEI NOVA NANOSEM 600 instrument equipped with an EDAX® instrument. Data were acquired with an accelerating voltage of 20 kV and a 100 s accumulation time. The EDAX analysis was performed using P/B-ZAF standardless method (where, Z = atomic no. correction factor, A = absorption correction factor, F = fluorescence factor, P/B = peak to background model) on selected spots and points.

3.2.5. Transmission electron microscopy (TEM)

TEM images and selected area electron diffraction (SAED) patterns were collected using a JEOL 200 TEM instrument. Samples for these measurements were

prepared by sonicating the nanocrystalline powders in ethanol and dropping a small volume onto a carbon-coated copper grid.

3.2.6. Electrochemical Studies

All the electrochemical measurements were performed on a CHI 660A electrochemical workstation at 25 °C. Three electrode set-up was used with a glassy carbon electrode (having diameter 3 mm) as working electrode, platinum wire as counter and Hg/HgO (MMO) as reference electrode. All the solutions were purged with nitrogen gas for 20 minutes prior to the measurement. The catalyst ink was prepared by dispersing 5 mg of catalyst in 1 mL of mixed solvent solution (IPA:H_2O=1:1 v/v) and 10 µL of 1 wt.% Nafion binder. The Nafion binder (Signa Aldrich, 5 wt%) was diluted to 1 wt% with isopropyl alcohol (IPA). Twenty µL of the catalyst ink was dropcasted on to glassy carbon (GC) electrode and dried overnight at room temperature. Before depositing the catalyst, the GC was polished with 0.05 µm alumina slurry, washed several times with distilled water (16.2 mΩ) and IPA. Commercial Pd/C (10wt. %, Sigma Aldrich) was used for comparison of the activity with the Pd_2Ge catalyst. The blank cyclic voltammetry (CV) measurement was carried out with 1M KOH aqueous solution at a scan rate 50 mV/sec. CV and chronoamperometry (CA) measurements were performed in 1M KOH/1M EtOH electrolyte solution at a scan rate 50 mV/sec. Linear sweep voltammetry (LSV) was recorded with a sweep rate of 1 mV/sec at 1000 rpm in 1M KOH/1M EtOH electrolyte solution. Tafel plots (TP) were derived from LSV measurement.

3.2.7. Computational Details

The first principal calculations have been done by in collaboration with Prof. Umesh Waghmare and his group. The first principles calculations were performed on the density functional theory as implemented in quantum espresso package.[38] The exchange-correlation energy of electrons was treated with local density approximation with Perdew-

Zunger parametrized form.[39] We employed a periodic boundary conditions with 4X4 and 3X3 supercell of Pd and Pd_2Ge surfaces, respectively, and include a vacuum of about 14 Å to keep interaction between periodic images low. We have used a kinetic energy cut off of 35 Ry to truncate the plane wave basis. We use uniform mesh of 3X3X1 and 3X3X2 k-points for Pd and Pd_2Ge surfaces, respectively, in sampling integration over the brillouin zone. We have used different orientation of OH and CH_3CO on surface and relax the system until the Hellmann-Feynman forces on each atom are less than 0.03 eV/Å. We have considered Pd_2Ge_24 as a Ge-deficient surface and Pd_2Ge_36 as a pristine Pd_2Ge phase throughout our calculation.

3.3. Results and Discussions

3.3.1. PXRD analysis

A typical representation of the unit cell of the Pd_2Ge crystal structure is shown in **Figure 1a**. The coordination environments of the catalytically active palladium sites, are shown in **Figures 1b** and **1c**. Pd_2Ge crystallizes in the hexagonal Fe_2P structure type ($P\bar{6}2c$ space group), which is a vacancy ordered variant of the AlB_2 prototype. Among the four crystallographically different sites, two are occupied by the Pd atoms (Wyck. no. 3*f* and 3*g*) and the other two are occupied by the Ge atoms (Wyck. no. 2*a* and 1*b*). The open circle represents the deficiency at the Ge atoms, which is confirmed from the PXRD analysis of Pd_2Ge_24 and EDX measurements. **Figure 2** shows the PXRD patterns of Pd_2Ge nanoparticles synthesized at 220 ^oC varying the reaction time. Comparison of the experimental PXRD patterns with the simulated pattern of the bulk compound[16] confirmed that Pd_2Ge crystallizes in the ordered phase without any impurities. In the case of Pd_2Ge_24, the relative shift of the PXRD pattern with respect to the bulk compound to the lower angle (2θ) indicates the increase in lattice constant i.e. deficiency in Ge content (**Figure 2b**). However, there was no shift in the XRD pattern of Pd_2Ge_36 in comparison

to the simulated pattern suggests the absence of Ge deficiency (**Figure 2b**), which can be explained as either the vacancy of Ge filled slowly or the chemical etching of Pd due to the strain present in Pd_2Ge_24 sample. Although it is expected that the slow reduction of Ge compared to Pd, the filling of Ge vacancy can be ruled out due to the negligible difference in the atomic composition of Pd and Ge obtained from the EDAX measurements which shows the Pd and Ge contents in Pd_2Ge_24 and Pd_2Ge_36 samples are 72-76% and 28-24%, respectively (**Figure 3**). In addition, powder XRD of Pd_2Ge_36 sample contains sizable intense (111) peak at $2\theta = 40.1^{o}$ represents metallic Pd confirmed that Pd slowly etched out of the system and exist in the composition $Pd_x/Pd_{1-x}Ge_y$. This dealloying process, interestingly enhances the catalytic activity of Pd_2Ge_36 compared to Pd_2Ge_24. The crystallite sizes calculated using the Scherer formula for the compounds Pd_2Ge_24 and Pd_2Ge_36 are 15 and 18 nm, respectively.

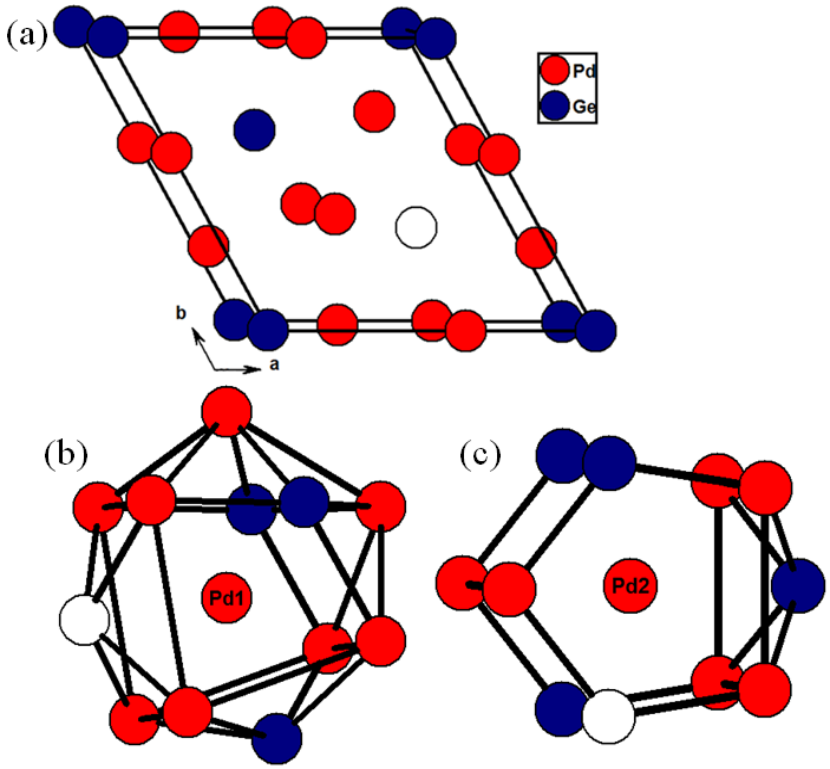

Figure 1. (a) Crystal structure of Pd_2Ge, the white atom represents a vacant site at Ge position for the sample Pd_2Ge_24; coordination sphere of (b) Pd1 and (c) Pd2.

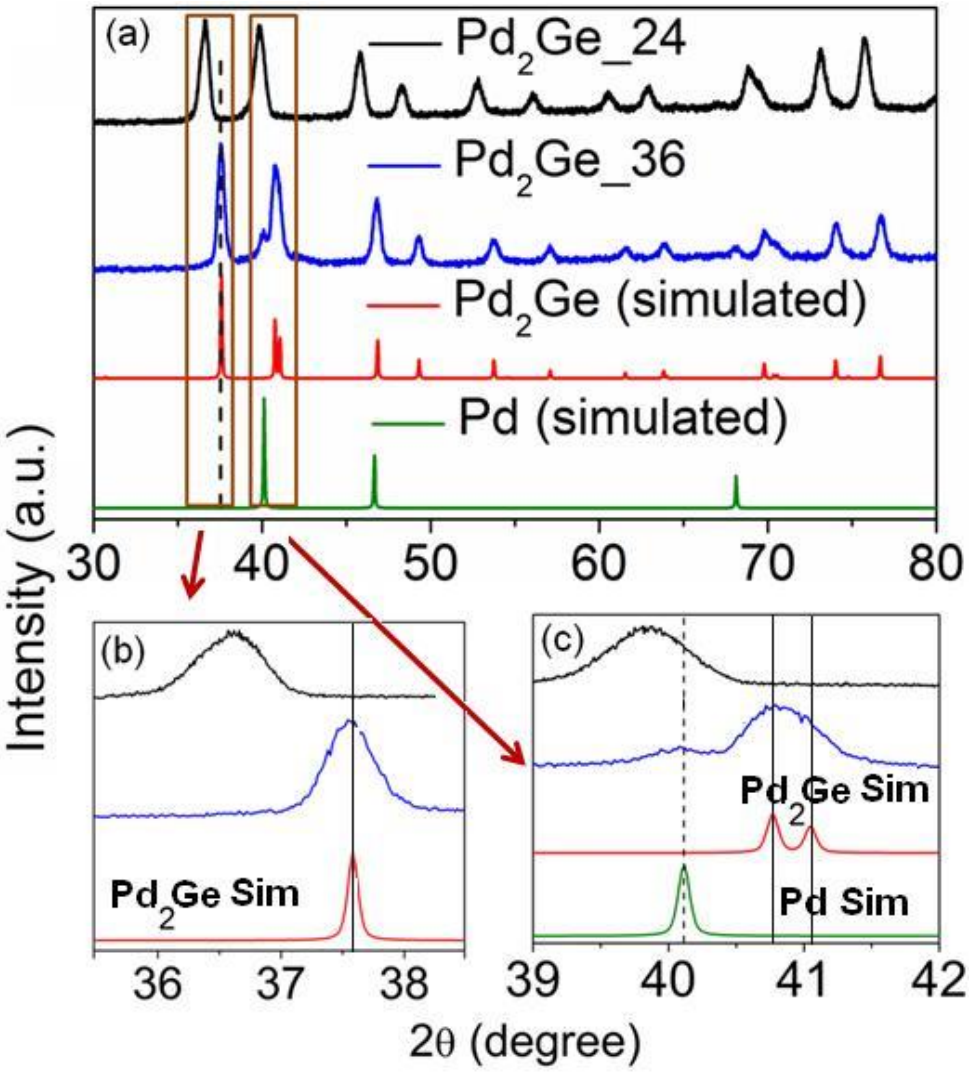

Figure 2. (a) Comparison of PXRD patterns of Pd_2Ge nanoparticles synthesized by solvothermal technique at 220 ^oC after 24 h and 36 h with simulated powder pattern from bulk Pd_2Ge intermetallic compound and Pd. (b) Enlarged plot showing the relative shift of Pd_2Ge_24 compared to the bulk compound. (c) Enlarged plot represent the presence of Pd in Pd_2Ge_36 sample.

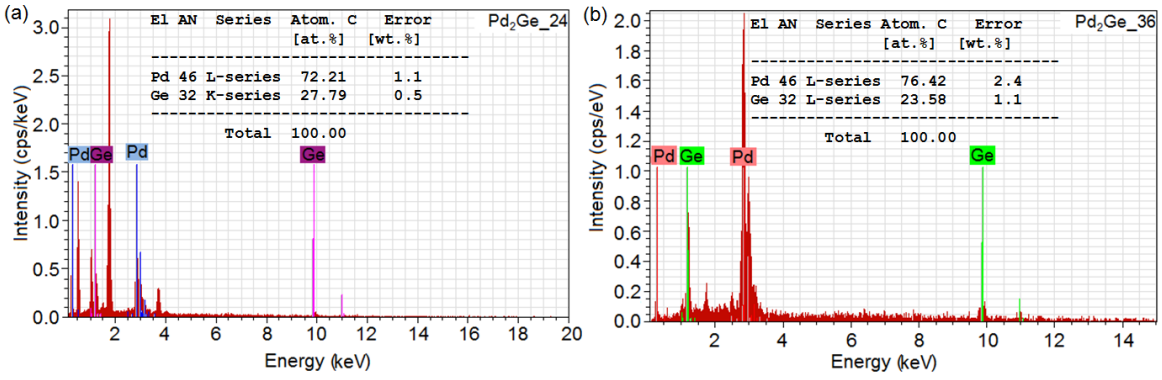

Figure 3. EDAX data of Pd_2Ge NPs synthesized after (a) 24 h and (b) 36 h of reaction time.

3.3.2. TEM analysis

Figure 4 shows the TEM images for Pd_2Ge_24. The sample mostly contains worm like one dimensional interconnected structures can also be called as nanowire of Pd_2Ge similar to PdAu.[40] From the TEM images it is clear that Pd^{2+} and Ge^{4+} are first co-reduced to form Pd_2Ge intermetallic nanoparticles and gradually grow with time. There are spherical particles in few parts of the grid as well (**Figure 4a and 4b**). From HRTEM image, d-spacing (between two lattice fringes) was calculated to be 0.240 nm clearly indicates the presence of (111) plane of ordered Pd_2Ge intermetallic nanoparticles. Formation of intermetallic Pd_2Ge nanoparticle was further proved by SAED pattern (**Figure 4a inset**). The diffraction pattern contains (001), (111), (210), (003) planes confirm the formation of ordered intermetallic Pd_2Ge nanoparticle.

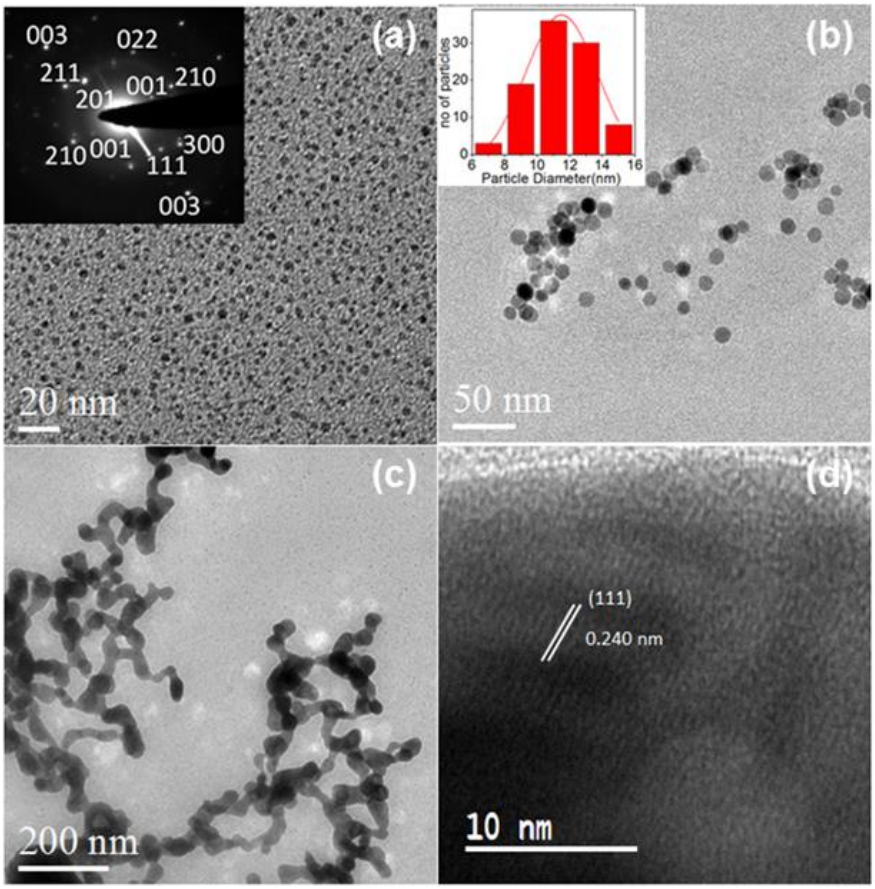

Figure 4. (a) TEM images of Pd_2Ge nanoparticles showing the growth from ultrasmall nanopartilcles (< 5 nm), (b) spherical shaped 5-10 nm particles and inset shows the

electron diffraction pattern on this region, (c) worm like network and (d) HRTEM image from the tape like network.

The bigger particles become ellipsoidal and smaller branches join up (**Figure 5a and 5b**) to form large connected network (**Figure 5c**). It is well known that conversion of spherical nanoparticles into nanowires occurs via an oriented attachment mechanism.[41] The network consists of several kinks and grains, which were also reported in case of AuCu nanowires grown by the same mechanism.[41] This is further supported by the observation of worm like network observed in Pd_2Ge_36 (**Figure 5c**).

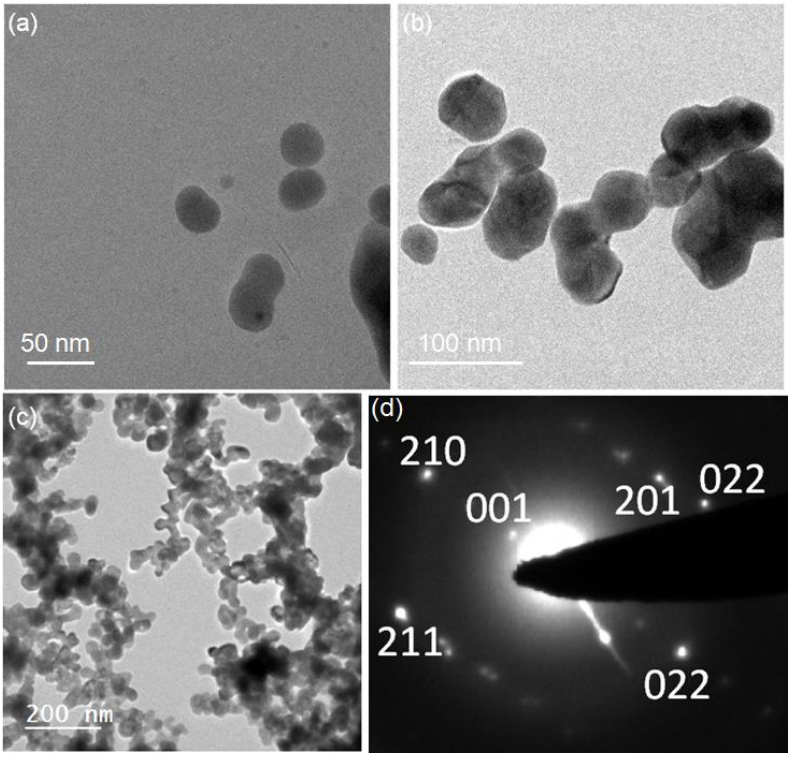

Figure 5. TEM images of Pd_2Ge_24 nanoparticles (a) growth of ellipsoidal particles from small nanopartilcles (<15 nm) (b) to smaller joined structures (c) highly connected network of Pd_2Ge_36 nanoparticles (d) shows SAED pattern from the Pd_2Ge_36 network.

3.3.2. Electrochemical Studies

The parameters obtained from the electrochemical measurements are given in **Table 1**. The stability of the catalysts was studied by running cyclic voltametric sweeps in the range -0.8 to 0.25 V in 1M aqueous KOH solution as shown in **Figure 6**. In the anodic sweep, the peaks correspond to the desorption of hydrogen (-0.8 to -0.6 V) and oxidation

of Pd (0.0 to 0.25) are quite prominent. In the cathode sweep part, the reduction of PdO (-0.05 to -0.3 V) and adsorption of hydrogen are also apparent. The processes desorption of hydrogen, oxidation of Pd, reduction of PdO and adsorption of hydrogen are marked as a, b, c and d in **Figure 6a**. Since the Pd_2Ge_36 sample proved to be a better catalyst compared to the Pd_2Ge_24 sample in terms of current, we studied the stability of this catalyst in alkaline medium upto 10 cycles (**Figure 6b**). The current value increases with increasing cycle numbers, which could be accounted by the dealloying process of Pd atoms from the bulk to the surface and hence there is an increment in the current value. This was supported by the powder XRD data with a shift of peaks towards higher 2θ (**Figure 2b**). Since PdO reduction peak current is proportional to the exposure of Pd catalytic surface to OH^- adsorption, the electrochemically active surface area (ECSA) was calculated by the integration of charges from PdO reduction region considering the value

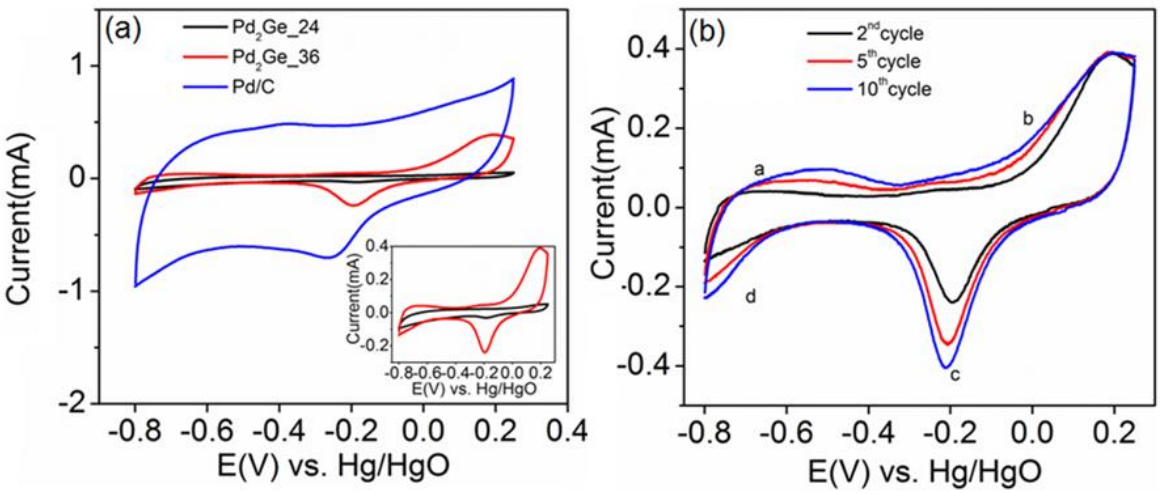

of 405μC/cm^2 for PdO monolayer reduction.[24]

Figure 6. (a) CV measurements obtained for Pd_2Ge_24, Pd_2Ge_36 and Pd/C in alkaline (1M KOH) solution at a scan rate of 50 mV/sec. The inset shows the comparison plot of CV for Pd_2Ge_24 and Pd_2Ge_36. **(b)** CV profile of Pd_2Ge_36 with respect to cycles (up to 10th cycle) at a scan rate of 50 mV/sec to check the stability of the catalyst in alkaline (1M KOH) medium.

Table 1. Summary of important parameters obtained from the ethanol oxidation.

Catalyst	ECSA (cm^2)	2^{nd} Cycle (Forward Sweep)		250^{th} Cycle (Forward Sweep)		j at -0.1V at 900s (mA/cm^2)
		J ($mAcm^{-2}$)	E (V)	J ($mAcm^{-2}$)	E (V)	
Pd/C	3.10	1.91	-0.081	0.73	-0.12	0.069
Pd_2Ge_24	0.096	2.19	-0.087	3.11	-0.11	0.138
Pd_2Ge_36	1.41	4.1	-0.074	4.64	-0.051	1.57

Typical cyclic voltammograms for EOR on Pd_2Ge_24h, Pd_2Ge_36h and Pd/C are shown in **Figure 7**. A significant increase in surface area normalized current density 4.1 $mAcm^{-2}$ (2.2 times) is observed for the sample Pd_2Ge_36 in comparison with commercial Pd/C (1.94 $mAcm^{-2}$) for the same loading clearly indicating that Ge plays a very important role in enhancing the EOR activity. A plausible reason for this could be efficient interaction of Ge with OH^- synergetic with adsorption and desorption of ethanol on Pd, which is also seen observed case of Pd-Sn catalysts.[33] Pd_2Ge_24 shows marginal increase in current density 2.12 $mAcm^{-2}$ as compared to Pd/C 1.94 $mAcm^{-2}$ for forward oxidation process in the second cycle.

The ethanol oxidation efficiency of Pd_2Ge_36 was better than its counterpart, Pd_2Ge_24 and Pd/C as observed in the cycling study (**Figure 7a and 7b**). It was seen that the catalyst is highly active till 250^{th} cycle with current density of 4.6 $mAcm^{-2}$, whereas 4.1 $mAcm^{-2}$ for the 2^{nd} cycle. The high stability of the catalyst in terms of current density upto such large cycle life infers that the catalyst is greatly resistant to surface poisoning. Still the shift of forward peak potential with 100^{th} and 250^{th} (-0.07V to -0.04V) shows the catalyst is prone to catalytic poisoning at higher cycles. In **Figure 7a**, it was noticed that the difference in current density between Pd_2Ge_24 and Pd/C was marginal but the same comparison plot for 250^{th} cycle for ethanol oxidation (**Figure 7c**), the current density of Pd_2Ge_24 has increased by 4.3 times more than that of commercial Pd/C with negligible change in peak potential strongly suggesting that the ordering in the structure plays

significant role in the stability of Pd_2Ge towards EOR activity. Interestingly, the current density of Pd/C has dropped by 2.7 times at the 250th cycle as compared to the 2nd cycle. In addition, as expected, the efficient catalyst Pd_2Ge_36 showed highest current density, which is 6.4 times more than that of Pd/C.

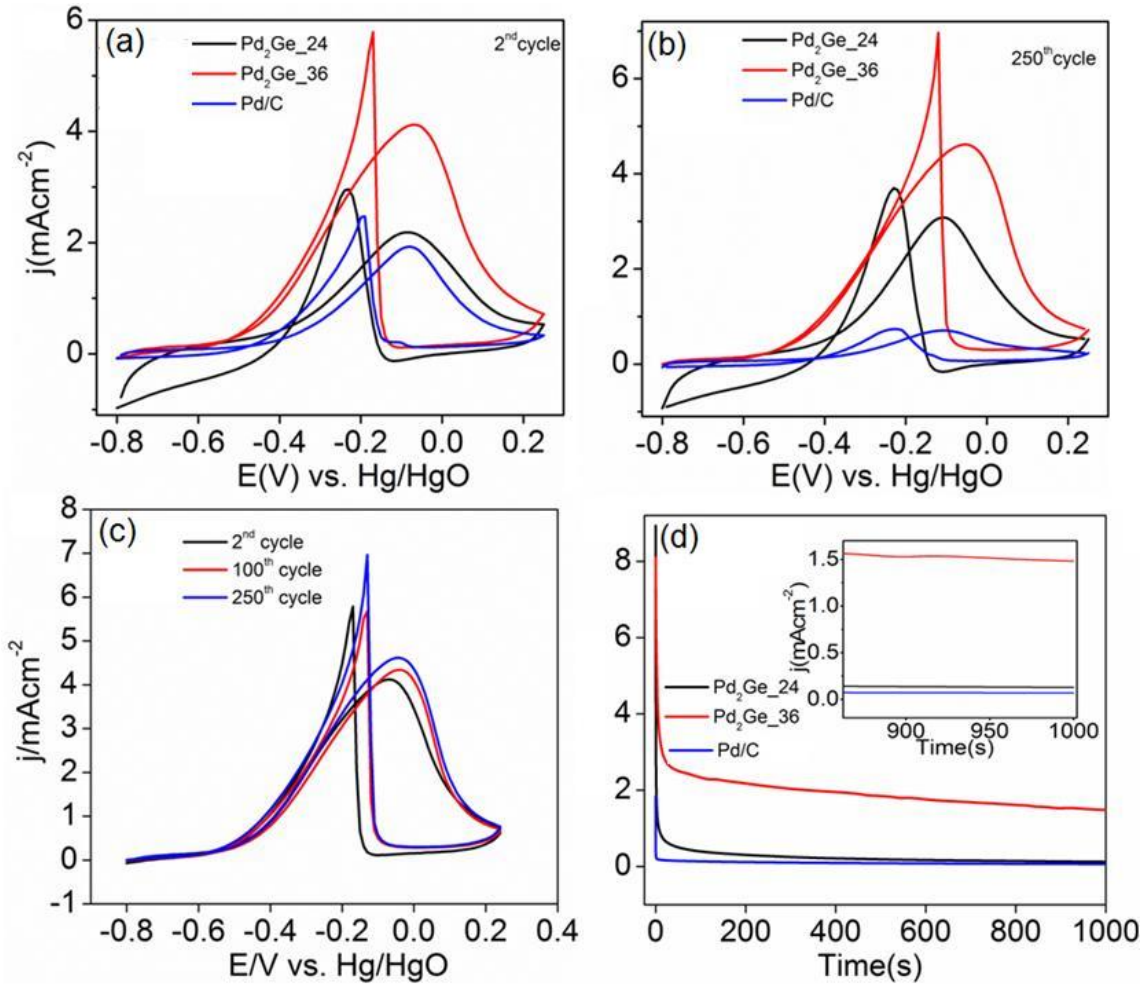

Figure 7. (a) CV curves measured for the 2nd cycle for the catalysts Pd_2Ge_24, Pd_2Ge_36 and Pd/C, (b) CV curves measured for the catalyst Pd_2Ge_36 with respect to cycle and (c) CV curves measured for the 250th cycle for the catalysts Pd_2Ge_24, Pd_2Ge_36, Pd/C. In all above cases 1 M KOH containing 1 M ethanol solution at a scan rate of 50 mV/sec were used. **(d)** Chronoamperometric measurements (CA) of Pd_2Ge_24, Pd_2Ge_36, Pd/C in 1 M KOH + 1M ethanol solution for 1000 sec at electrode potential of -0.1V vs Hg/HgO.

Figure 7d shows the chronoamperometric (CA) measurement for Pd_2Ge_36, Pd_2Ge_24 and Pd/C at -0.1V vs. Hg/HgO for the catalytic ethanol oxidation of 1M ethanol in 1M KOH for 1000s was carried out to follow the electrochemical stability of the catalyst. The stability of Pd_2Ge_36 is better than the other two catalysts. The order of decay observed was in the order of Pd_2Ge_36< Pd_2Ge_24< Pd/C, with Pd/C showing 21.7 times decay profile than Pd_2Ge_36 between 900-1000s. **Table 1** summarises the comparable data for ethanol oxidation over Pd_2Ge_24, Pd_2Ge_36 and Pd/C. The presence of Ge in Pd_2Ge crystal lattice increases the stability of the catalysts for the elelctrocatalytic oxidation of ethanol in alkaline medium. This clearly suggests that more ordering or in other words less deficiency in Pd_2Ge favours better catalytic activity and more stability towards EOR.

Figure 8 shows the charge transfer kinetic behaviour for Pd_2Ge_36 and Pd/C for EOR on based on Tafel plots obtained from the LSV measurements. Since Pd_2Ge_36 showed better activity than Pd_2Ge_24, it was chosen for the investigation of quasi steady state Tafel polarization in comparison with Pd/C. The onset potential obtained are -0.52 and -0.49 for Pd_2Ge_36 and Pd/C, respectively (**Table 2**) used in the calculation Tafel slope, which is a measure of charge transfer kinetic activity. Inset in **Figure 8** shows the linear Tafel plot obtained from the plot of log current density Vs. potential, where the potential range is -0.5V to -0.2V. The expression relating current density and potential is

$$\eta = 2.303RT\log (j/j_o)/\alpha nF$$

Where ŋ is the overpotential ($\eta = E - E_{theory}$), α is the anodic transfer coefficient, n is the number of electrons transferred in the reaction and j_o is the exchange current density, j is the current density obtained experimentally at a particular potential.

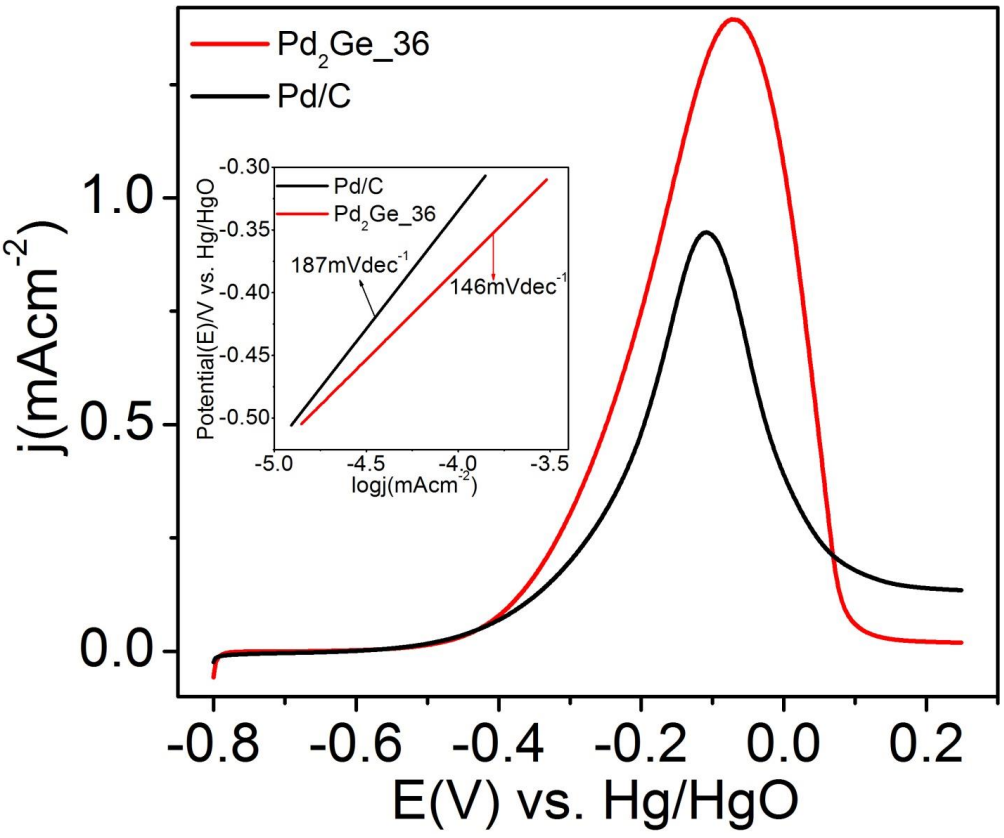

Figure 8. Quasi-steady state linear scan voltammograms of Pd/C and Pd_2Ge_36 catalysts in 1 M KOH + 1M ethanol solution , at 1.0mV/sec (Inset is the Tafel plot of Pd/C andPd_2Ge_36 in 1 M KOH + 1M ethanol solution).

The starting potential observed as 230 mV and is higher than the theoretical potential (E_{theory}) -0.87 mV.[17] Tafel slope obtained for Pd_2Ge_36 (146 $mVdec^{-1}$) is lower than Pd/C (187 $mVdec^{-1}$) indicating that Pd_2Ge_36 possess higher charge transfer kinetic activity for the EOR on the electrode surface. As a result, it can be stated that the catalyst Pd_2Ge_36 has higher efficiency for the adsorption of OH^-, which in turn affects the kinetics of EOR.[17,24] This leads to the oxidation of intermediates adsorbed on the electrode surface.

Exchange current density was calculated by extrapolating the Tafel line, where the over potential is zero. The surface activity normalized exchange current density (j_O/$mAcm^{-2}$) for Pd_2Ge_36 (38.9 $mAcm^{-2}$) is 6.6 times higher than Pd/C (5.8 $mAcm^{-2}$), as

shown in **Table 2**. Based on the Tafel slope and j_O it can be concluded that Pd_2Ge_36 is kinetically more active than the commercial Pd/C for the EOR on the catalyst surface.

Table 2. Parameters obtained from the Tafel plot based on LSV studies.

Catalyst	Onset Potential (V vs Hg/HgO)	Tafel Slope (mV/dec)	Exchange current density(mA/cm^2)
Pd/C	-0.49	187	5.8
Pd_2Ge_36	-0.52	146	38.9

3.3.3. Theoretical analysis

Most catalytic reactions are governed by Sabatier principle, which states that catalytic activity will be optimum when binding of reactive intermediates with catalytic surface has *intermediate free energies of adsorption* (*binding energies*).[42] We used this principle as a basis to rationalize the catalytic activity of Pd_2Ge. The ethanol electro-oxidation reaction in alkaline medium on the metal surface involves many steps and intermediates among which the formation of CH_3COOH (shown below) is the rate determining step.[43]

$$M-(CH_3CO)_{ads} + M-(OH)_{ads} \longrightarrow M-CH_3COOH + M$$

The main intermediate species during ethanol electro-oxidation are CH_3CO[43] and OH,[43] the latter helps in cleaning the surface of the catalyst through oxidizing the carbonecious species. We have used various initial configurations of CH_3CO and OH on Pd_2Ge and Pd (111) surfaces.

The most favorable binding configurations of CH_3CO and OH adsorbed on Pd_2Ge are determined through minimization of energy (**Figures 9a and 9b,** respectively). OH adsorbs at a minimum distance of 1.2 Å, 1.1 Å and 1.2 Å from the surface atoms on Pd (111), Pd_2Ge _24 and Pd_2Ge _36 surfaces respectively, whereas, CH_3CO adsorbs at a minimum distance of 1.79 Å, 1.49 Å and 1.79Å from the surface atoms on Pd (111), Pd_2Ge__24 and Pd_2Ge_36 surfaces, respectively. Corresponding adsorption energies are

summarized in **Table 3**. On the basis of adsorption energy it can clearly be seen that OH binds quite strongly with Pd_2Ge surfaces compared to Pd (111) surface. After OH adsorption, Pd_2Ge surface undergoes strong relaxation of about 0.2 Å compared to ~0.1 Å in case of Pd surface. This strong relaxation of Pd_2Ge surfaces shows the strong interaction between the surface and the adsorbate and hence stronger binding of OH compared to Pd (111) surface. This is also evident in density of states as shown in **Figure 10**. In case of Pd_2Ge _24and Pd_2Ge _36, OH binds strongly to the former. Also, Pd_2Ge binds strongly to CH_3CO followed by Pd (111) and Pd_2Ge_36.

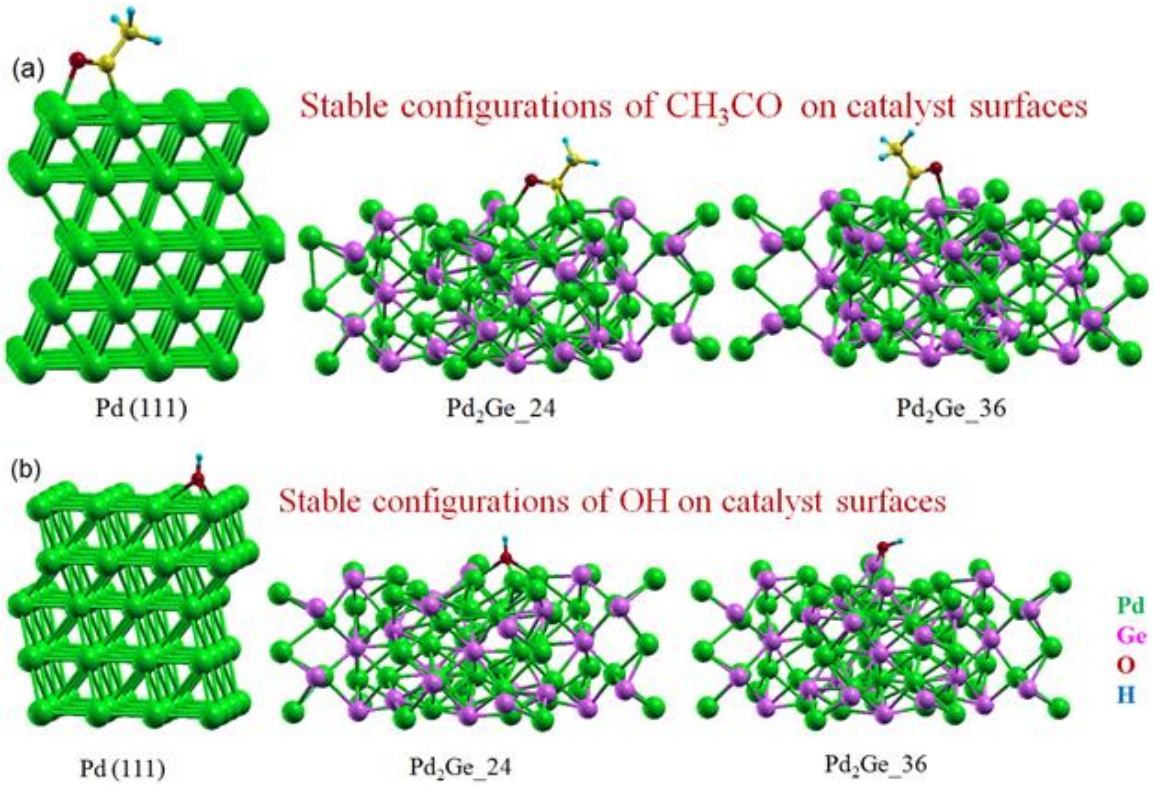

Figure 9. Adsorption of a) CH_3CO and b) OH on Pd(111), Pd_2Ge_24 and Pd_2Ge_36 samples.

To get a better insight into it, we applied d-band model proposed by Hammer and Nørskov.[44] According to this model, higher the d-band centre greater is the binding and hence, the catalytic activity. The d-band center (ε_d) is given by the following relation in this model:

$$\varepsilon_d = \frac{\int_{-\infty}^{E_F} E\rho_d(E)dE}{\int_{-\infty}^{E_F} \rho_d(E)dE}$$

where, ρ_d is the projected density of d-states of surface atoms, E is the energy and E_F is the Fermi level.

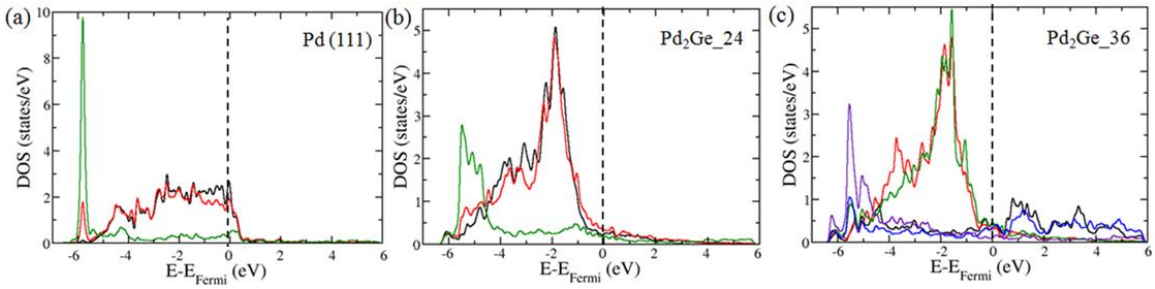

Figure 10. Projected density of states of Pd-4d, Ge-4p, and O-2p orbitals of surfaces. In case of figs. (a) and (c) surface Pd atoms, Pd atom to which O is attached and O has been represented by black, red and green curves respectively. Surface Ge and Pd, Ge and Pd to which O is attached and O is represented by black, red, green, blue and indigo curves respectively.

We have obtained the average d-band center for CH_3CO and OH adsorbed on the surface atoms (**Table 3**). The d-band model fails for Pd (111) and Pd_2Ge_24 surfaces but value of d-band center of Pd_2Ge_36 correlates well with its binding energy. Pd_2Ge _36 has fairly high value of d-band center and hence can bind strongly with OH. In case of CH_3CO adsorption d-band center lie below the Fermi level and hence binds weakly with the Pd_2Ge_36 surface. Pd_2Ge _24 is Ge-deficient and hence possesses vacant Ge sites on its surface, which have two important consequences on the binding ability with the adsorbate: first, these vacant sites themselves act as an active adsorption sites[45] and secondly, Ge vacancies will expose Pd sites to both CH_3CO and OH radicals (which also act as a catalyst poison at higher adsorption energy) to a greater extent leading to decreased coordination number,[46] and high adsorption energy (**Table 3**). Thus, the too much strong binding of adsorbate will poison the catalyst surface by decreasing the effective coverage of incoming CH_3CH_2OH molecules. Also, a good catalyst for ethanol oxidation should bind strongly with OH and weakly with CH_3CO, these two criteria are

well satisfied by Pd_2Ge_36 and Pd_2Ge_24 shows the intermediate catalytic activity between Pd (111) and Pd_2Ge_36.

The potential required for ethanol oxidation for different catalysts has been shown in **Table 1**. Using the relation, E(NHE) = E(Hg/HgO) + 0.108 V[47] we converted the potentials to NHE scale. On NHE scale, the minimum potential required for ethanol oxidation is around 4.5 eV. We obtained the work function (ϕ_s) (**Table 3**) using the following relation:

$$\phi_s = V_{vacuum} - V_{Ferni}$$

Here, V_{vacuum} and V_{Fermi} are the potentials in the vacuum and at Fermi level.

ϕ_s value clearly shows that the Pd (111) lies below on the potential scale of ethanol oxidation compared to Pd_2Ge surfaces. This also confirms the strong catalytic activity of Pd_2Ge surfaces in comparison to Pd (111) surface.

Table 3. Adsorption energies (kJ/mol) for CH_3CO and OH radical on different catalyst surfaces. Average value of d-band centers (eV) of CH_3CO and OH adsorbed surface atoms has been shown in the brackets. The work functions for different catalyst surfaces also listed in Table.

Catalyst	CH_3CO	OH	ϕ_s (eV)
Pd (111)	-335.0 (-2.50)	388.10 (-2.24)	5.7
Pd_2Ge_24	-368.78 (-2.73)	489.53 (-2.40)	5.0
Pd_2Ge_36	-288.0 (-2.90)	436.42 (-2.33)	4.9

3.4. Conclusion

Pd_2Ge nanoparticles were synthesized for the first time using the solution based chemistry. The ordered intermetallic nature of this compound was confirmed by X-ray and electron diffraction techniques. The material was tested for its electrochemical activity towards ethanol oxidation and was found to be highly active and durable upto 250 cycles compared to the commercially available catalyst (Pd/C). Our work establishes the fact that *p*-block elements can also be used like the first row transition metals as an active

constituent along with the noble metals in the form of bimetallic/alloys and/or intermetallic compound and paves the way to the detailed study of other unexplored compounds of this class. Moreover, ordered Pd_2Ge nanoparticles can also be regarded as a model system where a perfect balance between the adsorption energies of CH_3CO and OH on the catalyst surface dictates its electrocatalytic activity and the presence of vacancies in the inactive sites undoubtedly affects the course of reactivity.

3.5. References

(1) W. X. Chen, J. Y. Lee and Z. L. Liu, *Chem. Commun.*, **2002**, 2588-2589.

(2) T. T. H. Van, K. C. Pillai, H. L. Chou, C. J. Pan, J. Rick, W. N. Su, B. J. Hwang, J. F. Lee, H. S. Sheu and W. T. Chuang, *Energ. Environ. Sci.*, **2011**, 4, 4194-4200.

(3) E. Antolini, J. R. C. Salgado and E. R. Gonzalez, *J. Power Sources*, **2006**, 160, 957-968.

(4) B. Lim, M. J. Jiang, P. H. C. Camargo, E. C. Cho, J. Tao, X. M. Lu, Y. M. Zhu and Y. N. Xia, *Science*, **2009**, 324, 1302-1305.

(5) D. L. Wang, H. L. L. Xin, R. Hovden, H. S. Wang, Y. C. Yu, D. A. Muller, F. J. DiSalvo and H. D. Abruna, *Nat. Mater.*, **2013**, 12, 81-87.

(6) Y. J. Kang, L. Qi, M. Li, R. E. Diaz, D. Su, R. R. Adzic, E. Stach, J. Li and C. B. Murray, *ACS Nano*, **2012**, 6, 2818-2825.

(7) B. Y. Xia, H. B. Wu, X. Wang and X. W. Lou, *J. Am. Chem. Soc.*, **2012**, 134, 13934-13937.

(8) M. H. Huang, G. F. Dong, N. Wang, J. X. Xu and L. H. Guan, *Energ. Environ. Sci.*, **2011**, 4, 4513-4516.

(9) Y. C. Hsieh, Y. Zhang, D. Su, V. Volkov, R. Si, L. J. Wu, Y. M. Zhu, W. An, P. Liu, P. He, S. Y. Ye, R. R. Adzic and J. X. Wang, *Nat. Comm.*, **2013**, 4.

(10) Y. Lee, J. Kim, D. S. Yun, Y. S. Nam, Y. Shao-Horn and A. M. Belcher, *Energ. Environ. Sci.*, **2012**, 5, 8328-8334.

(11) J. F. Chang, L. G. Feng, C. P. Liu, W. Xing and X. L. Hu, *Energ. Environ. Sci.*, **2014**, 7, 1628-1632.

(12) E. H. Yu, X. Wang, U. Krewer, L. Li and K. Scott, *Energ. Environ. Sci.*, **2012**, 5, 5668-5680.

(13) C. Koenigsmann and S. S. Wong, *Energ. Environ. Sci.*, **2011**, 4, 1161-1176.

(14) S. Y. Shen, T. S. Zhao, J. B. Xu and Y. S. Li, *Energ. Environ. Sci.*, **2011**, 4, 1428-1433.

(15) S. J. Guo, S. J. Dong and E. K. Wang, *Energ. Environ. Sci.*, **2010**, 3, 1307-1310.

(16) E. Antolini, *Energ. Environ. Sci.*, **2009**, 2, 915-931.

(17) C. Xu, P. k. Shen and Y. Liu, *J. Power Sources*, **2007**, 164, 527-531.

(18) J. E. Mcmurry and R. C. Fay, Pearsons publications, New Delhi, **2008**.

(19) S. Meenakshi, P. Sridhar and S. Pitchumani, *RSC Advances*, **2014**, 4, 44386-44393.

(20) J. Bagchi and S. K. Bhattacharya, *J. Power Sources*, **2007**, 163, 661-670.

(21) M. Wang, D. J. Guo and H. L. Li, *J. Solid State Chem.*, **2005**, 178, 1996-2000.

(22) K. F. Zhang, D. J. Guo, X. Liu, J. Li, H. L. Li and Z. X. Su, *J. Power Sources*, **2006**, 162, 1077-1081.

(23) C. W. Xu, P. K. Shen and Y. L. Liu, *J. Power Sources*, **2007**, 164, 527-531.

(24) H. T. Zheng, Y. L. Li, S. X. Chen and P. K. Shen, *J. Power Sources*, **2006**, 163, 371-375.

(25) C. W. Xu, Z. Q. Tian, P. K. Shen and S. P. Jiang, *Electrochim. Acta.*, **2008**, 53, 2610-2618.

(26) D. B. Chu, J. Wang, S. X. Wang, L. W. Zha, J. G. He, Y. Y. Hou, Y. X. Yan, H. S. Lin and Z. W. Tian, *Catal. Commun.*, **2009**, 10, 955-958.

(27) Z. P. Sun, X. G. Zhang, R. L. Liu, Y. Y. Liang and H. L. Li, *J. Power Sources*, **2008**, 185, 801-806.

(28) Z. Y. Zhang, L. Xin, K. Sun and W. Z. Li, *Int. J. Hydrogen. Energ.*, **2011**, 36, 12686-12697.

(29) S. C. Lin, J. Y. Chen, Y. F. Hsieh and P. W. Wu, *Mat. Lett.*, **2011**, 65.

(30) L. H. Shi, A. Q. Wang, Y. Q. Huang, X. W. Chen, J. J. Delgado and T. Zhang, *Eur. J. Inorg. Chem.*, **2012**, 2700-2706.

(31) Q. F. Yi, F. J. Niu, L. H. Song, X. P. Liu and H. D. Nie, *Electroanal.*, **2011**, 23, 2232-2240.

(32) T. Herranz, M. Ibáñez, J. L. Gómez de la Fuente, F. J. Pérez-Alonso, M. A. Peña, A. Cabot and S. Rojas, *Chem. Electro. Chem.*, **2014**, 1, 885-895.

(33) W. X. Du, K. E. Mackenzie, D. F. Milano, N. A. Deskins, D. Su and X. W. Teng, *ACS Catal.*, **2012**, 2, 287-297.

(34) R. Kodiyath, G. V. Ramesh, E. Koudelkova, T. Tanabe, M. Ito, M. Manikandan, S. Ueda, T. Fujita, N. Umezawa, H. Noguchi, K. Ariga and H. Abe, *Energ. Environ. Sci.*, **2015**.

(35) L. Rao, Y.X. Jiang, B.-W. Zhang, Y.R. Cai and S.G. Sun, *Phys. Chem. Chem. Phys.*, **2014**, 16, 13662-13671.

(36) W. Hong, J. Wang and E. Wang, *ACS App. Mater. Inter.*, **2014**, 6, 9481-9487.

(37) W. S. Wopersnow, K. , *J. Less-Common Met.*, **1977**, 52.

(38) G. Paolo, B. Stefano, B. Nicola, C. Matteo, C. Roberto, C. Carlo, C. Davide, L. C. Guido, C. Matteo, D. Ismaila, C. Andrea Dal, G. Stefano de, F. Stefano, F. Guido, G.

Ralph, G. Uwe, G. Christos, K. Anton, L. Michele, M.-S. Layla, M. Nicola, M. Francesco, M. Riccardo, P. Stefano, P. Alfredo, P. Lorenzo, S. Carlo, S. Sandro, S. Gabriele, P. S. Ari, S. Alexander, U. Paolo and M. W. Renata, *J. Phys. Condens. Matter.*, **2009**, 21, 395502.

(39) J. P. Perdew and A. Zunger, *Phys. Rev. B*, **1981**, 23, 5048-5079.

(40) W. Hong, J. Wang and E. Wang, *Acs Appl. Mater. Inter.*, **2014**, 6, 9481-9487.

(41) L. H. Shi, A. Q. Wang, Y. Q. Huang, X. W. Chen, J. J. Delgado and T. Zhang, *Eur. J. Inorg. Chem.*, **2012**, 2700-2706.

(42) P. Sabatier, *Ber. Deutschen Chem. Gesellschaft*, **1911**, 44, 1984-2001.

(43) Z. X. Liang, T. S. Zhao, J. B. Xu and L. D. Zhu, *Electrochimica Acta*, **2009**, 54 2203–2208.

(44) B. Hammer and J. K. Nørskov, *Surf. Sci.*, **1995**, 343, 211-220.

(45) E. Gonzalez, P. Jasen, G. Gonzalez, L. Moro and A. Juan, *Phys. Status Solidi*, **2009**, B246, 1275–1285.

(46) F. Calle-Vallejo, J. I. Martinez, J. M. Garcia- Lastra, P. Sautet and D. Loffreda, *Angew. Chem. Int. Ed.*, **2014**, 53, 8316 –8319.

(47) R. A. Nickell, W. H. Zhu, R. U. Payne, D. R. Cahela and B. J. Tatarchuk, *J. Power Sources*, **2006**, 161, 1217-1224.

Chapter 4

Effect of Morphology of Ordered $PdCu_3$ Nanocrystals on Electrocatalytic Oxygen Reduction Reaction in Alkaline Medium

Abstract

We have synthesized ordered intermetallic $PdCu_3$ nanocrystals in different morphology by facile solvothermal method using oleylamine both as solvent, surfactant and reducing agent. The particle size of the nanoparticles obtained is in the range 10-15 nm. High resolution transmission electron microscopy confirms that sphere ($PdCu_3$_S) and cube ($PdCu_3$_C) shaped nanocrystals are composed of (111) and (100) planes, respectively. We have evaluated the catalytic activities of both types towards Oxygen Reduction Reaction (ORR) in alkaline medium. The activity of the catalyst for ORR was found in the order of $PdCu_3$_S < $PdCu_3$_C. The limiting current density and mass activity of $PdCu_3$_C is 1.24 and 3.58 times higher than $PdCu_3$_S. The activity of $PdCu_3$ is comparable to the state of art Pt/C catalyst.

4.1. Introduction

Although fuel cells are considered as one of the major sources of green energy as they directly convert hydrogen and oxygen into electricity and water,[1] one of the major issues towards the high efficiency of the fuels cells is the sluggish reaction kinetics of the Oxygen Reduction Reaction (ORR) at the cathode.[2,3] Therefore, development of highly active and stable electrocatalyst for ORR is one of the major challenges in fuel cells and metal-air batteries. As a part of improving the activity of the catalyst in fuel cell, currently alkaline fuel cell research is gaining more interest because of enhanced stability and activity of the catalysts under basic conditions and the absence of specific adsorption of spectator ions present in acidic medium.[4-10] In comparison with Pt relatively more abundance and low cost and having less poisoning effect[11,12] Pd makes it as promising alternative electrocatalysts for ORR. But the intrinsic ORR activity of Pd is at least five times lower than that of Pt counterparts.[13,14] It has been reported that combination of Pd with other metals like Ni,[15,16] Fe,[14,17] Sn,[18] Co,[19,20] Ti,[21] Cr,[22] Cu[23-25] and Bi[26] in bimetallic, alloy or intermetallic structures enhances the ORR activity as well as stability compared to pure Pd metal. The increase in ORR activity of Pd based alloys has been proposed as the modification of electronic structure of Pd upon alloying with other metals.[13,27,28] Another way to activity enhancement can be the crystal facet engineering. Due to different OH_{ads} coverage and available active sites in different planes of Pd, the activity order for different crystallographic planes of Pd are found to be in the order: Pd (110)< Pd (111) < Pd (100) in both acidic and alkaline medium.[29-31]

There are two objectives have put to achieve the goal on the development of a catalyst with activity on par or better than the existing Pt based materials; first one is to develop an ordered Pd based compound and secondly crystallographically engineer the

facets. In order to achieve these, we have synthesized ordered $PdCu_3$ nanocrystals using a facile one pot solvothermal synthesis. The morphology has been controlled by varying solvent, stabilizer and reducing agent. To the best of our knowledge, this is the first attempt has been done on the synthesis and shape variation of ordered intermetallic nanoparticles without using any external reducing agent. The use of intermetallic nanocrystals is advantageous over alloys and bimetallic because of uniform surroundings of the active sites. Cube shaped $PdCu_3$ ($PdCu_3$_C) nanocrystals are found to be more active than that of sphere analogue ($PdCu_3$_S) and having comparable activity to the state of art commercial Pt/C catalyst.

4.2. Experimental Section

4.2.1. Chemicals

Palladium acetylacetonate ($Pd(acac)_2$), oleylamine and nafion binder (5 wt%) were purchased from Sigma-Aldrich, hexdecyltrimethylammonium bromide (CTAB) were purchased from SDFCL and copper acetylacetonate ($Cu(acac)_2$) was purchased from Alfa Aesar. All the chemicals (more than 99% purity) were used as purchased without further purification. Millipore water of conductivity 18.2 MΩcm was used for the synthesis and all other studies.

4.2.2. Synthesis

$PdCu_3$ intermetallic nanoparticles were synthesized in different sizes and morphology by solvothermal method. In a typical solvothermal procedure, 0.1 mmol $Pd(acac)_2$, 0.3 mmol $Cu(acac)_2$ and 75 mg CTAB were mixed together in 18 ml oleylamine with vigorous stirring and loaded in 23 ml Teflon lined autoclave. The autoclave was kept at 180 ^oC for 24 hrs. $PdCu_3$ nanocubes were obtained by changing the solvent from oleylamine to 8:1 ratio of oleylamine and oleic acid, respectively. The

product was repeatedly washed several times with a 1:1 mixture of hexane and ethanol and dried in vacuum oven at 60 ^{o}C for 6hrs.

4.2.3. Powder X-ray Diffraction (PXRD)

PXRD measurements were done at room temperature on a Rigaku Miniflex X-ray diffractometer with Cu-K_α X-ray source (λ = 1.5406 Å), equipped with a position sensitive detector in the angular range $20^o \leq 2\theta \leq 80^o$ with the step size 0.02^o and scan rate of 0.5 s/step calibrated against corundum standards. The experimental patterns were compared to the pattern simulated from the data reported in the literature.[32]

4.2.4. Elemental Analysis

Quantitative microanalysis on all the samples were performed with a FEI NOVA NANOSEM 600 instrument equipped with an EDAX® instrument. Data were acquired with an accelerating voltage of 20 kV and a 100 s accumulation time. The EDAX analysis was performed using P/B-ZAF standardless method (where, Z = atomic no. correction factor, A = absorption correction factor, F = fluorescence factor, P/B = peak to background model) on selected spots and points.

4.2.5. Transmission electron microscopy (TEM)

TEM and high resolution TEM (HRTEM) images, selected area electron diffraction (SAED) patterns were collected using a JEOL 200 TEM instrument. Samples for these measurements were prepared by dropping a small volume of sonicated nanocrystalline powders in ethanol onto a carbon-coated copper grid.

4.2.6. X-ray photoelectron spectroscopy (XPS)

XPS measurement has been performed with Mg-Kα (1253.6 eV) X-ray source with a relative composition detection better than 0.1% on an Omicron Nanotechnology spectrometer.

4.2.7. Electrochemical Studies

All the electrochemical measurements were performed on a CHI 660C electrochemical workstation with three electrode channels at room temperature. Three electrode set-up consists of a glassy carbon (GC) (having diameter 3 mm) rotating disk electrode (RDE) (Pine Research Instrumentation) as working electrode, platinum foil as counter electrode and Hg/HgO (MMO) as reference electrodes. The electrolyte was 0.5M KOH solution prepared with ultrapure water (Millipore, 18.2 MΩcm). The catalyst ink was prepared by dispersing 2 mg of catalyst in 1 mL of mixed solvent solution (IPA: H_2O=1:1 v/v) and 10 µL of 1 wt% nafion binder. The nafion binder (5 wt%) was diluted to 1 wt% with isopropyl alcohol (IPA). From the prepared catalyst ink 20 µL was dropcasted on GC electrode and dried overnight in air. Before depositing the catalyst, the GC electrode was polished with 0.05 µm alumina slurry, washed several times with distilled water. Commercial Pt/C (40 wt%, Sigma Aldrich) was used for comparison of activity with the $PdCu_3$ catalysts. The geometrical surface area of the GC electrode exposed to the electrolyte solution was 0.07065 cm^2. The electrolyte solution was deaerated by purging nitrogen gas into the solution at least 30 min before each experiment. The cyclic voltammetry (CV) measurements were performed between -0.7V-0.1V at a scan rate of 50 mV/sec. The ORR electrocatalytic activity of $PdCu_3$ were performed in 0.5M KOH solution purged with high purity O_2 gas for at least 30 min to ensure O_2 saturation. Linear sweep voltammetry (LSV) measurements during ORR were carried out in O_2-saturated 0.5M KOH solution 5 mV/sec with the electrode rotated at 100-1600 rpm. The kinetic current density for the ORR was derived from the Koutecky-Levich equation:

$$1/j = 1/j_k + 1/j_d = 1/j_k + 1/Bw^{1/2}$$

Where j is the measured current density, w is the electrode rotation speed and j_k, j_d are kinetic and diffusion limited current densities respectively and "B" is called "B-factor" which is given by the following equation:

$$B= 0.62nFD_0^{2/3} v^{-1/6}C_0$$

Where n is the apparent no of electron transferred in the reaction, F is the Faraday constant, D_o is the diffusion co-efficient of O_2 (D_o= $1.65\times 10^{-5}cm^2s^{-1}$), C_0 is the concentration of O_2 dissolved in electrolyte (C_0= 1.03×10^{-6} $molcm^{-3}$), v is the kinematic viscosity of the solution (v= 0.01 cm^2s^{-1}).

4.3. Results and Discussions

4.3.1. Structure, Morphology and Composition Analysis

A typical representation of the unit cell of intermetallic $PdCu_3$ is shown in **Figure1**. $PdCu_3$ crystallizes in cubic phase with space group $Pm\bar{3}m$. Pure palladium metal has a face centered cubic crystal structure ($Fm\bar{3}m$) where all the corners and faces are occupied by the Pd atoms (Wyckoff no. 4*a*). While, in $PdCu_3$ the Pd atoms occupy the corner positions (Wyckoff no. 1*a*) and the Cu atoms occupy half of the octahedral holes (Wyckoff no. 3*c*). Such an ordered arrangement of Cu atoms within the lattice of Pd is

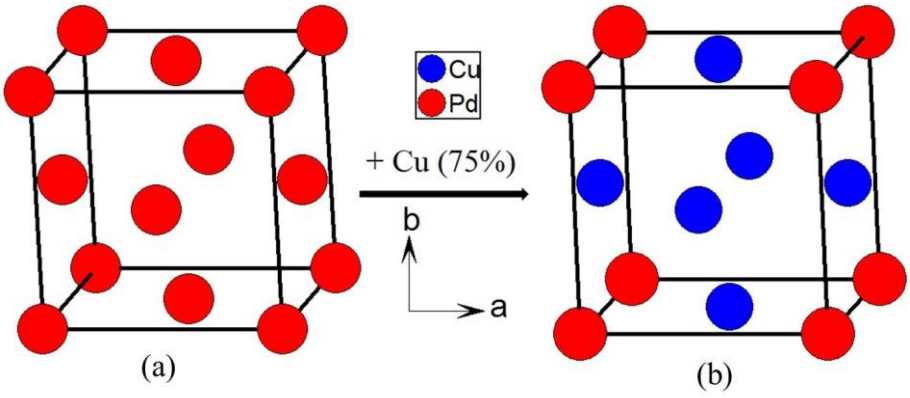

Figure 1. The crystal structure comparison of Pd (a) and $PdCu_3$ (b) along the *c*-direction.

expected to increase the catalytic activity. **Figure 2** shows the PXRD pattern of the as synthesized $PdCu_3$ in different morphology at 180 ^oC varying ratio of the co-solvent (oleylamine: Oleic acid) and surfactant. Comparison of the experimental PXRD with the simulated pattern of the bulk compounds clearly shows pure phase without any impurity.

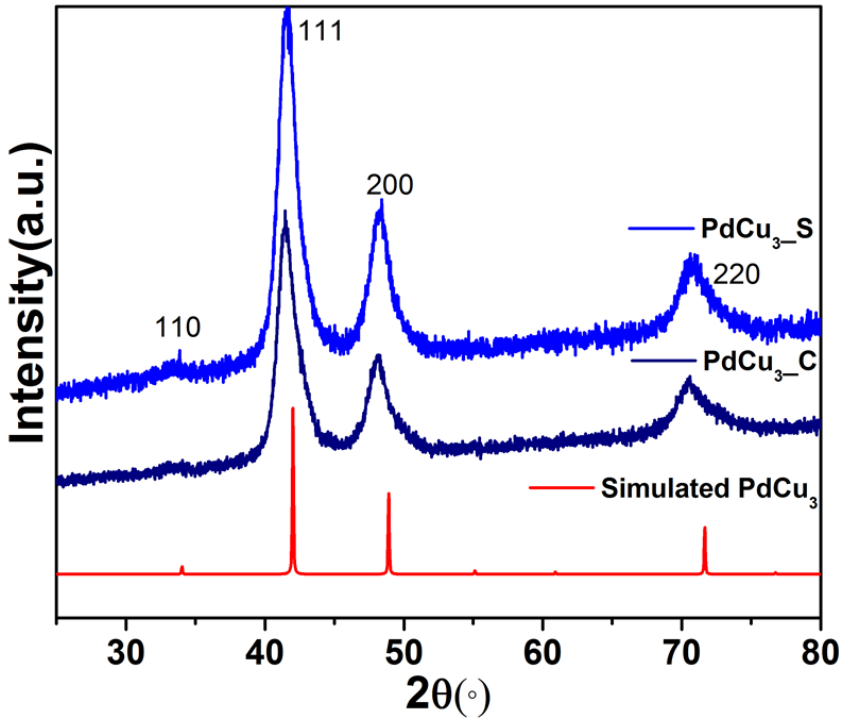

Figure 2. Comparison of PXRD patterns of different shaped $PdCu_3$ nanoparticles synthesized by solvothermal technique at 180 ^oC in different solvents with simulated powder pattern from bulk $PdCu_3$ intermetallic compound.

The crystallite size obtained from Scherer formula for $PdCu_3$_S and $PdCu_3$_C are respectively 6 and 9 nm, which is close to the particle size obtained from the TEM images (**Figures 3a and b**). It has already been reported that oleylamine can simultaneously act as solvent, reducing agent and stabilizer for the synthesis of metal nanocrystals.[33] The tailoring of morphology from sphere to cube/truncated cube is dependent on both oleic acid and CTAB. Only in oleylamine sphere shaped nanoparticle is forming. But in the 8:1 mixture of oleylamine and oleic acid along with CTAB, $PdCu_3$_C was formed. A probable explanation can be based on the specific binding of the surfactant/capping agent to a particular crystal facet. It is well known that oleylamine with $–NH_2$ group binds onto the

(100) crystal facet and hinders the growth along (100).[34,35] On the other hand, oleic acid with a carboxylic group, -COOH has a selective binding on the (111) facet,[34] thus facilitating the growth along (100) direction. Additionally, CTAB also plays an important role in cube formation as no cube shaped particle was formed in the absence of CTAB (**Figure 4**). Firstly, CTAB preferentially binds parallel to the (110) planes of the crystals and favours the growth along (100) direction.[36,37] Secondly, the presence of CTAB can affect the reduction rates of the Pd and Cu salt by the advanced formation of Cu nanocrystal although the standard reduction potential (E) for Pd^{II}/Pd (0.98V) is more positive than that of Cu^{II}/Cu (0.34V). Finally, galvanic replacement of Cu nanocrystals with Pd species in the solution leads to the formation of cube/truncated cube shaped nanoparticles.[38,39] The d-spacing calculated from HRTEM images (**Figures 3c and 3d**) are 0.225 nm and 0.389 nm, respectively for $PdCu_3$_S and $PdCu_3$_C nanoparticles. This clearly indicates that the exposed facets for $PdCu_3$_S and $PdCu_3$_C nanoparticles are (111) and (100), respectively. Formation of intermetallic $PdCu_3$ was further confirmed by SAED patterns (**Figures 3e and 3f**) containing (111), (200), (300), (311) planes of the ordered structure.

EDAX elemental analysis gave the atomic percentage 78.87± 2.6, 77.71±3.4 and 21.13±1.1, 22.29±1.5 respectively for Cu and Pd which is very close to the expected stoichiometric ratio 3:1 for $PdCu_3$_C and $PdCu_3$_S nanoparticles (**Figure 5**). The core-level XPS spectra of Pd 3d, Cu 2p are presented in **Figure 6**. **Figures 6a** and **6c** show the core-level spectra of Pd $3d_{5/2}$ (~335.5 eV), Pd $3d_{3/2}$ (~340.5 eV) and Cu $2p_{3/2}$(~932.5 eV), Cu $2p_{1/2}$(~952 eV) for $PdCu_3$_S and Pd $3d_{5/2}$(335.2 eV) clearly indicates the Pd^{0+} and Cu^{0+} states in the synthesized $PdCu_3$ compounds.[40]

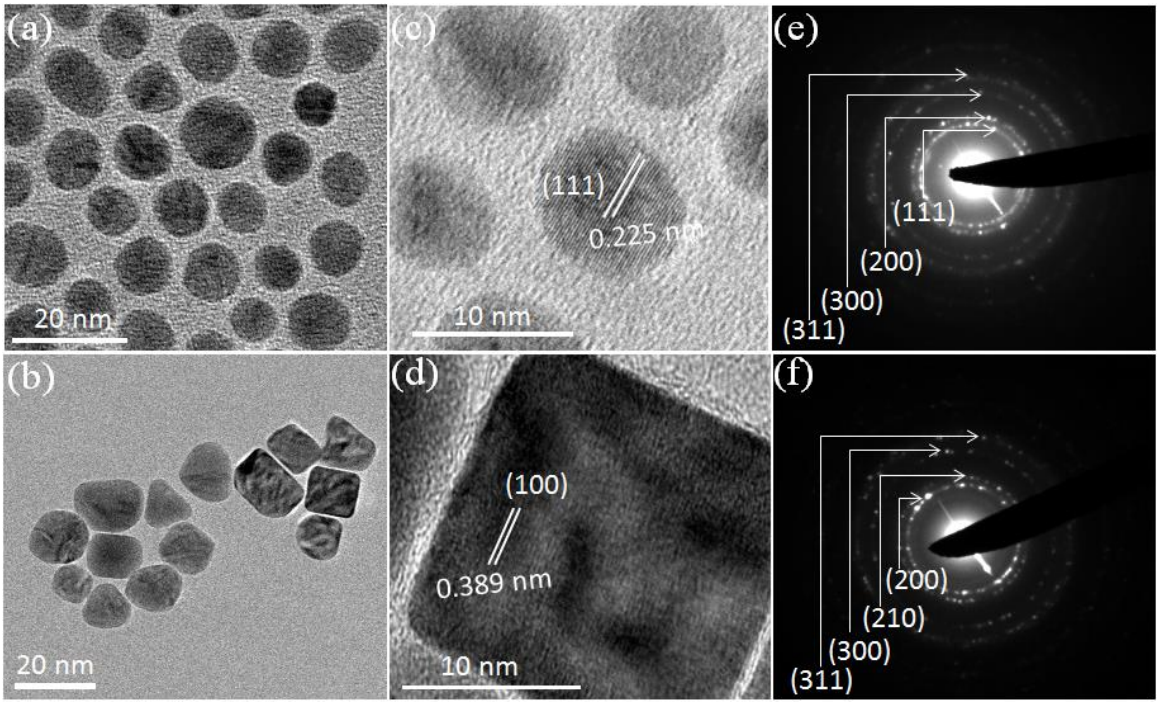

Figure 3. (a, b) TEM images, (c, d) HRTEM images, (e, f) SAED patterns of $PdCu_3$_S $PdCu_3$_C, respectively.

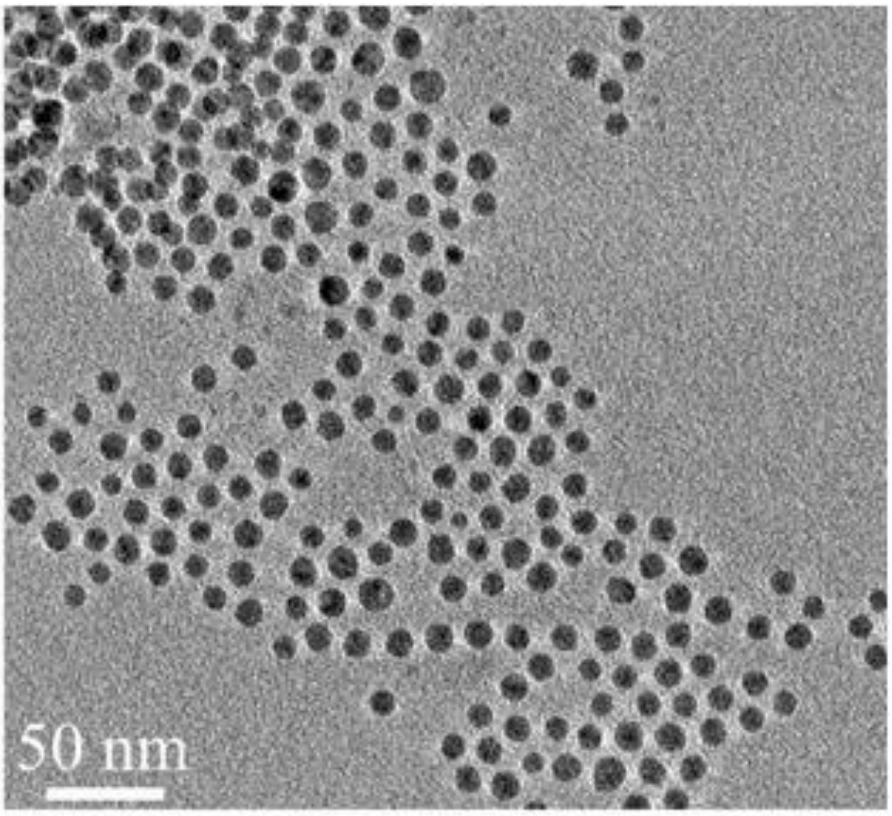

Figure 4. $PdCu_3$ nanoparticles synthesized in 8:1mixture of oleylamine and oleic acid in absence of CTAB.

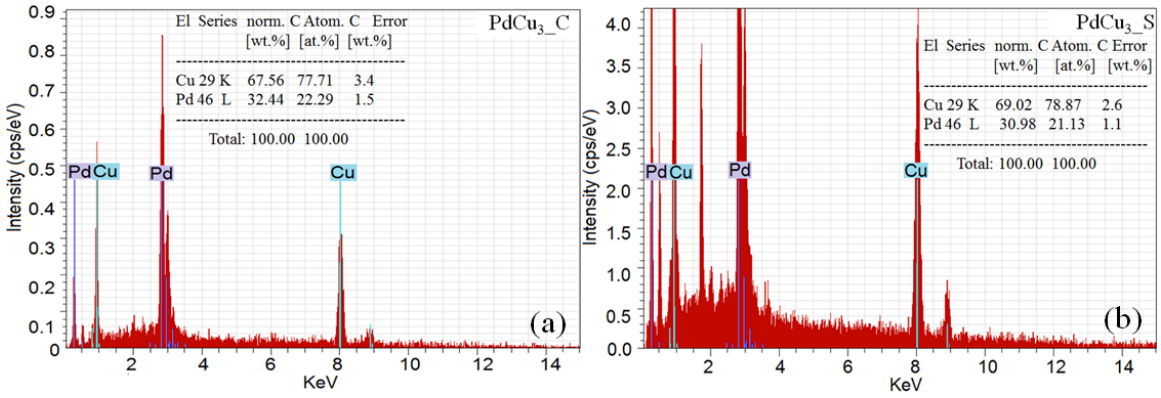

Figure 5. EDAX spectrum of (a) $PdCu_3$_S, (b) $PdCu_3$_C nanocrystals. The average chemical compositions of Pd and Ge are listed in the figure.

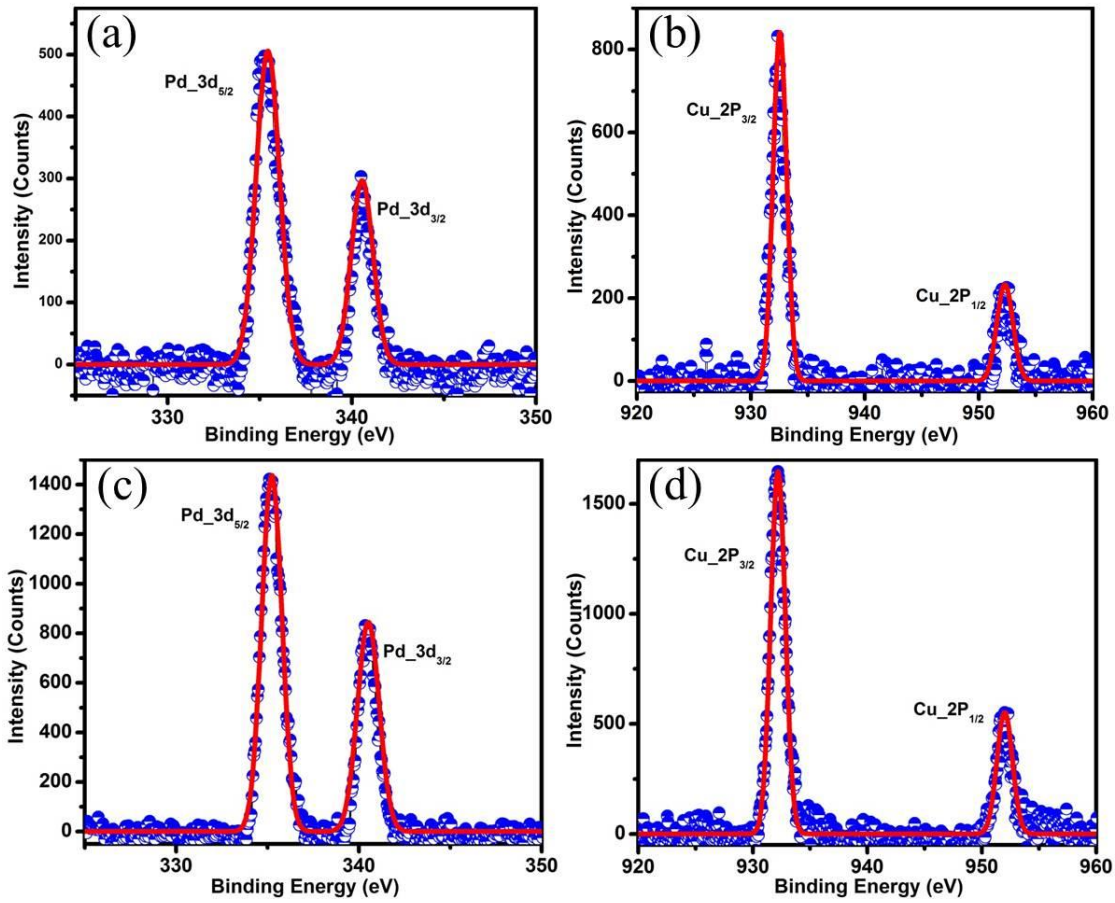

Figure 6. Core-level XPS spectra of $PdCu_3$ samples (a-c) for $PdCu_3$_S, (c-d) $PdCu_3$_C.

4.3.2. Electrocatalytic Activity of ordered $PdCu_3$ nanocrystals

Cyclic voltammetry (CV) of a typical $PdCu_3$ nanoparticle coated on GC in both O_2-saturated and N_2-saturated 0.5 M KOH solution is shown in **Figure 7**. In the

voltametric profile, PdO formation (-0.3 to 0.1V) and reduction (-0.25 to -0.4V) regions are well defined. But hydrogen adsorption/desorption region is not so clear which is common for Pd based catalysts in alkaline medium due to the influence of OH^-.[12,40-42] In the potential region (-0.15 to -0.4V) the onset potential for PdO reduction region is shifted to more positive potential with enhancement in current in case of O_2-saturated solution. This suggests oxygen adsorption at low potential and thus enhancement of the ORR kinetics.[43,44]

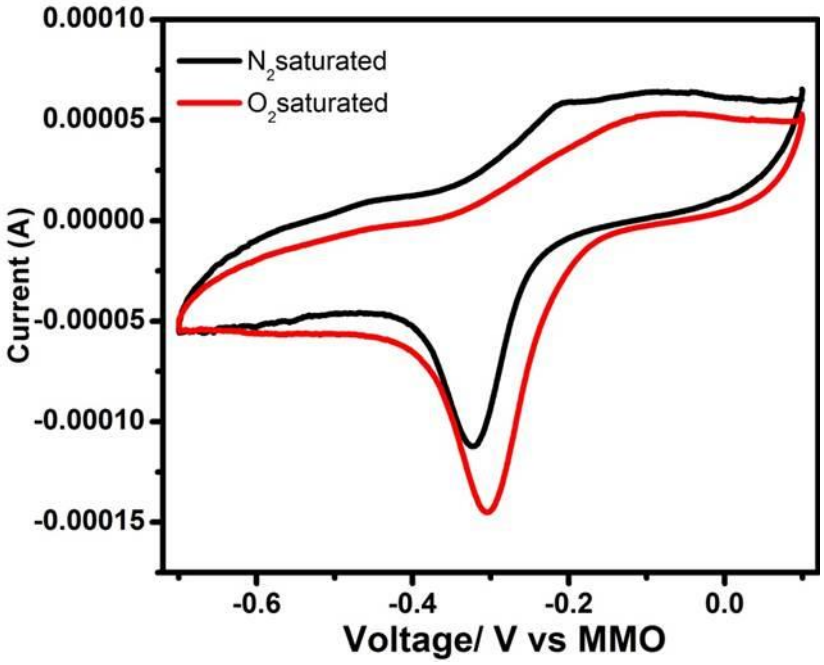

Figure 7. Cyclic Voltametry of $PdCu_3$ nanoparticle in both N_2 and O_2-saturated 0.5 M KOH solution with a sweep rate of 50 mV/sec.

The polarization curves for ORR the on both $PdCu_3$ nanospheres and nanocubes at different rotation rates are shown in **Figure 8(a, b)** in which current densities are normalised with respect to the geometrical surface area (0.07065 cm^2). They all reached a well-defined diffusion limited current. **Figure 8(c, d)** shows the corresponding K-L plot obtained from the inverse current densities (j^{-1}) as a function of inverse square root of rotation rate ($w^{-1/2}$) at different potentials, respectively. The K-L plots are linear indicating

first order dependence of the kinetics of ORR on $PdCu_3$ surface. The slope and intercept of the straight lines will give "B-factor" and kinetic current (i_k) respectively. The number of electrons calculated from the slope of K-L plots is close to four in each case. Hence the ORR on the $PdCu_3$ surface proceed with n= $4e^-$ reaction pathway.

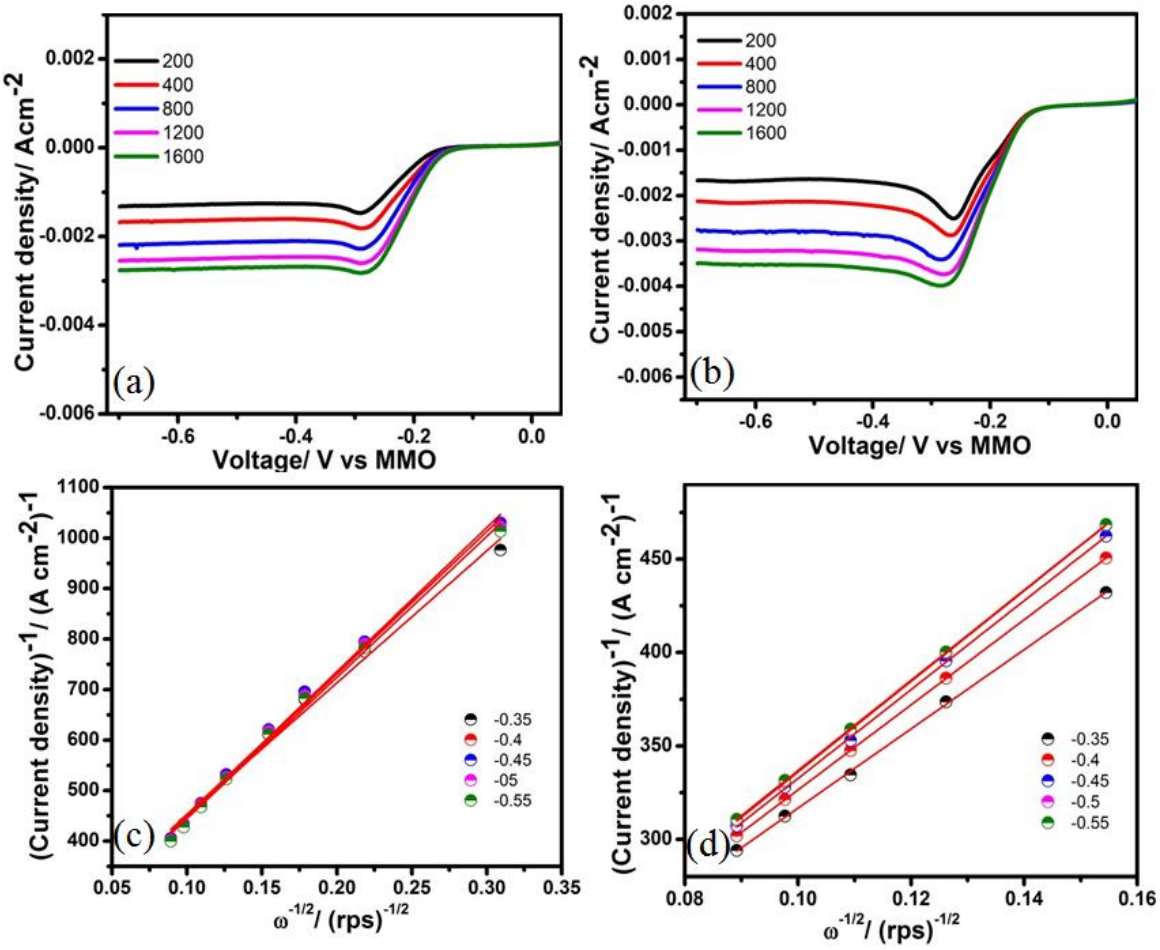

Figure 8. LSV polarisation curves for the ORR on $PdCu_3$_S (a), $PdCu_3$_C (b) in O_2-saturated 0.5M KOH at a scan rate of 5mV/sec, Koutecky- Levich plots of sphere (c), cube (d) electrode at different potentials.

The comparison between ORR activities on $PdCu_3$_S, $PdCu_3$_C and commercial Pt/C (40 wt%) is shown in **Figure 9**. The currents shown were measured at 1200 rpm. The activity for ORR in terms of onset potential follows the trend: $PdCu_3$_S< $PdCu_3$_C ~ commercial Pt/C (40 wt %). There is a positive shift of 30 mV and negative shift of 10 mV in the onset potential of $PdCu_3$_C as compared to $PdCu_3$_S and commercial Pt/C. The

limiting current densities increase as follows: $PdCu_3$_S ~ commercial Pt/C< $PdCu_3$_C. $PdCu_3$_C was found to be 1.24 times more active than that of $PdCu_3$_S and commercial Pt in terms of limiting current density value.

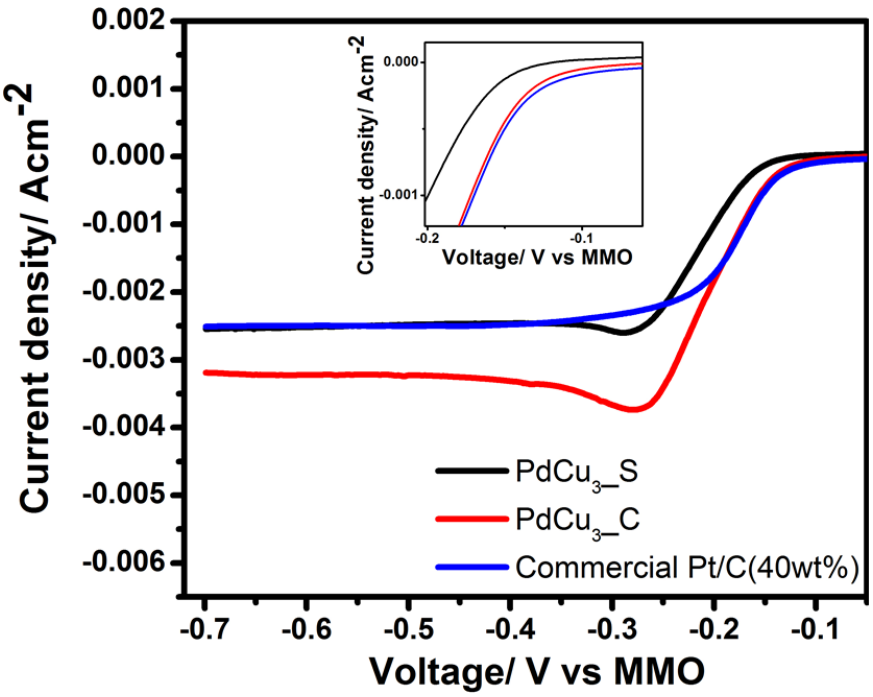

Figure 9. Comparison of oxygen reduction currents measured on $PdCu_3$_S, $PdCu_3$_C and commercial Pt/C at a rotation speed of 1200 rpm with a sweep rate of 20mV/sce.

After 500 cycles, the current density value for the $PdCu_3$_S was found to be decreased by 1.77 times whereas for $PdCu_3$_C it is almost same (**Figure 10**). This result indicates $PdCu_3$_C electrode is highly stable compared to $PdCu_3$_S. **Figure 11a** shows the mass activity order close to onset potential (-0.15V) follows the order $PdCu_3$_S< $PdCu_3$_C ~ commercial Pt/C (40 wt %). The mass activity of $PdCu_3$_C was found to be 3.58 times more than $PdCu_3$_S and 1.12 times less than commercial Pt. From the comparison data in terms of current densities, onset potential and stability, it can be told the overall ORR activity order is as follows: $PdCu_3$_S< $PdCu_3$_C ~ commercial Pt/C (40 wt %). To evaluate ORR activity in presence of methanol-containing electrolyte, chronoamperometric measurement was performed at -0.3V where ORR kinetics was high.

From the **Figure 11b**, $PdCu_3$ catalysts were found to be methanol tolerant whereas commercial Pt/C ORR kinetics was affected by methanol.

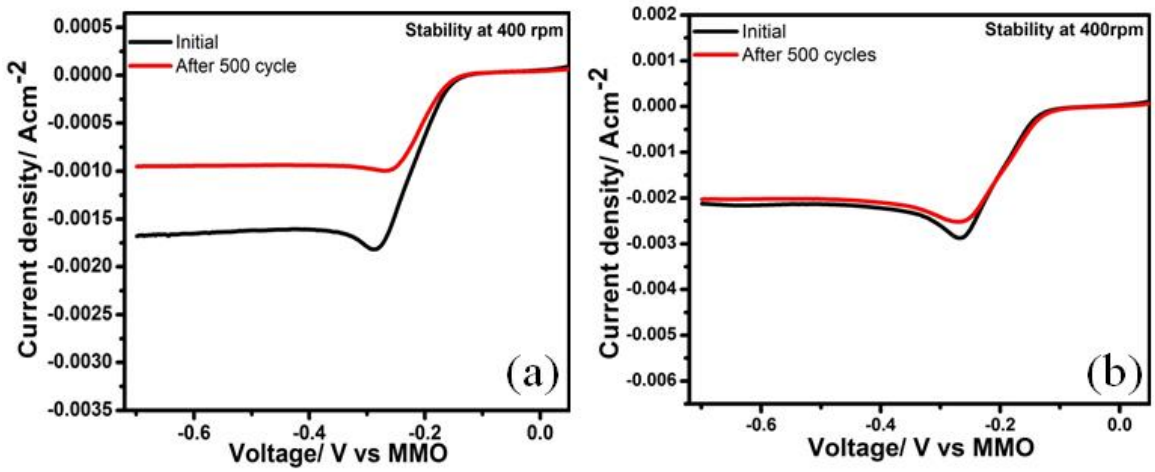

Figure 10. ORR polarisation curves before and after 500 potential cycles between 0.1 to -0.7V at a rotation speed of 400 rpm.

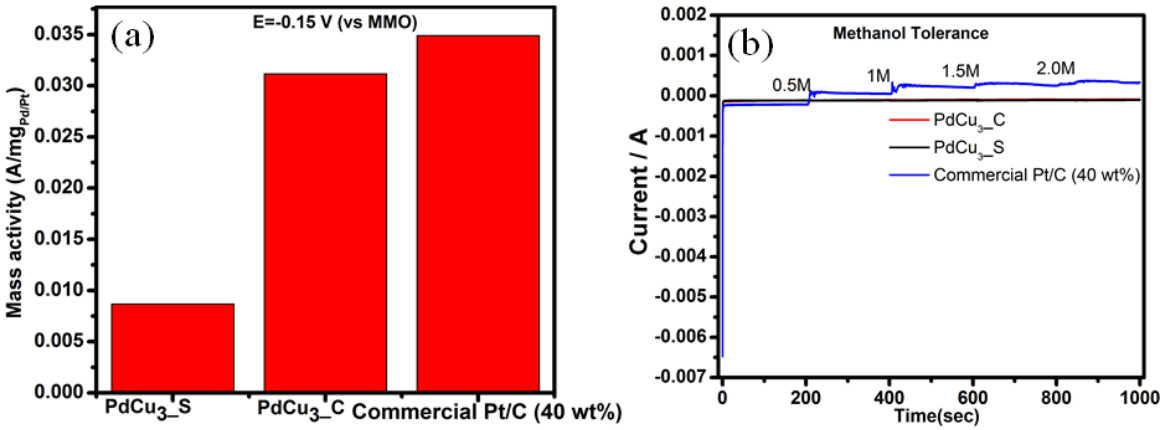

Figure 11. (a)Mass activity comparison between $PdCu_3$ and Pt/C catalysts normalized in reference to the loading amount of noble metals (Pd/Pt). Experiments were performed in O_2-saturated 0.5 M KOH at a rotation speed of 1200 rpm with a sweep rate of 5 mV/sec, (b) Methanol Tolerance Study: Chronoamperometry (CA) measurement performed at -0.3V on these three catalysts with addition of different concentration of methanol in a particular time interval.

Shao[28] and Suo[27] et al. has performed DFT calculation and showed that electronic structure of Pd surface can modified by strain and electronic distribution between Pd and its substrate (other alloying metal) (i.e. ligand effect), which in turn modifies the reactivity of Pd surface. The induced strain in the Pd surface due to the

insertion of Cu lowers the d-band centre and hence ORR activity is enhanced. Kondo et al. have showed[29] that ORR activity of different planes in acidic media goes in the trend Pd (110) < Pd (111) < Pd (100). Lee et al.[30] have successfully demonstrated the same order of reactivity of the Pd planes in alkaline medium. In another study Shao et al. investigated effect of different planes of Pd on ORR kinetics and proposed that low OH_{ads} coverage on Pd (100) plane creates more available reaction sites and hence an enhancement of ORR activity can be expected.

4.4. Conclusion

Ordered $PdCu_3$ nanocrystals have been synthesized successfully in different shapes for oxygen electroreduction in alkaline medium. From HRTEM analysis analysis, it can be concluded that nanospheres ($PdCu_3$_S) and nanocubes ($PdCu_3$_C) are essentially composed of (111), (100) planes, respectively. Our studies confirmed that ordered $PdCu_3$ alloy shows the activity trend $PdCu_3(111) < PdCu_3(100)$ in alkaline solution similar as reported for Pd. The activity of $PdCu_3$_C was found to be comparable to the state of art commercial Pt/C (40 wt %) catalyst. These findings provide a better understanding of the relationship between crystallographic planes and ORR activities of Pd based alloy catalysts in alkaline medium and will be helpful in the design and development of new Pd based cathode materials in PEMFCs.

4.5. References

(1) Dresselhaus, M. S.; Thomas, I. L. *Nature* **2001**, *414*, 332-337.

(2) Adzic, R. R., in: Lipkowski,J. : *P.N. Ross (Eds.),Electrocatalysis,Wiley, New York,* **1998**, 197.

(3) Gasteiger, H. A.; Kocha, S. S.; Sompalli, B.; Wagner, F. T. *Appl. Catal. B* **2005**, *56*, 9.

(4) Calegaro, M. L.; Lima, F. H. B.; Ticianelli, E. A. *J. Power Sources* **2006**, *158*, 735-739.

(5) Lima, F. H. B.; de Castro, J. F. R.; Ticianelli, E. A. *J. Power Sources* **2006**, *161*, 806-812.

(6) Alexeyeva, N.; Shulga, E.; Kisand, V.; Kink, I.; Tammeveski, K. *J. Electroanal. Chem.* **2010**, *648*, 169-175.

(7) Kruusenberg , I. M., L . ; Shah , Q . ; Kannan , A . M .; Tammeveski, K. *Int. J. Hydrogen Energy* **2012**, *37*, 4406 −4412.

(8) Wu, J. J.; Zhang, D.; Wang, Y.; Wan, Y.; Hou, B. R. *J. Power Sources* **2012**, *198*, 122-126.

(9) Sarkar, A.; Manthiram, A. *J. Phys Chem C* **2010**, *114*, 4725-4732.

(10) Oezaslan, M.; Hasche, F.; Strasser, P. *J. Electrochem. Soc.* **2012**, *159*, B444-B454.

(11) Genies, L.; Faure, R.; Durand, R. *Electrochim. Acta* **1998**, *44*, 1317-1327.

(12) Jiang, L.; Hsu, A.; Chu, D.; Chen, R. *J. Electrochem. Soc.* **2009**, *156*, B643-B649.

(13) Shao, M. *J. Power Sources* **2011**, *196*, 2433-2444.

(14) Shao, M. H.; Sasaki, K.; Adzic, R. R. *J. Am. Chem. Soc.* **2006**, *128*, 3526-3527.

(15) Ramos-Sánchez, G. Y.-M., H. ; Solorza-Feria,O. *Int. J. Hydrogen Energy* **2008**, *33*, 3596.

(16) Zhao, J.; Sarkar, A.; Manthiram, A. *Electrochim. Acta* **2010**, *55*, 1756-1765.

(17) Tarasevich, M. R.; Zhutaeva, G. V.; Bogdanovskaya, V. A.; Radina, M. V.; Ehrenburg, M. R.; Chalykh, A. E. *Electrochim. Acta* **2007**, *52*, 5108-5118.

(18) Miah, M. R.; Alam, M. T.; Okajima, T.; Ohsaka, T. *J. Electrochem. Soc.* **2009**, *156*, B1142-B1149.

(19) Wei, Y. C. L., C.W. Chang, Y.W.; Lai,C.M; Lim,P.Y.; Tsai, L.D.; Wang,K.W. *Int. J. Hydrogen Energy* **2010**, *35*, 1864.

(20) Tominaka, S.; Hayashi, T.; Nakamura, Y.; Osaka, T. *J. Mater. Chem.* **2010**, *20*, 7175-7182.

(21) Fernandez, J. L.; Raghuveer, V.; Manthiram, A.; Bard, A. J. *J. Am. Chem. Soc.* **2005**, *127*, 13100-13101.

(22) Lee, K.; Savadogo, O.; Ishihara, A.; Mitsushima, S.; Kamiya, N.; Ota, K. *J. Electrochem. Soc.* **2006**, *153*, A20-A24.

(23) Wang, X. P.; Kariuki, N.; Vaughey, J. T.; Goodpaster, J.; Kumar, R.; Myers, D. J. *J. Electrochem. Soc.* **2008**, *155*, B602-B609.

(24) Xu, C. X.; Zhang, Y.; Wang, L. Q.; Xu, L. Q.; Bian, X. F.; Ma, H. Y.; Ding, Y. *Chem. Mater.* **2009**, *21*, 3110-3116.

(25) Fouda-Onana, F.; Bah, S.; Savadogo, O. *J. Electroanal. Chem.* **2009**, *636*, 1-9.

(26) Xia, D. G.; Chen, G.; Wang, Z. Y.; Zhang, J. J.; Hui, S. Q.; Ghosh, D.; Wang, H. J. *Chem. Mater.* **2006**, *18*, 5746-5749.

(27) Suo, Y.; Zhuang, L.; Lu, J. *Angew. Chem. Int. Ed.* **2007**, *46*, 2862-2864.

(28) Shao, M. H.; Liu, P.; Zhang, J. L.; Adzic, R. *J. Phys. Chem. B* **2007**, *111*, 6772-6775.

(29) Kondo, S.; Nakamura, M.; Maki, N.; Hoshi, N. *J. Phys. Chem. C* **2009**, *113*, 12625-12628.

(30) Lee, C. L.; Chiou, H. P.; Liu, C. R. *Int. J. Hydrogen Energy* **2012**, *37*, 3993-3997.

(31) Shao, M. H.; Yu, T.; Odell, J. H.; Jin, M. S.; Xia, Y. N. *Chem. Commun.* **2011**, *47*, 6566-6568.

(32) Guymont, M.; Gratias, D. *Physica. status. solidi. (a)* **1976**, *36*, 329-334.

(33) Xu, Z. C.; Shen, C. M.; Hou, Y. L.; Gao, H. J.; Sun, S. S. *Chem. Mater.* **2009**, *21*, 1778-1780.

(34) Xiao, J. Y.; Qi, L. M. *Nanoscale* **2011**, *3*, 1383-1396.

(35) Yang, H. T.; Ogawa, T.; Hasegawa, D.; Takahashi, M. *J. Appl. Phys.* **2008**, *103*.

(36) Murphy, C. J.; San, T. K.; Gole, A. M.; Orendorff, C. J.; Gao, J. X.; Gou, L.; Hunyadi, S. E.; Li, T. *J. Phys. Chem. B* **2005**, *109*, 13857-13870.

(37) Liu, M. Z.; Guyot-Sionnest, P. *J. Phys. Chem. B* **2005**, *109*, 22192-22200.

(38) Wang, D. S.; Li, Y. D. *Adv. Mater.* **2011**, *23*, 1044-1060.

(39) Xia, B. Y.; Wu, H. B.; Wang, X.; Lou, X. W. *J. Am. Chem. Soc.* **2012**, *134*, 13934-13937.

(40) Cochell, T.; Li, W.; Manthiram, A. *J. Phys. Chem. C* **2013**, *117*, 3865-3873.

(41) Du, W. X.; Mackenzie, K. E.; Milano, D. F.; Deskins, N. A.; Su, D.; Teng, X. W. *ACS Catal.* **2012**, *2*, 287-297.

(42) Ahmed, M. S.; Jeon, S. *ACS Catal.* **2014**, *4*, 1830-1837.

(43) Chen, L. Y.; Chen, N.; Hou, Y.; Wang, Z. C.; Lv, S. H.; Fujita, T.; Jiang, J. H.; Hirata, A.; Chen, M. W. *ACS Catal.* **2013**, *3*, 1220-1230.

(44) Mukerjee, S.; Srinivasan, S.; Soriaga, M. P.; Mcbreen, J. *J. Electrochem. Soc.* **1995**, *142*, 1409-1422.

Summary and Future Directions

In this research, we have investigated the electrocatalytic activity of various ordered Pd based intermetallic nanomaterials. The compounds were synthesized in different size and shapes by adopting facile solution based approaches. The objective of this work was to develop Pd based catalysts having efficiency more than commercially available Pd/C and Pt/C and on par and more stable than current stat-of-the-art expensive Pt and Pd based compounds. Motivated on the recent developments in the area of Pd and other nanocrysatlline materials for various applications, we have selected a few interesting compounds, which was never reported in the nanocrystalline morphology. While going through the literature during the selection of Pd based compounds for various electrocatalytic properties, we noticed that only the tip of the iceberg has been touched. Three different compounds Pd_3Pb, Pd_2Ge and $PdCu_3$ have been synthesized in various morphology by using solvothermal and polyol methods. Another challenge was to develop these materials in ordered crystallographic arrangement. Due to the large difference in the reduction potential of the components, often resulted in disordered alloys or bimetallic materials. Ordering of the active sites in the special crystallographic position is very crucial to improve the catalytic activity. So optimizing the reaction conditions are required to achieve this objective. Towards this, we have varied the reaction time, temperature of the reaction, solvent and precursor salts. All three compounds we have synthesized in the ordered structure.

Other strategy of this work was to develop material in nano dimension aimed to increase the surface area and enhancing the catalytic activity. On the top of that, if these nanomaterials can be produced in different morphology with well directed crystal growth direction, the activity can be improved further. We have used various structure directing agents to produce nanomaterials with different morphology and active crystallographic

facets as we got it in the case of $PdCu_3$ nanoparticles. Another strategy was to control the crystallographic deficiency of selected atoms, which often reported as one aspect to improve the activity. We have optimized the reaction time in the case Pd_2Ge to achieve this and found that deficiency has a role in the ethanol oxidation reaction.

Powder XRD and TEM are powerful technics to probe the phase purity, particle size, deficiency of the atom and crystal growth direction. After every synthesis step, we have characterized the compound by these two techniques and redesign the experiment until we obtained the desired materials.

We have thoroughly studied electrocatalytic properties of the materials in both acidic and alkaline medium as an anode as well as cathode electrodes. Pd_2Ge and Pd_3Pb were used in the oxidation of small organic molecules such as formic acid and ethanol. In most of the cases our catalysts are found to be more active and stable with respect to the commercially available Pd/C catalysts. We have shown effect of crystal facets in electrocatalytic Oxygen Reduction Reaction (ORR) in alkaline medium for the ordered $PdCu_3$ nanocrystals. Cubic $PdCu_3$ nanocrystals composed of (100) crystal facets are found to be as active as the state of art material Pt in alkaline medium. In addition to that all compounds showed remarkable stability compared to the commercial materials.

After the successful results of these initial approaches, we would like to expand our work on different compounds. We already have preliminary results on Pd_2In_3 for the methanol oxidation. Other extension of this work in future is to dope the deficient atomic position with a third element, which can promote the activity further. We already observed the Ge deficiency in the crystal lattice of Pd_2Ge. We are planning to dope the Ge position with other metals (like Pt, Sb, Ni, Cu) with almost similar atomic radii to check how doping in the ordered structure changing the kinetics of the ethanol oxidation

in alkaline medium. We have planned to synthesize the first row transition metal substituted Pd_3Pb, Pd_2Ge and $PdCu_3$ nanocrystals and investigate their catalytic activities in near future as transition metals are expected to enhance the electrocatalytic properties. We have also planned to do study the change in co-ordination environment of the active sites of the ordered structures after substitution through XAFS measurements and correlate the change in electrocatalytic properties with structural variation. It is always important to understand the mechanism of the oxidation and reduction reactions. If the reaction happens through the indirect pathway, it can lead into the surface poisoning of the catalysts. We are planning to attach IR spectrometer to the existing electrochemical work station to understand the reaction mechanism during the electrocatalytic process. One of the best ways to develop stable catalyst is to avoid the indirect pathway, which may lead into the catalytic positioning by CO molecule. This will help us to design the catalyst for the better activity.

List of Publications

Publications included in Thesis

1. Facile and Ultrafast Synthesis of Pd_3Pb Nanocrystals towards Enhanced Activity and Durability in Direct Ethanol and Formic acid Fuel Cells; **Rajkumar Jana**, Udumula Subbarao and Sebastian C. Peter (manuscript under revision).

2. Ordered Pd_2Ge Intermetallic Nanoparticles for Enhanced Activity and Stability towards Ethanol Oxidation; Sumanta Sarkar, **Rajkumar Jana**, Suchithra, Umesh V. Waghmare, Balamurugan Thapa, S. Sampath and Sebastian C Peter (manuscript under revision).

3. Effect of Morphology of Ordered $PdCu_3$ Nanocrystals on Electrocatalytic Oxygen Reduction Reaction in Alkaline Medium; **Rajkumar Jana**, Anupam Bhim, Anju V Gopinath, S. Sampath and Sebastian C Peter (manuscript under preparation).

Publications not included in Thesis

4. Nanofication and Dimensional Reduction Mediated Valence Transition as a Tool towards Environmentally Stable Materials; Udumula Subbarao, Sumanta Sarkar, **Rajkumar Jana**, Sourav S. Bera andSebastian C. Peter (manuscript under submission).

5. $Yb_7Ni_4InGe_{12}$: a quaternary compound having mixed valent Yb atoms grown from indium flux; Udumula Subbarao, **Rajkumar Jana**, Maria Chondroudi, Mahalingam Balasubramanian, Mercouri G. Kanatzidis and Sebastian C. Peter, *Dalton Trans.*, **2015**, 44, 5797–5804.